

Hydrogel encapsulated biosensors for the detection of biologically significant vanadium and selenium

By

Francis Ntumba Muya

ND (CPUT), BSC. Honors (UWC), MSc (UWC)

This thesis is submitted in fulfillment of the requirements for the degree of **Philosophiae in Scientiae** to the Department of Chemistry, SensorLab
University of the Western Cape,

South Africa



UNIVERSITY *of the*
WESTERN CAPE

Supervisor

Prof. Priscilla Baker

Co-supervisor

Prof. Emmanuel Iwuoha

April

2017

ABSTRACT

Vanadium and selenium salts are toxic in large amounts, but trace amounts are necessary for cellular function in many organisms. Exposure to high level of selenium has been linked to delays in early childhood development as well as the development with onset of diabetes type II. Vanadium is a relatively controversial dietary supplement, used primarily for increasing insulin sensitivity. These metals have been identified as potential human carcinogens that disrupt cellular metabolic processes at high level, causing lung cancer, brain damage and DNA damage. Developing a sensor system that can monitor the level of vanadium and selenium in aqueous and selected real samples is a strong priority.

Biological sensors require a suitable micro-environment for the immobilization of enzyme or antibody (alkaline phosphatase and selenoprotein p antibody). Polysulfone hydrogel was selected as a suitable transducer for the construction of the biosensor due to its physical and chemical properties. The synthesized polysulfone hydrogel was characterized by cyclic voltammetry (CV), atomic force microscopy (AFM), scanning electron microscopy (SEM) and Raman spectroscopy and used for applications such as chemical sensors, adsorbents for metal remediation and transducers in the construction of biosensors.

The hydrogel sensors were applied for the detection of selenium and vanadium in aqueous medium. The oxidation states of selenium were confirmed as Se^{4+} , Se^0 and Se^{2-} . The oxidation states of vanadium were found to agree with V^{4+} , V^{3+} and V^{2+} , in terms of literature reference values. The sensor favoured Se^{4+} and V^{2+} , in terms of sensitivity, diffusion coefficient and limit of detection (LOD). The hydrogel was applied as an adsorbent for remediation of vanadium and selenium in aqueous systems. The adsorption process was investigated by swelling method, the adsorption capacity (Q) was found to be 0.189 mg/g and 0.559 mg/g for vanadium and selenium respectively.

Alkaline phosphatase (ALP) based biosensor was constructed by immobilizing ALP at hydrogel to produce Au-HGL/ALP biosensor. The biosensor was characterized by CV, AFM and Raman spectroscopy. The analytical performance of the biosensors was evaluated by SWV, EIS and amperometry. The biosensor displayed a linear response to the concentration of vanadium, in the range 0-30 μM which was modelled as Michaelis-Menten kinetics. The enzymatic binding efficiency displayed by the biosensor for vanadium in solution form 0-20 μM , was evaluated to have a LOD and limit of quantification (LOQ) of 0.227 μM and 0.758 μM respectively. The biosensor was employed for the detection of vanadium in Centrum® over 50+. Au-HGL/ALP biosensor exhibited high sensitivity for vanadium detection with a good reproducibility ($n=4$) and a relative standard deviation (RSD) of 8%.

The immunosensor was constructed by immobilizing Selenoprotein p (SePP) antibody at hydrogel electrode (HGL) resulting in Au-HGL/SePP immunosensor. The Au-HGL/SePP immunosensor was characterized by contact angle, AFM and CV. The immunosensor response to selenium in solution, investigated by amperometry produced a linear response to the detection of selenium with LOD and LOQ of 0.035 μM and of 0.104 μM respectively. However reproducibility was a challenge due to the hydrophobic nature of the antibody emulsion.

DEDICATION

This project is dedicated

To

Family members

My Parents

Mrs. Noella Nkongolo and Mr. Frederick Nkongolo Kabwe



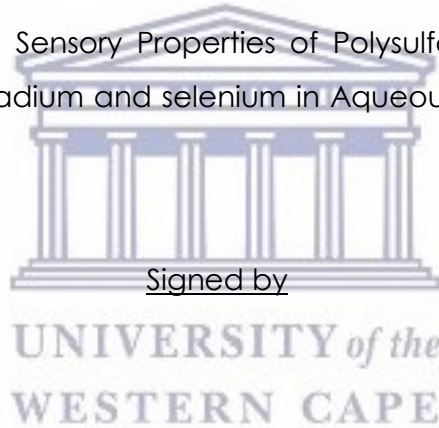
UNIVERSITY *of the*
WESTERN CAPE

DECLARATION

I declare that **Hydrogel encapsulated biosensors for the detection of biologically significant vanadium and selenium** is my own work, that it has not been submitted before for any degree or examination in any other university, and that all the sources I have used or quoted have been indicated and acknowledged as complete references. However part of this work have been published in the scientific journals, with references below:

Ref A: **Muya, F.N**, et al. *Environmental remediation of heavy metal ions from aqueous solution using hydrogel as adsorbent: Critical review*. Journal of water science and technology 2016, 73 (5) 983-992; **DOI**: 10.2166/wst.2015.567

Ref B: **Muya, F.N**, et al. "Sensory Properties of Polysulfone Hydrogel for Electro-Analytical Profiling of vanadium and selenium in Aqueous Solutions," J. Nano Res., vol. 44, pp. 142–157, 2016



Author

Francis Ntumba Muya

January 2017

Sign

A handwritten signature in black ink, appearing to read "Francis Ntumba Muya", is placed on a light yellow rectangular background.

Approved by

Supervisor

Prof Priscilla Baker

Sign.....

LIST OF PUBLICATIONS

1. **Muya, F.N.**, L. Phelane, P. Baker, and E. Iwuoha, *Synthesis and characterization of polysulfone hydrogels*. Journal of Surface Engineered Materials and Advanced Technology., 2014(4): p. 227-236.
2. Phelane, L., **F.N. Muya**, H.L. Richards, P.G.L. Baker, and E.I. Iwuoha, *Polysulfone nanocomposite membranes with improved hydrophilicity*. Electrochimica Acta 2014. **128** p. 326-335.
3. **Muya, F.N**, Ward .M, .E Sunday, P. Baker and E. Iwuoha, *Environmental remediation of heavy metal ions from aqueous solution using hydrogel as adsorbent: Critical review*. Journal of water science and technology 2016, 73 (5) 983-992; **DOI:** 10.2166/wst.2015.567
4. **Muya, F.N**, F. N. Muya, X. T. Ngema, P. G. L. Baker, E. Iwuoha. "Sensory Properties of Polysulfone Hydrogel for Electro-Analytical Profiling of vanadium and selenium in Aqueous Solutions," J. Nano Res., vol. 44, pp. 142–157, 2016
5. **Muya, F.N**^{1a}, Priscilla Baker¹, Emmanuel Iwuoha¹, Selim Boudjaoui², Nedjila H², Abdullatif Baraket², Nicole Jaffrezic², and A. Errachid². *Novel highly selective enzymatic gas biosensor for detection of formaldehyde*. Submitted for Patenting (pending)
6. **Muya, F.N**, Phelane, L. Baker P and Iwuoha E (2016). Selectively functionalized polysulfone hydrogel biosensors for vanadium and selenium detection. Paper presented at the international society of electrochemistry (ISE) 67th conference, The Hague Netherlands 21-27 August 2016, Viewed on the 22 August 2016.

ACKNOWLEDGEMENT

I would like to take this opportunity to sincerely express my gratitude to the following bodies in absolutely no specific order for a tremendous contribution to my entire academic life. I doubt it would have been possible for me to get to this level without their support, whether financial social or spiritual.

- **God** Almighty to Him all the glory, honor and adoration for giving me the strength and wisdom through the Holy Spirit to complete this work.
- University of the Western Cape (UWC), and Universite de Claude Bernard Lyon 1
- To my supervisors Prof. Priscilla Baker and Prof. E. Iwuoha, thank you very much for seeing my potential and guiding me all the way.
- To my postdoctoral fellow Dr. Tesfaye T. Waryo, and Dr Masikini Milua, thank you very much for putting in the time and effort to supervise, advise and help through my studies
- To my colleagues in SensorLab, University of the Western Cape, specially Dr Fanelwa Ajayi, Dr Chinwe Ikpo, Dr Natasha Ross, Dr. Noluthando Mayetwa Lisebo Phelane, Meryck Ward, Lindsay Willson, Candice Rassie, Keagan Pokpas, Xolani Ngema, Wonderboy, OLwetu and all
- To All my spiritual family (Grace a la Grace) for your spiritual support and prayer.
- To my uncle David Kabamba and his wife Mitchou Mbuyi and my lovely niece Esther Kabamba thanks for all your support in my life which are uncountable, keep it up and don't stop.
- To you my fiancé the love of my life Lilianne Ngandu much love and thanks for being patient with me.
- To all SensorLab's research team, you guys rock! Thank you very much
- SARchil chair (Nano electrochemistry and sensor technology) for grants holder linked bursary.

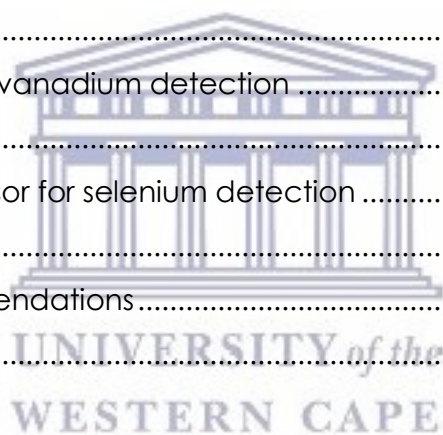
Much appreciation to all my family members for their love, support and care during the period of study. I felt highly encouraged and loved. Thank you so much. Lastly, not least to my parents **Frederick Nkongolo Kabwe** and **Noella Nkongolo**, this is for you. Thank you very much for your love, care, education and upbringing. You are just the best gift from God.



UNIVERSITY *of the*
WESTERN CAPE

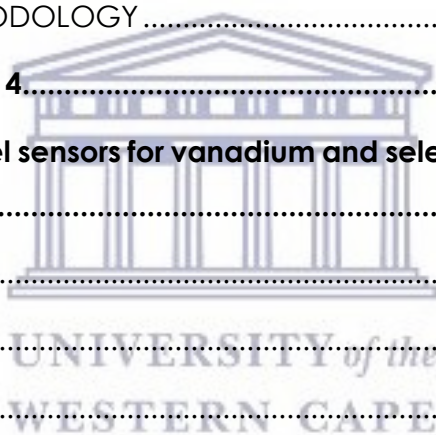
TABLE OF CONTENTS

Chapter 1	1
Chapter 2	11
Literature review	11
Chapter 3	42
Materials and Methodology	42
Chapter 4	59
Hydrogel sensors for vanadium and selenium in aqueous solutions	59
Chapter 5	91
Raman spectra of hydrogel biosensors	91
Chapter 6	101
Au-HGL/ALP biosensor for vanadium detection	101
Chapter 7	138
Au-HGL/SePP immunosensor for selenium detection	138
Chapter 8	151
Conclusions and recommendations	151
REFERENCES	154
ABSTRACT	ii
DEDICATION	iv
DECLARATION	v
LIST OF PUBLICATIONS	vi
ACKNOWLEDGEMENT	vii
TABLE OF CONTENTS	ix
LIST OF FIGURES	xiv
LIST OF UNITS	xxi



Chapter 1.....	1
INTRODUCTION.....	1
1. BACKGROUND AND OVERVIEW.....	1
2. MOTIVATION.....	3
3. PROBLEM STATEMENT	3
4. AIMS :	5
5. OBJECTIVES	6
6. CONCEPTUAL DIAGRAM.....	7
7. OUTLINE OF THE THESIS	8
Chapter 2.....	11
Literature review	11
Abstract	11
2. INTRODUCTION.....	11
2.1. GENERAL OVERVIEW	13
2.2. MECHANISM OF BIO-SORPTION.....	14
2.3. HYDROGELS AS ADSORBENTS	16
2.4. FACTORS AFFECTING ADSORPTION	18
2.5. ELECTROCHEMICAL DETECTION OF METALS	26
2.6. VANADIUM	29
2.7. Selenium	35
2.9. CHEMICAL SENSORS.....	39
Chapter 3.....	42
Materials and Methodology	42
3. REAGENTS	42
3.1. PREPARATION OF SOLUTION AND HYDROGEL SYNTHESIS	43

3.2.	ANALYTICAL TECHNIQUES USED FOR THIS STUDIES	43
3.2.1	Electrochemical techniques	44
3.2.2.	Spectroscopic techniques.....	52
	Raman spectroscopy	52
	Fourier transformer infrared spectroscopy (FTIR)	53
	Ultra-violet-visible spectroscopy.....	53
3.2.3.	Morphological techniques	54
	Scanning electron microscopy	54
	Atomic force microscopy	55
3.3.	RESEARCH METHODOLOGY	55
	Chapter 4.....	59
	Hydrogel sensors for vanadium and selenium in aqueous solutions	
	59
	ABSTRACT.....	59
4.	INTRODUCTION	59
4.2.	EXPERIMENT	60
4.3.	ELECTROCHEMICAL CHARACTERIZATION OF SYNTHESIZED POLYSULFONE HYDROGEL.....	60
4.4.	SPECTROSCOPY CHARACTERIZATION	64
4.5.	PHYSICAL TESTING OF SYNTHESIZED HYDROGEL	65
4.6.	HYDROGEL STABILITY	67
4.7.	MICROSCOPIC CHARACTERIZATION OF HYDROGEL	69
4.8.	HYDROGEL APPLICATION	71
4.8.1.	HYDROGEL SENSOR FOR DETECTION OF Vanadium	74
	Table 4.6: Adsorption capacity of various hydrogels systems	80



4.8.2.	HYDROGEL SENSOR FOR DETECTION OF SELENIUM	81
	Electrochemical studies of selenium at hydrogel interface	83
	Chapter 5.....	91
	Raman spectra of hydrogel biosensors	91
	ABSTRACT.....	91
5.	INTRODUCTION	91
5.1.	PRINCIPLE OF RAMAN	92
5.2.	PARTS OF RAMAN SPECTROMETER.....	93
5.3.	EXPERIMENTAL.....	94
5.4.	RESULTS AND DISCUSSIONS.....	96
5.5.	CHARACTERIZATION OF AU-HGL/ALP BY RAMAN SPECTROSCOPY	97
5.6.	CHARACTERIZATION OF AU-HGL/SePP BY RAMAN SPECTROSCOPY	99
5.7.	CONCLUSION.....	100
	Chapter 6.....	101
	Au-HGL/ALP biosensor for vanadium detection	101
	ABSTRACT.....	101
6.	INTRODUCTION	101
6.1.	EXPERIMENT	102
6.2.	ELECTROCHEMICAL RESPONSE OF ALKALINE PHOSPHATASE AT GLASSY CARBON ELECTRODE	103
6.3.	ELECTROCHEMICAL DEPOSITION OF HYDROGEL AT GOLD ELECTRODE	104
6.4.	IMMOBILIZATION AND CHARACTERIZATION OF ALKALINE PHOSPHATASE (ALP) ONTO AU/HGL ELECTRODE.....	110
6.5.	MICROSCOPIC CHARACTERIZATION OF ALP-HGL BIOSENSOR BY ATOMIC FORCE MICROSCOPY (AFM).....	113

6.6.	OSTERYOUNG SQUARE WAVE SPECTROSCOPY OF AUE-HGL/ALP BIOSENSOR RESPONSE TO VANADIUM	117
6.7.	ELECTROCHEMICAL IMPEDANCE ANALYSIS OF Au-HGL/ALP BIOSENSOR RESPONSE TO VANADIUM	122
6.8.	AMPEROMETRIC RESPONSE OF Au-HGL/ALP BIOSENSOR TO VANADIUM	126
6.9.	COMPARISON BETWEEN THE VOLTAMMETRY, IMPEDANCE AND AMPEROMETRIC BIOSENSOR FOR DETECTION OF VANADIUM.....	130
6.10.	KINETIC AND METABOLIC STUDIES OF THE AU-HGL/ALP BIOSENSOR.....	131
6.11.	Au-HGL/ALP BIOSENSOR RESPONSE TO VANADIUM DETECTED IN REAL SAMPLE 133	
6.12.	INTERFERENCE STUDIES	135
6.13.	CONCLUSION.....	136
	Chapter 7.....	138
	Au-HGL/SePP immunosensor for selenium detection.....	138
	ABSTRACT	138
7.	INTRODUCTION.....	138
7.1.	EXPERIMENTAL.....	139
7.2.	ELECTROCHEMICAL RESPONSE OF SELENOPROTEIN P ANTIBODY AT GLASSY CARBON ELECTRODE.....	140
7.3.	OSTERYOUNG SQUARE WAVE SPECTROSCOPY OF Au-HGL/SePP IMMUNOSENSOR RESPONSE TO SELENIUM.....	145
7.4.	AMPEROMETRIC RESPONSE OF Au-HGL/SePP IMMUNOSENSOR TO SELENIUM 147	
7.5.	CONCLUSION.....	150



UNIVERSITY of the
WESTERN CAPE

Chapter 8.....	151
Conclusions and recommendations.....	151
REFERENCES	154

LIST OF FIGURES

Figure 2.1: Two stage bio-sorption diagram	16
Figure 2.2: Hydrogel adsorption mechanism	17
Figure 2.3: Comparison of kinetics parameters (q_m and q_e) of different metals ions and adsorbents	21
Figure 2.4: Comparison of kinetics parameters (K_f) of different metals ions and adsorbent	22
Figure 2.5: Vanadium image	29
Figure 2.6: Vanadium in steels production	31
Figure 2.7: Vanadium pentoxide	31
Figure 2.8: Vanadium sulfate	32
Figure 2.9: Essential anti-diabetic effect of vanadium compounds [112].	33
Figure 2.10: Anti- and pro-tumor actions of vanadium compounds [55,113].	34
Figure 2.11: Selenium salt	35
Figure 2.12: Mechanism of anti-cancer activity of selenium	36
Figure 2.13: Ribbon diagram (rainbow-color, N-terminus = blue, C-terminus = red) of the 3D structure of bacterial alkaline phosphatase.	40
Figure 2.14: Rainbow-color of the 3D structure of Selenoprotein p antibody.	41
Figure 3.1: Typical OSWV for film containing the forward, reverse and reverse currents.	47

Figure 3.3: Sinusoidal current response to potential perturbation as a function of time.	49
Figure 3.4: Randles equivalent circuit.....	49
Figure 3.6: ALP biochemistry: Ribbon diagram (rainbow-color, N-terminus = blue, C-terminus = red) of the 3D structure of bacterial alkaline phosphatase.	57
Figure 3.7: SePP-biochemistry/SePP in selenium homeostasis and transport of the testis, brain and kidney.....	58
Figure 4.1: Cyclic voltammetry of PSF at SPCE in 1 M HCl vs Ag/AgCl.....	61
Figure 4.2: Cyclic voltammetry of PVA and at SPCE in 1 M HCl vs Ag/AgCl.....	62
Scheme 4.1: Schematic representation of hydrogel synthesis.....	62
Figure 4.3: Cyclic voltammetry of hydrogel at SPCE in 1 M HCl vs Ag/AgCl.....	63
Figure 4.4: FTIR spectra of hydrogel powder at SPCE.....	64
Figure 4.5: Swelling capacity of hydrogel.....	66
Figure 4.6: CV of time interval studies of selenium at hydrogel interface in 1 M HCl vs Ag/AgCl.....	68
Figure 4.7: HR-SEM spectrum of a) PSF and b) PSF-hydrogel at SPCE at 10 x magnification with EHT 5 W.....	69
Figure 4.8: AFM images of a) PSF and b) PSF-hydrogel at SPCE.....	70
Figure 4.9: CV of bare SPCE in solution and vanadium at unmodified SPCE In 1M HCl vs Ag/AgCl.....	72
Figure 4.10: SWV A) Oxidation and B) Reduction of bare electrode and vanadium at unmodified SPCE in 1 M HCl vs Ag/AgCl.....	73
Figure 4.11: Cyclic voltammetry of (a) Vanadium at hydrogel interface and (b) vanadium at Hydrogel immobilized at electrode in 1 M HCl vs Ag/AgCl.....	75
Figure 4.12: calibration curves plot based on the influence of concentration of vanadium on the peak current response at hydrogel interface in 1 M HCl vs Ag/AgCl.	76

Figure 4.13: Effect of time on heavy-metal ions adsorption ($C_0 = 100 \text{ m g/L}$, $m = 0.5000 \text{ g}$, $V = 40 \text{ mL}$, $\text{pH}=6$, $T = 25^\circ\text{C}$).....	77
Figure 4.14: HR-SEM image of (a) Vanadium at SPCE, (b) Vanadium at hydrogel interface after electrochemical analysis and dried for 24 hrs.....	79
Figure 4.15: CV of bare SPCE and selenium at SPCE in 1 M HCl vs Ag/AgCl	82
Figure 4.16: CV of unmodified electrode, Hydrogel at SPCE and selenium at hydrogel SPCE interface in 1 M HCl vs Ag/AgCl	84
Figure 4.17: Series of CV recorded at different scan rates for the same solution containing only Se^{4+} at hydrogel interface in 1 M HCl vs Ag/AgCl	85
Figure 4.18: Influence of concentration of selenium on the peak current response at hydrogel interface in 1 M HCl vs Ag/AgCl	86
Figure 4.19: Effect of time on heavy-metal ions adsorption ($C_0 = 100 \text{ m g/L}$, $m = 0.5000 \text{ g}$, $V = 40 \text{ mL}$, $\text{pH}=6$, $T = 25^\circ\text{C}$).....	88
Figure 4.20: HR-SEM EDS image of (a) Selenium at SPCE, (b) Selenium at hydrogel interface after electrochemical analysis and dried for 24 hrs.....	89
Figure 5.1: Different possibilities of light scattering.....	93
Figure 5.2: travel in the Raman spectrometer.....	94
Figure 5.3: Image of Xplora HORIBA Raman spectroscopy	95
Figure 5.4: Raman spectrum of PSF and PSF-hydrogel at SPCE.....	97
Figure 5.5: Raman spectra of (a) Au-electrode, (b) hydrogel electrochemical deposited at gold electrode (AuE-HGL) and alkaline phosphatase incubated to the hydrogel interface (AuE-HGL-ALP).....	98
Figure 5.6: Representation of electrode modification.....	99
Figure 5.7: Raman spectra of (a) hydrogel electrochemical deposited at gold electrode (AuE-HGL), (b) Au-electrode, and (c) Selenoprotein p antibody incubated to the hydrogel interface (AuE-HGL-SePP)	100
Figure 6.1: UV-vis of ALP in 10mM Tris-buffer solution.....	103

Figure 6.2: CV of (1) bare GCE in Tris-Buffer pH 7.9 at scan rate of 50 mV/s and (2) with 10 μ L ALP added to the buffer at GCE.....	104
Figure 6.3: Electrochemical deposition of Hydrogel unto Au (10 cycles) in 0.2 M HCl vs Ag/AgCl.....	105
Figure 6.4: Characterization of the deposited polysulfone Hydrogel unto Au electrode in fresh 0.2 M HCl vs Ag/AgCl	106
Figure 6.5: Randle Sevčik plot of peak current versus root of scan rate in 0.2M HCl Ag/AgCl obtained after electrochemical characterization of HGL/Au	107
Figure 6.6: Characterization of Au-HGL in 1%BSA, 10mM Tris-buffer pH 7.9 vs Ag/AgCl	109
Figure 6.7: Au-HGL response to ALP in solution	110
Figure 6.8: SWV of Au-HGL/ALP biosensor at different incubation time interval by (A) oxidation and (B) reduction	112
Figure 6.9: AFM images of (a) Bare AuE, (b) AuE-HGL and (c) AuE-HGL/ALP.....	115
Figure 6.10: AFM height distribution of (a) Bare AuE, (b) AuE-HGL and (c) AuE-HGL/ALP.....	116
Figure 6.11: SWV of vanadium (A) oxidation and (B) reduction in Tris-buffer 1% BSA, scan at 50 mV/s.....	117
Figure 6.12 Michaelis-Menten plots of the AuE-HGL/ALP biosensor response to vanadium.....	118
Figure 6.13. Calibration plot for the AuE-HGL/ALP biosensor response to vanadium in the linear range between 0-25 μ M (n=4).....	120
Figure 6.14: Effect of ALP in the biosensor construction	121
Figure 6.14: Electrical model.....	122
Figure 6.15: EIS (Nyquist plot) of Au-HGL/ALP response to vanadium.	123
Figure 6.17: EIS (Bode plot) of Au-HGL/ALP response to vanadium.....	125

Figure 6.18: Current response of biosensor to concentration addition of vanadium in Tris-buffer vs Ag/AgCl	126
Figure 6.19: Calibration plot of vanadium response to the amperometric biosensor monitored at - 850mV in fresh Tris-buffer vs Ag/AgCl (n=4).	127
Figure 6.20: Amperometric effects of ALP in Au-HGL/ALP biosensor.....	129
Figure 6.21: UV-vis response of vanadium solution (1) before and (2), (3) after being exposed to the Au-HGL/ALP biosensor.....	132
Figure 6.22: Au-HGL/ALP biosensor response to Centrum Tablet in Tris-buffer 1% BSA, scan at 100 mV/s.....	133
Figure 6.23: Au-HGL/ALP biosensor response to vanadium in centrum	134
Figure 6.24: Au-HGL/ALP biosensor response to interference (a) Centrum (b) Boron, (c) Nickel and (d) Potassium solution in Tris-buffer 1% BSA, scan at 100 mV/s.	135
Figure 7.1: UV-vis of SePP in phosphate buffer solution	139
Figure 7.2: Cyclic voltammograms of SePP at GCE in PBS pH 7.1 at 50 mV/s Vs Ag/AgCl.	140
Figure 7.3: Scan rate dependence studies of SePP at Bare GCE in PBS pH 7.1 vs Ag/AgCl	141
Figure 7.4: Contact angle of SePP	142
Figure 7.5 OSWV of SePP immobilized at Au-HGL in PBS pH 7.1 Vs Ag/AgCl (A) oxidation and (B) reduction	144
Figure 7.6 OSWV (Reduction) of the increasing in selenium concentration using AuE-HGL/SePP immunosensor in PBS pH 7.1, scan at 100 mV/s	145
Figure 7.7: Calibration plot for the Au-HGL/SePP immunosensor to the different concentration of selenium in the linear range between 0-8 μ M.	146
Figure 7.8: Amperometry immunosensor for selenium detection at - 0.200 V in PBS pH 7.1 vs Ag/AgCl.....	148

Figure 7.9: Calibration plot of selenium response to the amperometric immunosensor monitored at -0.200 V in PBS pH 7.1 vs Ag/AgCl..... 149

LIST OF TABLES

Table 2.1: Coefficient of pseudo-first and second order kinetics models.....	23
Table 2.2: Summary Table of metal ions concentrations dependence based on pH, adsorbent time and concentration	24
Table 2.3: Summary of most source of selenium [59].....	37
Table 2.4: Tolerable upper intake levels (ULs) for selenium[9].....	38
Table 4.1: Summary table of peak potential.....	64
Table 4.2: PSF-PVA hydrogel functional group identification	65
Table 4.3 Swelling capacity of hydrogel in various electrolyte	67
Table 4.4: Vanadium redox potential at SPCE.....	74
Table 4.5: Summary of hydrogel performance sensor in the presence of vanadium	76
Table 4.6: Adsorption capacity of various hydrogels systems	80
Table 4.7: Selenium redox at bare SPCE.....	83
Table 4.8: Summary of hydrogel performance sensor in the presence of selenium.....	86
Table 6.1: Kinetic parameters of Polysulfone hydrogel film deposited at Au electrode in 0.2M HCl	108
Table 6.2: Analytical parameters of ALP incubation time.....	113
Table 6.3: Analytical parameters of AuE, HGL and ALP derived from AFM image	115
Table 6.4: Analytical performance of Au-HGL/ALP response to vanadium.....	120
Table 6.5: EIS fitting data	123

Table 6.6: Analytical performance of Au-HGL/ALP response to vanadium 128

Table 6.6: Comparison for various techniques used 130

Figure 7.4: Contact angle of SePP 142

Table 7.1: Analytical performance of Au-HGL/SePP response to selenium..... 147

Table 7.2: Analytical performance of Au-HGL/SePP response to selenium..... 149



UNIVERSITY *of the*
WESTERN CAPE

LIST OF UNITS

Micro litter

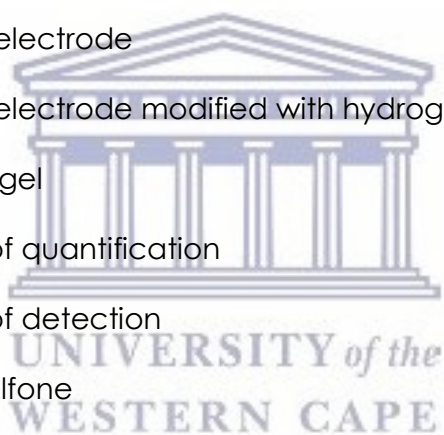
A	:	Ampere
μA	:	Micro-Ampere
mA	:	Mili-Ampere
nm	:	nano meter
Cm^2/s	:	Centimeter square per second
Ω	:	Ohms
V	:	Voltage
KHz	:	Kilohertz
μF	:	micro-farad



UNIVERSITY *of the*
WESTERN CAPE

KEY WORDS AND ABBREVIATIONS

Amp	:	Amperometry
ALP	:	Alkaline phosphatase
AFM	:	Atomic force microscopy
AuE-HGL/ALP:		Alkaline phosphatase immobilized at AuE-HGL
BSA	:	Bovine Serum albumin
CV	:	Cyclic voltammetry
EIS	:	Electrochemical impedance spectroscopy
ECS	:	Electrochemical sensor
AuE	:	Gold electrode
AuE-HGL	:	Gold electrode modified with hydrogel
HGL	:	Hydrogel
LOQ	:	Limit of quantification
LOD	:	Limit of detection
PSF	:	Polysulfone
R _c T	:	Resistance
ROS	:	Reactive oxygen species
Se	:	Selenium
SWV	:	Square wave Voltammetry
SePP	:	Selenoprotein p antibody
SEM	:	Scanning electron microscopy
SPCE	:	Screen printed carbon electrode
V	:	Vanadium



Chapter 1

INTRODUCTION

This chapter gives a brief introduction of the project and general introduction to problem identification associated with heavy metals. As well as the author of the thesis illustrate the project proposal; objectives of the project and expected outcome followed by methodology to be applied are presented.

1. BACKGROUND AND OVERVIEW

It has been reported for the past few decades that nature could effectively handle hazardous substances such as toxic heavy metals, dye pollutants, etc. [1]. Nowadays human beings are more concerned about their sensitive natural environment. Experts estimate that industrial processes release up to a million different pollutants into the atmosphere and the aquatic ecosystem as metal ions and complexes [2]. Subsequently, industrialization and population growth approximately by 61.5% as well as the quality of life required have increased [3–6]. Exposure to air pollution coming from industrial activities, traffic and energy production become unescapable. Of interest, mining industries have introduced different types of heavy metals as wastes into the environment. Recently, the term “heavy metals” has become widely used in biology and environmental studies related to their potential toxicity and ecotoxicity [7]. Humans are exposed to heavy metals through foods, water, industry products and occupational exposure. The poisoning effects of heavy metals are due to their interference with the normal body biochemistry in the normal metabolic processes [8]. The Kidneys, bones and lungs are the critical target organs with regard to environmental exposure. Heavy metals

such as vanadium and selenium are common air pollutants, being emitted mainly as a result of various industrial activities and agriculture. These heavy metals are persistent in the environment and are subject to bioaccumulation in food-chains. Selenium salts are toxic in large amounts, but small amounts are necessary for cellular function in many organisms [9–13]. It is also found as an ingredient in many multi-vitamins and other dietary supplements, including infant formula. In humans, selenium is a trace element nutrient that functions as cofactor for the reduction of antioxidant enzymes, such as glutathione peroxidases and certain forms of thioredoxin reductase [14]. Recently, selenium exposure has been linked to early childhood developmental delays as well as development of diabetes type II [15]. Vanadium is a relatively controversial dietary supplement, used primarily for increasing insulin sensitivity and body-building [16–22]. Deficiencies in vanadium have been linked to reduced growth and impaired reproduction in rats and chickens [23]. Inhalation exposures to vanadium and vanadium compounds result primarily in adverse effects on the respiratory system [16–20,24–27]. Vanadium and selenium have been identified as potential human carcinogens that disrupt cellular metabolic processes at high level, causing lung cancer, brain damage and DNA damage [28][29–31]. A fundamental understanding of metal species bioavailability and transformation in various matrices is crucial to the development of sensor and biosensor systems. This lead to the main objectives of this research, the development of a highly selective immunosensor for detection of selenium based on the affinity of selenoprotein P Antibody, whereas the biosensor for vanadium will draw on the inhibition mechanism of alkaline phosphatases. However both these sensors require a biocompatible electroactive platform.

2. MOTIVATION

Electrochemical sensors with rapid and highly sensitive detection capabilities of various bio/chemical species are in great demand in many areas of science. Developing easy-to-use electrochemical device for detecting the concentration and activities of the various species has become very important. Hydrogels are advanced polymer systems that hold special advantages in drug delivery based on their loading capacity and control release of drug [32,33]. As a result, hydrogels and polymer technologies owned by some company may offer particular advantages as vehicles that can be loaded with trace metals after manufacturing, permitting their use with a broad range of active agents including anti bacteria. Consequently hydrogels have been used extensively in the development of the smart drug delivery systems [34,35]. Therefore, since they can change their properties in response to specific stimuli. However, they usually require continuous stimulation to maintain these changes. Now, researchers have developed an approach that could allow more delicate control and timing of entrap and release of heavy metals [36]. In addition the new technique uses hydrogels, as a type of smart polymer for entrapment and controlled release. Therefore hydrogels being able to control entrapment and release of metals by triggering a change in oxidation state, this could help in the design of programmable device for monitoring drugs metabolism of toxic metals in human body and improved methods for environmental hazards recognition.

3. PROBLEM STATEMENT

Vanadium is a trace mineral that is needed by human body in small amounts [23,28,37–39]. It is commonly found in vegetables (black pepper, mushrooms, parsley, and corns) and sea foods [40–42]. The presence of vanadium in the brain inhibits cholesterol from forming in the blood vessels [43–46]. Vanadium is active in many chemical reactions that take place in the body [47]. However it is believed

that vanadium is involved in energy production, as a cofactor of enzymes to accelerate chemical reactions in the body [48]. It also participates in blood metabolism, bones and teeth development. There is more to vanadium than the benefits mentioned above. It's believed to play a significant role in the transfer of blood sugar (glucose) to the muscles [47–49]. Apart from its blood sugar lowering effect, it is also seen to increase the sensitivity of muscles to insulin [50–52]. Thus, if you have type 2 diabetes and insulin resistance is responsible for your condition, vanadium sulfate can be a prescribed treatment [51,53]. Since vanadium can increase adsorption of sugar in the muscles, it can store more energy within the muscles [54]. This means the body will not have as much as glucose to store as fat. As a result, it can increase muscles mass, vascularity and blood flow for a time [8,55]. Vanadium has been regarded to cure much disease. However, it has been found to be toxic at higher concentrations [53]. The toxicity of vanadium blocks the reactivity of essential functional groups of biomolecules, and disrupts the integrity of bio membranes [56,57]. Above the tolerance levels vanadium causes poisoning cancer, brain damage and kidney failure. It also participates in DNA damaging, blocking of protein as well as oxidation of lipids which is a preliminary step in the development of cardiovascular disease [40]. Selenium on the other hands is an essential trace element, and its low status in humans has been linked to increased risk of various diseases [58]. In recent years, selenium research has attracted tremendous interest because of its important role in antioxidant selenoprotein for protection against oxidation stress initiated by excess reactive oxygen species. Selenocysteine is recognized as the 21st amino acid and it forms a predominant residue of selenoprotein and selenoenzymes in biological tissues [59]. During protein synthesis, the selenocysteine residue is cotranslationally inserted and encoded by the UGA codon, which is associated with a terminal codon. The molecular structure of selenocysteine is an analogue of Cysteine where a sulphur atom is replaced by selenium. Selenoenzymes have strong antioxidant activity which plays a significant role in protecting cells against oxidative damage from reactive oxygen species (ROS) [60]. However, an increased ROS production can exert oxidative stress in physiological system. If the excess is not regulated they can cause damage to

cellular lipids, proteins and DNA [30]. This damage is linked to various human disease including heart disease, and atherogenesis [56,60]. Therefore it is imperative to having a system implemented that can address issues such as, improved health care. The current studies focus on the new development of biological sensors and chemical sensor for the detection and monitoring of selenium and vanadium in aqueous solution and selected real sample to improved methods for health hazards recognition.

Recently hydrogels have attracted particular attention in the novel and most intensively developing field of polymers with sensor-actuator functions [35,61]. The sensitivity of hydrogels to a large number of physical factors like temperature, electrical voltage, pH concentration and salt concentration make them promising materials for a broad range of applications as microsensors [62]. However, most hydrogels still suffer from a number of limitations such as low tensile strength which limit their use in load-bearing applications and result in the premature dissolution or flow away of the hydrogel for a targeted purpose. Therefore it is essential to identify new hydrogel composites with the appropriate physical and chemical properties that will be used in the design of biological sensor for vanadium and selenium detection. This brings us to the aim and main objectives of this studies as elaborated below:

4. AIMS :

- I. Development of chemical hydrogel sensors for vanadium and selenium remediation from waste water
- II. Development and characterization of the impregnated gold functionalized with hydrogel biosensor for detection of vanadium and immunosensor for the detection of selenium.
- III. The study of the metabolism of selected vanadium and selenium complexes to evaluate kinetic behaviour and reaction mechanism.

- IV. Application of the biological sensors to real samples such as commercialise centrum multivitamins.

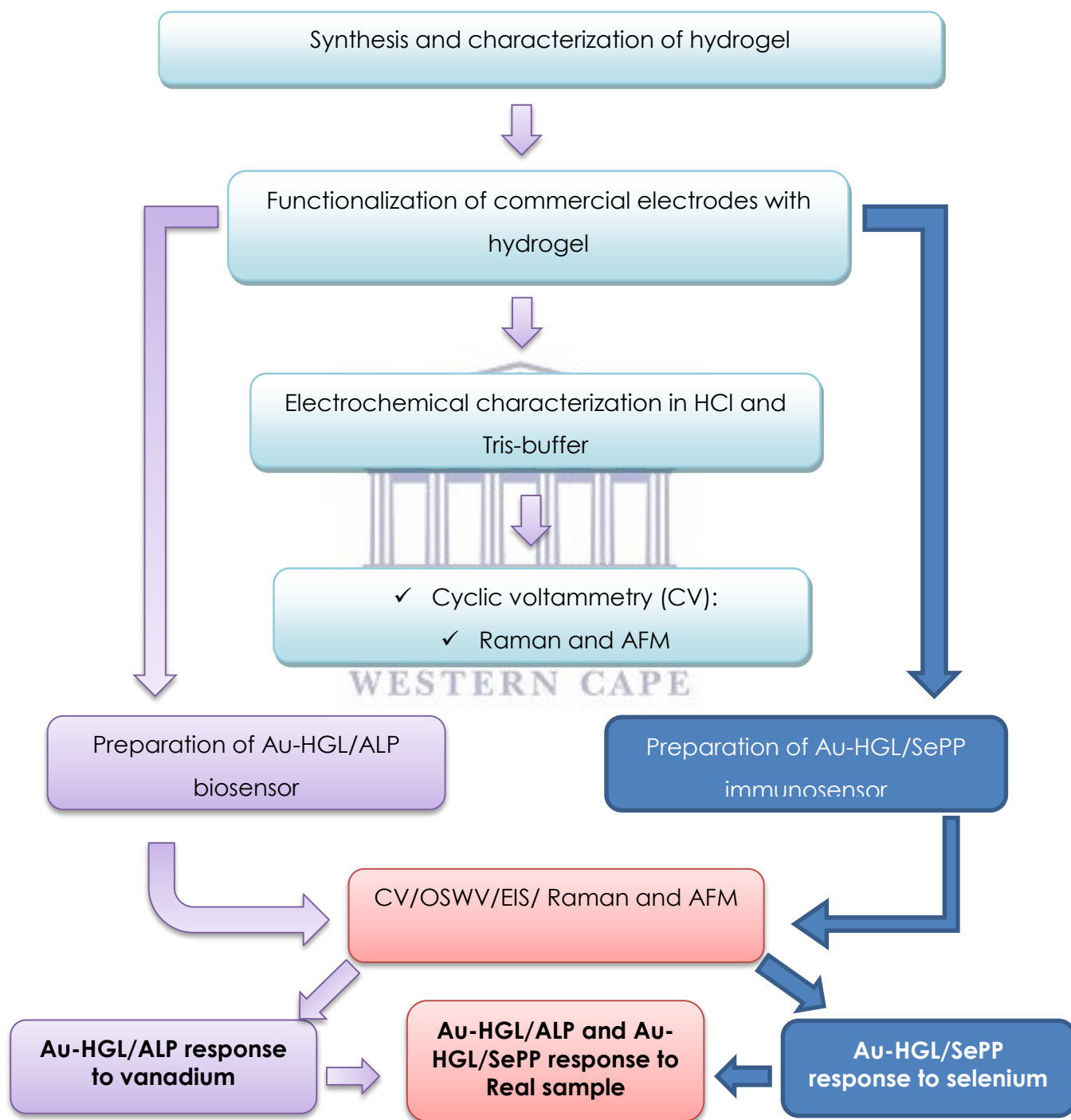
The proposed biosensor and immunosensor development will find applications in quality control and daily uses due to their fast recognition and efficiency. The biosensors reactivity will be modelled using electrochemical impedance spectroscopy (EIS), amperometry or direct potentiometry and cyclic voltammetry techniques.

5. OBJECTIVES

- Investigation of polysulfone hydrogel sensory properties for remediation of heavy metal of biological significant such as vanadium and selenium in environment waste water.
- Development of hydrogel encapsulated biosensors for the detection of vanadium and selenium based on the analytical signal.
- Functionalization of hydrogel onto a gold electrode based on the electrochemical deposition.
- Immobilization of alkaline phosphatase enzyme at gold functionalized hydrogel interface for vanadium recognition
- Immobilization of selenoprotein p antibody at gold functionalized with hydrogel interface for selenium recognition.

6. CONCEPTUAL DIAGRAM

In line with the study objectives and experiment programmed



7. OUTLINE OF THE THESIS

The aims and objectives of the research may be divided into the following chapters, which provide pertinent details of vanadium and selenium at immobilized and mobilized hydrogel interface. As well as biological recognitions of vanadium and selenium at hydrogel interface after immobilization with alkaline phosphatase and selenoprotein P antibody respectively.

Chapter 1

This chapter gives a brief introduction of the project and general introduction to problem identification associated with heavy metals. As well as illustrate the project proposal, objectives of the project and expected outcome followed by methodology to be applied are presented. Also introduced hydrogels general structure, properties and application.

Chapter 2

In this chapter, a critical review on environmental remediation of heavy metal ions from aqueous solution using hydrogel as an adsorbent are discussed. The short come of existing methods and what can be done in order to enhance the performance of the adsorbent in term of adsorption capacity are also being specified. This section has been published in the journal of water science and technology. A brief description and general information regarding the metals of choice such as vanadium and selenium is elaborated. Furthermore provides some information on the heath benefit and problem associated to vanadium and selenium based on the world health organization (WHO) protocols.

Chapter 3

This chapter gives a synopsis on the various analytical techniques used and detailed of the research methodology are elaborated. General experimental procedures for the chemical and electrochemical preparation of the material are explained. Follow by characterization and application of the developed polysulfone hydrogel for recognition of biological significant free radicals.

Chapter 4

This chapter deals with synthesis and characterization of polysulfone-hydrogel. Physical properties were interrogated using techniques such as FTIR, SEM, AFM and swelling. Whereas, electrochemical properties of the material was also investigated using CV and OSWV. The electron diffusion and ionic transport properties of the hydrogels as immobilized thin films in aqueous solutions were evaluated by CV. Aspects of sensory properties of polysulfone hydrogel for electro-analytical profiling of vanadium and selenium in aqueous solutions has been published in the Journal of Nano Research.

Chapter 5

In this chapter we demonstrate the use of Raman spectroscopy has emerged as a useful tool for sensor and biosensor characterization. Characterization was based on the principle of surface-enhanced Raman spectroscopy (SERS), a technique for molecular fingerprinting. Here we have used Raman spectroscopy for the characterization of the various stages of biosensors development.

Chapter 6

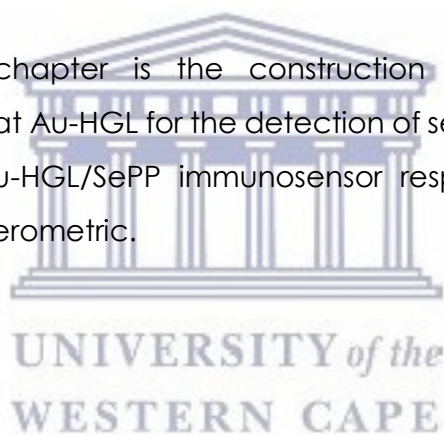
This chapter provides the electrochemical approach such as voltammetry, amperometry and electrochemical impedance spectroscopy on the construction Au-HGL/ALP biological sensor for the detection of vanadium based on the alkaline phosphatases inhibition protocol. Here we capture major results and application of ALP electrochemical biosensor to vanadium and selected real sample, also its performance in terms of kinetic and metabolism.

Chapter 7

The approach in this chapter is the construction of immunosensor using selenoprotein p antibody at Au-HGL for the detection of selenium. Here we present the first results of The Au-HGL/SePP immunosensor response to selenium using voltammogram and amperometric.

Chapter 8

This chapter provide the main conclusion of the entire thesis based on the performances of both biosensor and immunosensor constructed on alkaline phosphatase and selenoprotein p antibody and recommendations for future work are elaborated.



Chapter 2

Literature review

Abstract

This chapter, introduced a critical review on environmental remediation of heavy metal ions from aqueous solution using hydrogel as an adsorbent. The short come of existing methods and what can be done in order to enhance the performance of the absorbent in term of adsorption capacity are specified. A brief description and general information regarding the metals of choice such as vanadium and selenium are elaborated. Furthermore provides some information on heath benefit and problem associated with vanadium and selenium according to world health organization (WHO) protocols. This section of my work was published in the journal of water science and technology as reference below.

UNIVERSITY of the
WESTERN CAPE

Muya, F.N, .E Sunday, P. Baker* and E. Iwuoha, Environmental remediation of heavy metal ions from aqueous solution using hydrogel as adsorbent: Critical review. Journal of water science and technology 2016, 73 (5) 983-992; DOI: 10.2166/wst.2015.567

2. INTRODUCTION

Heavy metal ions from industrial waste water such as Cd^{2+} , Pb^{2+} , Cu^{2+} , Mg^{2+} , Hg^{2+} , etc. constitute a major cause of pollution for ground water sources. The toxicity of these ions to mankind and aquatic life causes many health problem. Therefore they should be removed from wastewater before disposal. Various treatment technologies such as adsorption, precipitation and coagulation have been applied to remediate the potential toxic elements from aqueous mediums [63–65]. However most of these methods are facing some challenges in terms of effectiveness,

applicability and cost. In the light of these challenges, recently adsorption methods have been recognized as an alternative method that can remove effectively heavy metals at very low concentration (1-100 mg/L). Numerous adsorbents have been reported in the literature for this purpose. However very few researches focused on the application of hydrogel as an effective adsorbent for heavy metal removal in aqueous solutions. This review section provides information from the last four to five years up to date on the various applications of hydrogel and its composites in removing heavy metal ions from aqueous solutions at micro and nano-scale.

Industrialization has remarkably increased the level of heavy metal pollution of ground water in the last two decades. This has caused serious environmental problems owing to their level of toxicity to various life forms. Despite the fact that it's believed nature could handle hazardous substances. However, millions of different pollutants have been introduced into the atmosphere and the aquatic ecosystem per annum by industrial processes [66].

Heavy metals found in wastewaters are harmful to the environment and their effects on biological systems are very severe. The toxicity of metals such as cadmium, vanadium and lead above the tolerance levels causes cancer [67], brain damage, kidney failure, DNA damaging [56], blocking of protein as well as oxidation of lipids which is a preliminary step in the development of cardiovascular diseases [28,30,68]. Heavy metals ions have the tendency to form complexes with biological matter. Some heavy metals ions are essential to many organisms but very toxic above certain concentration. These elements, along with amino and fatty acids and vitamins are required for normal biochemical processes such as respiration, biosynthesis and metabolism [69].

The efficient removal of these toxic metal ions is a very difficult task due to the high cost of treatment methods. In recent years, research interest has increased in terms of the production of low-cost alternatives. Microbe-based technologies can provide an alternative to the conventional methods for removal of these metals ions since

they are important in biological systems and in the environment at regulated concentrations. Environmental monitoring agencies have set permissible limits for heavy metals levels in drinking water due to their harmful effects. The removal and tepid decontamination of these heavy metal ions (Cd^{2+} , Pb^{2+} , Cu^{2+} , Mg^{2+} and Hg^{2+}) is very important for the environmental remediation.

Various processes have been employed in the removal of heavy metals from waste water includes chemical precipitation, coagulation, solvent extraction, membrane separation, ion exchange and adsorption. However, the common use of ion exchange and reverse osmosis is restricted by the high operating cost. As an alternative to chemical precipitation, membrane filtration or ion exchange and adsorption processes with wide variety of adsorbents have been used such as hydrogels [70]

2.1. GENERAL OVERVIEW

Adsorption processes are widely used by various researchers for the removal of heavy metals from waste streams, and activated carbon has been frequently used as an adsorbent as well. It is used extensively in water and wastewater treatment industries despite its high cost. In recent years, the need for safe and economical methods for the elimination of heavy metals from contaminated waters has necessitated research interest toward the production of low cost alternatives such as agriculture waste, polymeric material, hydrogels and commercially available activated carbon.

Agricultural and industrial by-products such as rice husk, wheat bran, wheat husk, saw dust of various plants, bark of the trees, ground-nut shells, coconut shells, black gram husk, hazelnut shells, walnut shells, cotton seed hulls, waste tea leaves, Cassia fistula leaves, maize corn cob, sugar-cane bagasse, apple, banana, orange peels, soybean hulls, grapes stalks, water hyacinth, sugar beet pulp, sunflower stalks,

coffee beans, Arjun nuts, cotton stalks etc. have been used for the elimination of heavy metals from wastewater after some physical or chemical modification [29]. Agricultural waste materials constitutes significant source of metal biosorption. The functional groups present in agricultural waste biomass viz acetamido, alcoholic, carbonyl, phenolic, amido, amino, and sulfhydryl groups have affinity for heavy metal ions and can form metal complexes or chelates [29-30].

2.2. MECHANISM OF BIO-SORPTION

The mechanism of biosorption process includes chemisorption, complexation, adsorption on surface, diffusion through pores and ion exchange. Conventional techniques have their inherent limitations such as less efficiency, sensitive operating conditions, production of secondary sludge and high cost of disposal [31]. The aforementioned adsorption of heavy metals by activated carbon is a powerful technology and has been applied mostly in treating domestic and industrial waste water. However the high cost of activated carbon and loss of the adsorbent during the regeneration process restricts its application. Since 1990's the adsorption of heavy metal ions by low cost renewable organic materials has gained popularity [32-33]. The utilization of sea weeds, moulds, yeasts, and other dead microbial biomass and agricultural waste materials for removal of heavy metals has been explored [34]. Recently attention has been diverted towards biomaterial which comes mostly as byproducts of large scale industrial operations. The major advantages of biosorption over conventional treatment methods include: low cost, high efficiency, minimization of chemical or biological sludge, no additional nutrient requirement, regeneration of bio sorbents, and possibility of metal recovery [36-37].

Agricultural materials particularly those containing cellulose shows potential metal biosorption capacity. The basic components of the agricultural waste materials biomass include hemicellulose, lignin, extractives, lipids, proteins, simple sugars, water hydrocarbons, starch containing variety of functional groups that facilitates

metal complexation which helps for the sequestering of heavy metals [38-40]. Most agricultural waste materials are environmental-friendly due to their unique chemical compositions, great abundance, low in cost and they are efficient option for heavy metal remediation. The removal of metal ions from aqueous streams using agricultural materials is based upon metal biosorption [71]. The process of biosorption involves a solid phase (sorbent) and a liquid phase (solvent) containing the dissolved species that will be adsorbed. Due to high affinity of the sorbent for the metal ion species, the latter is attracted and bound by complex process which is affected by several mechanisms involving chemisorptions, complexation, adsorption on surface and pores, ion exchange, chelation, adsorption by physical forces, entrapment in inter and intra-fibrillar capillaries, and spaces of the structural polysaccharides network as a result of the concentration gradient and diffusion through cell wall and membrane [72]. Functional groups present in biomass molecules such as (acetamido groups, carbonyl, phenolic, structural polysaccharides, amido, amino, sulfhydryl carboxyl groups, alcohols and esters) have the affinity for cadmium, copper and lead detection within a limit range of 150-350 mg/L [53]. Some bio sorbents are non-selective and bind to a wide range of heavy metals with no specific priority, whereas others are specific for certain types of metals depending on their chemical composition. The complexation of various functional groups with heavy metal ions (Cd^{2+} , Pb^{2+} , Cu^{2+} , Mg^{2+} and Hg^{2+}) during biosorption process has been reported by different research workers using spectroscopic techniques [1]. The processes of biosorption can be optimized to enhance the regeneration of the bio sorbents and recovery of heavy metal ions. Most of the optimizations are performed in the batch process; this allows the design of continuous flow systems for industrial remediation applications (Figure 2.1).

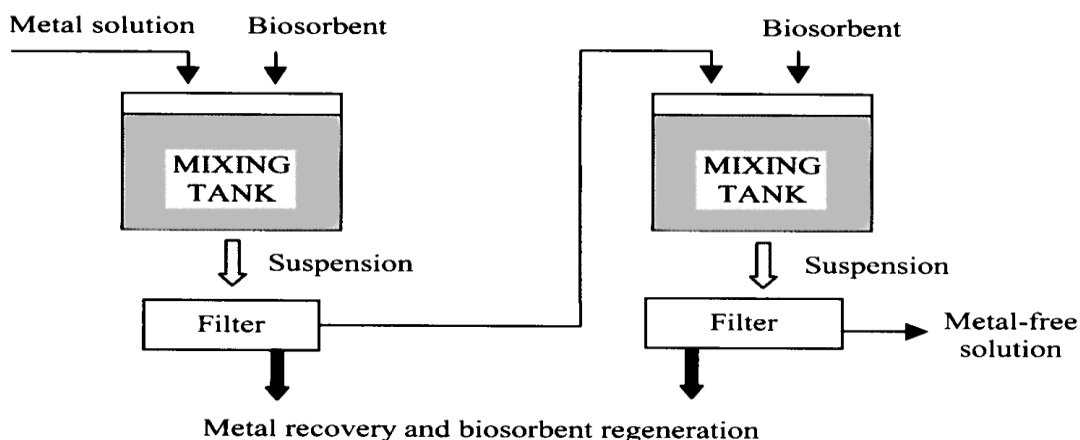


Figure 2.1: Two stage bio-sorption diagram

2.3. HYDROGELS AS ADSORBENTS

Hydrogels are three dimensional networks of crosslinked polymers which are able to swell rapidly and retain large volumes of water in their swollen structure (Figure 2.2). They are usually made of hydrophilic polymers molecules which are crosslinked either by chemical bonding or other cohesion forces such as ionic interaction, hydrogen bonding or hydrophobic interaction [10,42,73,74]. They are also used in the preparation of molecular recognition interfaces for biosensor [42,73]. Various hydrogels have been employed in biosynthesis processes and adsorbents such as cellulose graft acrylic acid (C-g-AA), chitosa hydrogel with 2, 5-dimercapto-1, 3, 4-thiodiazole (CTS-DMTD), PVA-Hydrogel biomass of penicillium cyclopium and starch graft acrylic acid/montmorillonite (S-g-AA/MMT) [35,75–77].

PVA-Hydrogel synthesis was achieved by precipitation of aqueous solution of PVA out of absolute ethanol [78]. Glutaraldehyde was used as cross linking agent to PVA polymer and HCl as catalyst. The hydrogel was further immobilized with *P. cyclopium* by dispersing a pre-weighed amount of wet biomass in the PVA aqueous solution prior to the precipitation. Hydrogels adsorptive capacities and absorption kinetics are influenced by many factors like metal concentration [79],

pH of the solution [80–82] composition of the absorbent [83–85] and contact time [55]. pH is an important parameter that affects hydrogel performance by influencing its swelling and metal ion chelation on chelating adsorbents. For selective adsorption, besides the use of a specific ligand modified sorbent, selectivity could be achieved by adjusting the pH to different values, and maximum adsorption is achieved at pH range 4-6 [12,86]. However pH control is the most important parameter for the selective adsorption of metal ions. pH 5.0 was found to be the optimal condition for Cd(II) and Pb(II) in controlled laboratory work [86]. The sorption of Cd (II) and Pb (II) ions by hydrogel was found to be minimal at pH 2. The minimum adsorption observed at low pH was due to higher mobility of H⁺ ions present favoring the preferential adsorption of hydrogen ions compared to metals ions (Cd²⁺, Pb²⁺, Cu²⁺, and Mg²⁺). At lower pH value, the surface of the adsorbent is surrounded by hydronium ions (H⁺), thereby preventing the metal ions from approaching the binding sites of the sorbent. This means that at higher H⁺ concentration, the bio sorbent surface becomes more positively charged such that the attraction between biomass and metal cations is reduced. In contrast, as the pH increases, more negatively charged surface becomes available thus facilitating greater metal removal. It is commonly agreed that the sorption of metal cations increases with increasing pH as the metal ionic species become less stable in the solution [39,87–89]

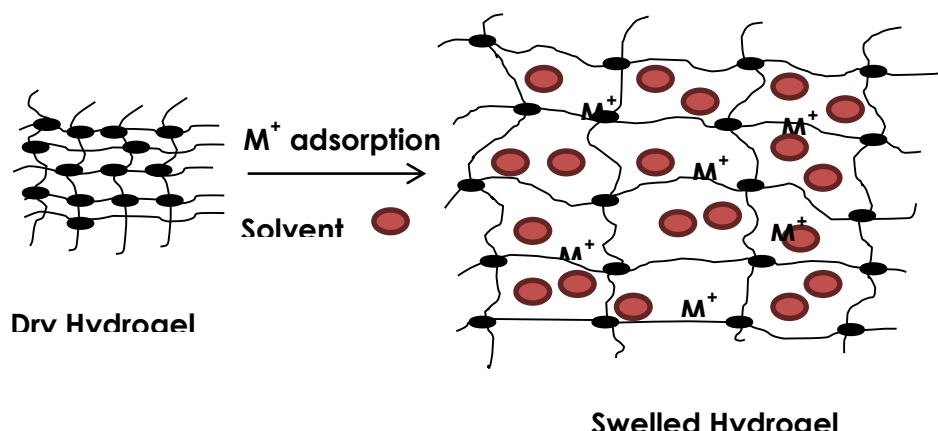


Figure 2.2: Hydrogel adsorption mechanism

2.4. FACTORS AFFECTING ADSORPTION

Effect of adsorbate solution pH

The pH of the metal ions strongly affects the adsorption properties of hydrogels as discussed [90]. At $\text{pH} > 6$, precipitations of hydroxides may occur simultaneously depending on the metals and its oxidation state, and may not lead to accurate interpretation of adsorption. However at low $\text{pH} \leq 3$ condition, the main effective adsorption sites of the hydrogel; namely the alcoholic and carboxyl groups; are both easily protonated leading to the reduction of the adsorptive activity. At higher pH conditions, the protonated functional groups may be deprotonated resulting in higher adsorption activity [78].

Effect of contact time and adsorption kinetics

The time for treatment is an important factor in metal uptake and thus, the effect of immersion time on the metal uptake of different metal ions was investigated. It could be observed that the increase in immersion duration is accompanied by an increase in metal ion adsorption and this reached its maximum value after 180 minutes of soaking, and then levels up [76]. The results of many research revealed that at the initial immersion time the metal ions adsorption is fast and it became slower near the equilibrium. Such behavior occurs due to the fact that during the initial stage, a large number of vacant active sites were available for adsorption after that repulsion occurred between the adsorbate molecules on the adsorbent surface which slows down the adsorption process [78]. Therefore it is imperative to consider positively in future research the times and monitor the adsorption during times intervals in order to maximize the adsorptions and detection of specific metals.

Effect of initial concentration and adsorption isotherms

Metal ions concentration has an effect on the adsorption capacity. It could be observed that as the initial concentration increased, the adsorption capacities also increased but the rate of increase becomes slow after the concentration reached 150 mg/L for Zn^{2+} , Co^{2+} and Mn^{2+} [91,92] This indicates that there were few empty adsorption sites on the adsorbents and suggests that the adsorption almost reached equilibrium. The initial concentration provided the driving force needed to overcome the resistance due to the mass transfer of metal ions between adsorbed and adsorbate. Therefore if the initial concentration is high, the driving force will also be high; consequently the adsorption capacity will be high. The adsorption capacity of hydrogels are based on adsorption isotherm and the kinetics of adsorption and typically modeled as first and secondary order kinetic models.

For this studies Langmuir equation is a fairly good fit to the adsorption isotherms of Pb^{2+} and Cd^{2+} ions on the hydrogels. The maximum adsorption capacity found for Pb^{2+} and Cd^{2+} ions by using Langmuir equation were in mg/g [93]. Therefore more research should be conducted on the same hydrogel to improve selectivity, sensitivity and enhance the detection of these metal ions at microgram per liter if not nano-gram per liter. Conversely the kinetics of the adsorption data was calculated using kinetic models to understand the dynamic of the adsorption process in terms of the order and rate constant of Pb (II) into hydrogel beads. These models were pseudo- first-order and pseudo-second-order models [83,86,93–95]. Adsorption models predicts the rate at which adsorption takes place for a given system and it is probably the most important factor in adsorption system design, with adsorbate residence time and the reactor dimensions controlled by the system's kinetics. The sorption isotherms represent the relationship between the amount adsorbed by a unit weight of solid sorbent and the amount of solute remaining in the solution at equilibrium [94]. Langmuir and Freundlich isotherm models are frequently used isotherm models for describing short- term and mono component adsorption of metal ions. The reaction orders based on the capacity of the adsorbents have also been studied, such as Lagergren's first-order equation, Redlich

Peterson model and BET model. However, Langmuir and Freundlich isotherm models have shown to be suitable for describing short-term and mono component adsorption of metal ions by different bio sorbents. The adsorption kinetic data were described by the Lagergren pseudo-first-order model, which is the earliest known equation describing the adsorption rate based on the adsorption capacity. The adsorption isotherm data were evaluated by means of the Langmuir and Freundlich adsorption models. The two models are expressed by the following equations:

$$\frac{C_e}{q_e} = \frac{1}{bq_m} + \frac{C_e}{q_m} \quad (\text{Eq 2.1})$$

$$q_e = kfCe^{1/n} \quad (\text{Eq 2.2})$$

In the above equations q_m (mg/g) is a representative of monolayer maximum uptake of metal ions and b (L/mg) is the Langmuir adsorption constant and is related to the free energy of adsorption. K_f (mg/g) (L/mg)^{1/n} and n , are the Freundlich adsorption constants indicative of the adsorption extent and adsorption intensity respectively. Based on these equations, the slope and intercepts of C_e/q_e versus C_e are used to determine q_m and b , and in the same way K_f and n can be obtained from the plot of $(\ln q_e)$ versus $(\ln C_e)$ [72,96].

Selected kinetics parameters for metal adsorption (cadmium, lead and copper) by common adsorbent materials have been extracted for comparison (Table 2.1). The performances of the hydrogel adsorbents have been extracted to highlight the sorption parameters (Figure 2.3). Alginate beads and chitosan nano-fibrils showed high adsorption capacity of Cd, Pd and Cu at pH 5 respectively (Table 2.1). Maximum adsorption was observed due to the fact that, at that pH the biomass becomes preferentially protonated and releases the reduced metal cations, which adsorb onto the alginate beads, resulting in improved metal removal. PAA hydrogels and PEGAMA Vin hydrogel showed very poor adsorptive capacity. The mobility of H⁺ ions present favored the preferential adsorption of hydrogels ions

compared to metals ions, and the surface of the adsorbent is surrounded by hydronium ions (H^+), thereby preventing the metal ions from approaching the binding sites of the sorbent and resulting in poor adsorptions (Figure 2.3). Alginate beads showed the highest sorption capacity of cadmium and lead respectively (182 and 165 mg/g). Chitosan indicated the second highest sorption for cadmium (140 mg/g), lowest for lead (61 mg/g) and highest for copper (169 mg/g), whereby PAA hydrogel adsorbed only lead with a maximum sorption of (113 mg/g), and PEGAMA Vin hydrogel displayed significant adsorption of cadmium (71 mg/g) and lead (118 mg/g). Based on the information provided (Figure 2.3), chitosan performed as the best adsorbent based on its sensitivity and selectivity toward a wide range of metal ions (Cd, Pd and Cu) compared to other adsorbents, in particular PAA hydrogel which was only capable of detecting lead.

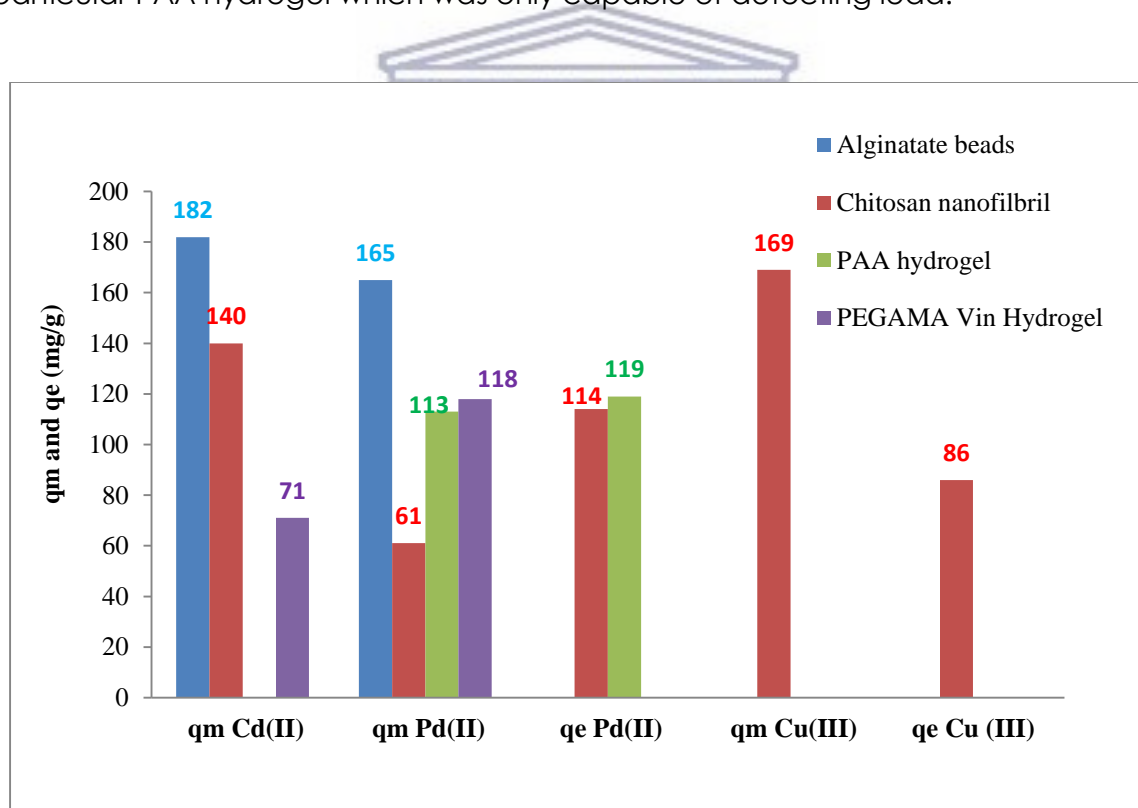


Figure 2.3: Comparison of kinetics parameters (q_m and q_e) of different metals ions and adsorbents

The adsorption capacity of hydrogels is based on isotherms and the kinetics of adsorption which predict the rate at which adsorption takes place for a given system. The data derived from comparing the different hydrogels showed that their reactions were mostly pseudo-first order kinetics. Chitosan nanofilbril, PEGAMA Vin hydrogel and alginate beads exhibited high pseudo first order rate constant for cadmium and lead respectively, whereas PAA hydrogel only showed a high value for lead (Figure 2.4). In contrast chitosan and alginate beads showed highest rate of adsorption for all four metals evaluated.

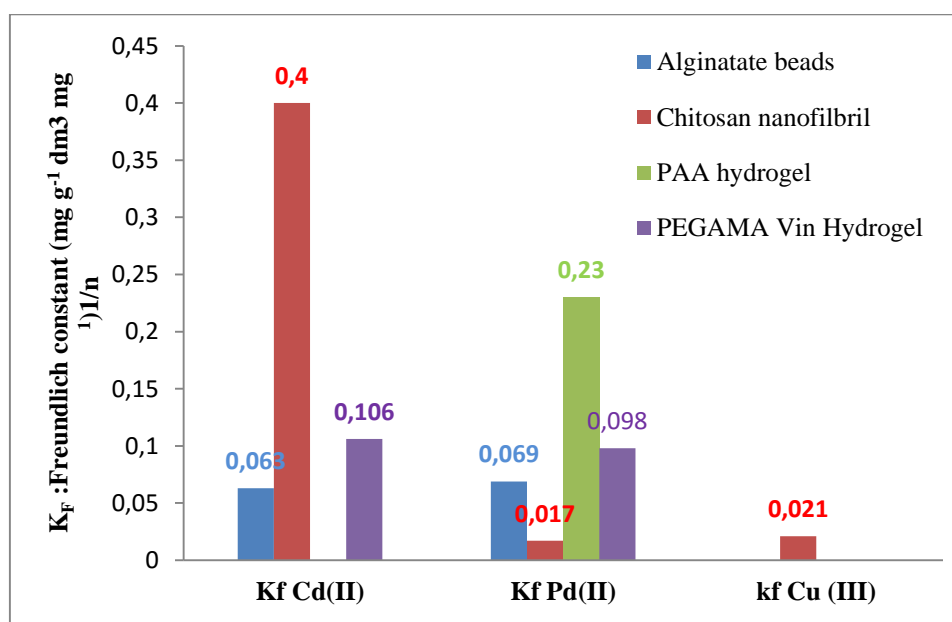


Figure 2.4: Comparison of kinetics parameters (K_f) of different metals ions and adsorbent

Table 2.1: Coefficient of pseudo-first and second order kinetics models

Adsorbent	Pseudo-first order kinetics					Pseudo- second order kinetics			
	Metal ions	Adsorption capacity (mg/g)	K_f (l/g)	q_e	R^2	K_s	η	R^2	Referenc es
Alginate beads	Cd^{2+}	182	0.063	---	0.898	8.07	2.97	0.992	[85]
	Pb^{2+}	165	0.069	---	0.910	6.55	3.65	0.994	
AMPS/PVAcCopoly mer hydrogel	Ni^{2+}	230	1.064	---	0.995	0.013	4.94	0.986	[97]
	Mn^{2+}	160	0.719	---	0.996	0.011	4.99	0.989	
Chitosan Nano fibril	Cd^{2+}	140	0.400	---	0.990	0.008	6.14	0.994	[98]
	Cu^{3+}	169	0.021	86	0.970	0.0008	0.41	0.999	
	Pb^{2+}	61	0.017	114	0.986	0.0001	0.44	0.995	
PVA/AAc hydrogel	Zn^{2+}	388	0.017	415	0.942	1,76	2.40	0.991	[99]
	Co^{2+}	245	0.015	278	0.960	5.17	2.03	0.998	
	Mn^{2+}	152	0.03	145	0/948	8.11	1.42	0.997	
PAA hydrogel	Pb^{2+}	113	0.23	119	1.000	51.85	6.32	0.857	[90]
PVA	Cu^{2+}	14	0.049	---	0.99	4.298	0.43	0.95	[100]
	Cd^{2+}	71	0.106		0.99	24	5.25	0.93	[101]

Adsorbent	Pseudo-first order kinetics					Pseudo- second order kinetics			References
	Metal ions	Adsorption capacity (mg/g)	K_f (l/g)	q_e	R^2	K_s	η	R^2	
Poly(EGDMA-VIM) hydrogel	Pb ²⁺	118	0.098		0.99	38	5.19	0.96	
	Hg ²⁺	172	0.070		0.99	43	4.17	0.90	



Table 2.2: Summary Table of metal ions concentrations dependence based on pH, adsorbent time and concentration

Pseudo-first and second order kinetics						
Adsorbent	Metal ions	Metal concentration	pH	Kinetic model	Adsorption capacity (mg/g)	references
PVA/AAc	Cu ²⁺	300 mg/l	4.5	K_s	13	[82]
Poly(EGDMA-VIM) hydrogel	Cd ²⁺	300 mg/l	3-5	K_s	69	[66]
	Pb ²⁺	300 mg/l	3-5	K_s	112	
	Hg ²⁺	300 mg/l	3-5	K_s	162	

Pseudo-first and second order kinetics						
Adsorbent	Metal ions	Metal concentration	pH	Kinetic model	Adsorption capacity (mg/g)	references
Alginate beads	Cd ²⁺	200-300 mg/l	6.5	K _s	182	[85]
	Pd ²⁺	100 mg/l	6.0	K _s	165	
AMPS/PVAcCopolymer hydrogel	Ni ²⁺	200 mg/l	6.5	K _s	230	[1]
	Mn ²⁺	350 mg/l	5.5	K _s	160	
PAA hydrogel	Pb ²⁺	150 mg/l	6.5	K _s	113	[90]
Chitosan Nano fibril	Cd ²⁺	300 mg/l	6.0	K _s	140	[98]
	Cu ³⁺	250 mg/l	5.5	K _s	169	
	Pb ²⁺	200 mg/l	6.7	K _s	61	

WESTERN CAPE

2.5. ELECTROCHEMICAL DETECTION OF METALS

Electrochemical hydrogel sensors are relatively not reported for the detection of metal ions and has found its way into commercial products and advanced integrated sensing systems. A steady effort has been made on the development of efficient and easy-use electrochemical sensors. Hydrogel sensors for heavy metals, with rapid and highly sensitive detection capabilities are in great demand in many areas of science. Developing hydrogel sensors for detecting lower concentration of heavy metal ions becomes very significant due to the ability the encapsulate and released properties. Electrochemical devices with accuracy and sensitivity have already been developed for certain applications. The detection of low concentration of toxic heavy metal ions in environment water is essential because of its lethal effects on the environment and living organisms. To date only few researcher have reported on hydrogel sensor for detection of heavy metal including; hydrogel sensor for metal oxide [35], PVA hydrogel sensor for heavy metal cations, P(MBTVBC-co-VIM)- coated QCM [80], P(NIPAM-co-BCAm) hydrogels [102]. However most of them couldn't detect heavy metals at lower level (μg and ng) except PVA hydrogel which detect Nickel at a range of (0.1- 0.214 $\text{nM}/\mu\text{M}$).

Maximum concentration for toxic heavy metals and precious metals in drinking water have established by World health organization and environmental protection agency (EPA). A permissible concentration of toxic heavy metals such as Ar, Cr, Cu and Pb is 5-20 $\mu\text{g}/\text{L}$ as well as 0.1 $\mu\text{g}/\text{L}$ for Hg. 500 $\mu\text{g}/\text{L}$ was assigned to precious metals (Zn, Mn) at their secondary oxidation states [103]. The use of hydrogels in heavy metal remediation showed better performance than precipitation methods, activated carbon, and agricultural waste and offers promising application prospects. To date research has focused mainly on specific metals including, copper, lead, silver, cadmium, nickel, chromium, gold and mercury. Other transition metals with high toxicity or transition metals which are known disease markers have not been as widely addressed. Vanadium and selenium have been identified as

carcinogenic agents that disrupt cellular metabolic processes at higher dosage 200 µg/L in drinking water. Evidence from literature indicates that exposure to selenium could induce neuro-mental effects on fetuses, infants and children development as well as development of diabetes type II [13]. These metals block the reactivity of essential functional groups of biomolecules and disrupt the integrity of bio-membranes. There is also a need to investigate the simultaneous removal of many co-existing pollutants in waste water. It is preferable to develop a multipurpose adsorbent which can remove different kinds of pollutants at micro and nano scale. To achieve these aims, new materials and methods are required that utilize our understanding of parameters which affects adsorption of heavy metal ions including pH, analyte concentration, contact time and adsorbent functional group. Hydrogels are a promising group of materials due to their compatibility with aqueous phase and future work should involve functionalization of hydrogel materials for selective and sensitive metal remediation as well as sensitive analytical methods for ultra-low concentration evaluation. Electrochemical methods for metal quantification and speciation have emerged as a promising tool for evaluation of a wide range of metal ion species. The success of electrochemical detection of nickel, lead, copper, mercury and cadmium has been established using chemical sensors (hydrogel sensor) with results possible in the µg/mL range [104]. Therefore combining the electrochemical methods with the removal efficiency of stimuli responsive hydrogel materials could produce highly efficient water treatment solutions in particular for metal remediation.

In conclusion a wide range of treatment technologies have been developed for heavy metal removal from wastewater. Agricultural waste and hydrogels are relatively new processes that have shown significant contribution for the removal of these contaminants from aqueous effluents. Hydrogel has also find a typical application in soft gel tablets and contact lenses [105–107]. However, it is evident from the literature that agricultural waste, activated carbon and hydrogel adsorbents do not adequately remove heavy metals at micro and nano scale. Even though hydrogels have shown improved adsorption efficiency they still suffer from a

number of limitations, such as low tensile strength. This limit their use in load-bearing applications and result in the premature dissolution or flow away from the hydrogel for a targeted purpose and hence low sorption capacity. Therefore it is essential to identify new hydrogel composites with the appropriate physical and chemical properties capable of comprehensive metal species adsorption from aqueous media. The advantages offered by electrochemical control of hydrogel sorption, shows great promise with respect to detections of a wide range of transition metal species at very low concentration.

Heavy metals are defined as metals of a density higher than 5 g/Cm³. They occur as pure elements, as ions and complexes. Heavy metals were brought into the environment by human activities. Additionally, heavy metals are released to the ecosystem with the exponential growth of metal mining, the following processes and their industrial use. They show a large tendency to form complexes, especially with nitrogen, sulphur and oxygen containing ligands of biological matter [108]. Toxicological effects can be explained by this interaction. As a result, changes in the molecular structure of proteins, breaking of hydrogen bonds or inhibition of enzymes can appear. Acute poisoning is rarely observed and usually the result of suicide attempts or accidents. Chronic toxicity is much more relevant and caused by repeated exposure over long periods of time. Mutagenic, carcinogenic or teratogenic effects have been described for some heavy metals [109]. Vanadium and selenium are important metals in biological systems and in the environment. Human cells contain metal ions that are "tied" up in proteins forming metal complexes such as selenoprotein or vanadyl cysteine complex. Selenoprotein are antioxidants used to prevent cellular cell damaging from chelatable or free radicals, and free radicals are by product of oxygen metabolism that contribute to the development of chronicle disease i.e. immune deficiency, cancer and heart disease. These trace elements can also be found in small quantities, and can have more negative impact on our bodies. Therefore these two elements have been found as potential elements of interest for future research.

2.6. VANADIUM

Vanadium is among transition metal that occurs naturally. It is extensively distributed in the earth at a concentration of 100 mg/kg. It also found in about 65 different minerals [45]. The color of Vanadium depends on its form; Vanadium can be a gray-white metal or light gray or white lustrous powder. Pure Vanadium is a bright white, soft, and ductile metal. [48]



Figure 2.5: Vanadium image

Large amounts of vanadium ions are found in a few organisms, possibly as a toxin. The toxicity of vanadium is associated with their oxidation states, the oxide and some other salts of vanadium have moderate toxicity [28,41,48]. Particularly in the ocean, vanadium is used by some life forms as an active center of enzymes, such as the vanadium bromo-peroxidase of some ocean algae. Vanadium is probably a micronutrient in mammals, including humans, but its precise role in this regard is unknown [54]. Vanadium's chemistry is defined by four adjacent oxidation states 2-5. In aqueous solution, it easily forms metal aqua complexes, and the colors are lilac $[V(H_2O)_6]^{2+}$, green $[V(H_2O)_6]^{3+}$, blue $[VO(H_2O)_5]^{2+}$, yellow VO_3^- and they can be classified as reducing or oxidizing agent depending on the nature of the compounds. [45].



From left: $[\text{V}(\text{H}_2\text{O})_6]^{+2}$ (lilac), $[\text{V}(\text{H}_2\text{O})_6]^{+3}$ (green), $[\text{VO}(\text{H}_2\text{O})_5]^{+2}$ (blue) and $[\text{VO}(\text{H}_2\text{O})_5]^{+3}$ (yellow).

Vanadium (IV) compounds often exist as vanadyl derivatives which contain the VO^{2+} center. Ammonium vanadate (V) (NH_4VO_3) can be successively reduced with elemental zinc to obtain the different colors of vanadium in these four oxidation states. Lower oxidation states occur in compounds such as $\text{V}(\text{CO})_6$, $[\text{V}(\text{CO})_6]^-$ and substituted derivatives. Vanadium is mostly commercialized as vanadium pentoxide. It is used as a catalyst for the production of sulfuric acid [110]. Vanadium compounds are found in different form depending on its occurrence and usage, including vanadium metal (V), vanadium pentoxide (V_2O_5), Vanadyl sulfate (VOSO_4) and sodium metavanadate (NaVO_3)

Vanadium metal (V)

Vanadium metal is frequently used in steel production, with approximately 80% of vanadium going into ferro-vanadium. It is also used for the production of rust resistant, spring and high speed tool steels. It is an important carbide stabilizer in making steels [43,48].



Figure 2.6: Vanadium in steels production

Vanadium pentoxide (V_2O_5) and vanadyl sulfate ($VOSO_4$)

Vanadium (V) oxide is well known as vanadium pentoxide; it is a brown or yellow solid closely to deep orange in aqueous. It is used in ceramics and as a catalyst as well as in the production of superconductive magnets [22,43] . Vanadyl sulfate and sodium metavanadate have been used in dietary supplements.



Figure 2.7: Vanadium pentoxide



Figure 2.8: Vanadium sulfate

Health benefits of vanadium

Humans are not exposed to vanadium only via environmental or anthropogenic sources but also from dietary supplementation. Vanadium is available in certain foods and sold as dietary supplement. Although it's thought that humans may need small quantities of vanadium for certain biological functions, scientists have not confirmed whether it should be considered an essential nutrient. In some medical articles vanadium supplements are touted as a natural remedy for a number of health conditions, including anemia, diabetes, cancer, bones health, heart disease, high blood pressure, high cholesterol and obesity [43,45,46,48]. In addition, vanadium have been identify as a treatment for hangovers, enhance exercise performance, and prevent cancer. Although research on health effect of vanadium is limited and dated, there's some evidence that vanadium may offer certain health benefits [28].

Diabetes

Vanadium is potentially beneficial in controlling blood-sugar levels in diabetes patients [46,108,111]. Research suggests that vanadate may help improve the body's metabolism of blood sugar (also known as glucose)[46,108,111]. Studies indicate that vanadium compounds and vanadate may promote the movement of glucose into cells. To date, few clinical trials have tested the use of vanadium in treatment of diabetes. However, one of the few human-based studies found that vanadyl sulfate had some beneficial effects on patients with type 2 diabetes [53]. After six weeks of treatment with vanadyl sulfate, the patients showed improvements in glucose metabolism and cholesterol levels [46,108,111]. Still, vanadyl sulfate did not appear to help regulate blood sugar levels.

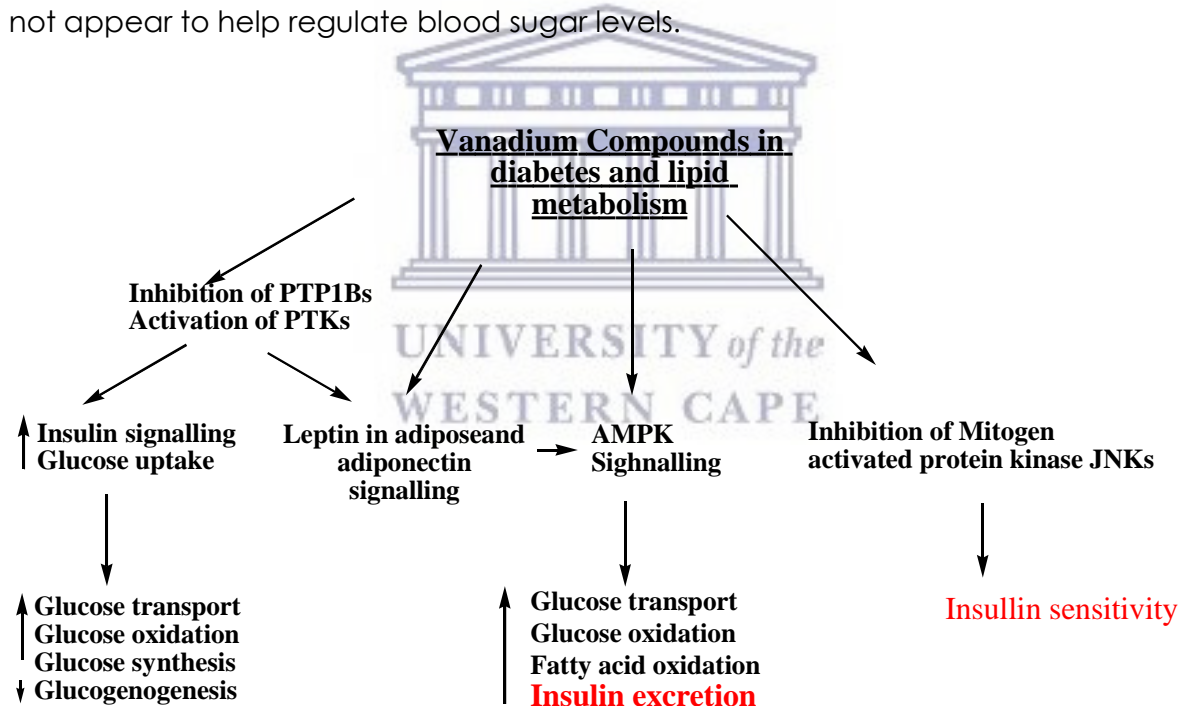


Figure 2.9: Essential anti-diabetic effect of vanadium compounds [112].

Abbreviations: PTP - protein tyrosine phosphorylase;

PTP-ase - protein tyrosine phosphatase; JNKs-c - Jun N-terminal protein kinases;

AMPK - AMP-activated protein kinase; PPAR γ -peroxisome proliferator-activated receptor gamma.

Cancer

According to a 2002 report published in Critical Reviews in Oncology/Hematology Vanadium shows promising result for cancer treatment [49,55]. Studies on human cells demonstrate that Vanadium may help promote apoptosis [49]. There's also some evidence that Vanadium may help suppress the growth of cancerous tumors [49,55]. To date there is a lack of clinical trials on Vanadium's effectiveness against cancer; therefore it's too soon to recommend Vanadium for cancer treatment (or cancer prevention).

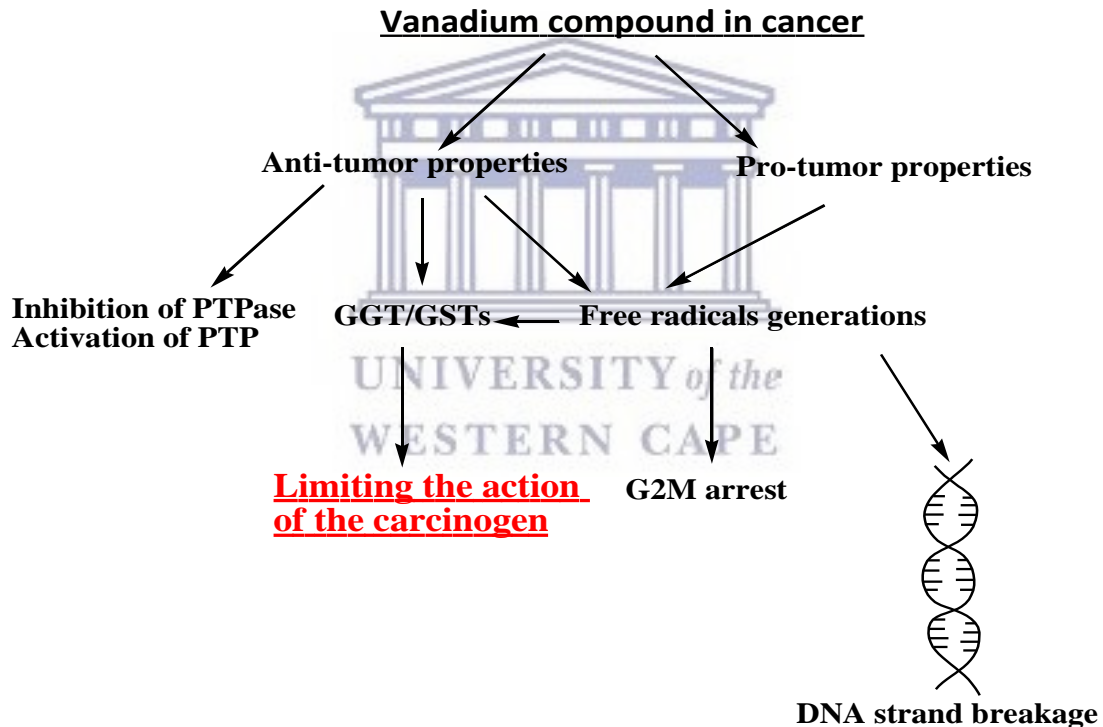


Figure 2.10: Anti- and pro-tumor actions of vanadium compounds [55,113].

Abbreviations: PTP - protein tyrosine phosphorylase; PTP-ase - protein tyrosine phosphatase; GGT-gamma-glutamylotransferase; GST-glutathione S-transferase.

Bone Health

Vanadium compounds were tested on animal and human cells and the results indicated that vanadium promoted osteogenesis (a process in which bone-forming cells lay down new bone material) [47]. However, no clinical evidence on the uses of vanadium compounds for the prevention and the treatment of bone disorders.

2.7. Selenium

Selenium is a transition metal found in group 4 of the periodic table and naturally occurs in two forms i.e. inorganic (selenate and selenite) and organic (selenomethionine and selenocysteine) [58]. Both forms can be good dietary sources of selenium [59]. Soils contain inorganic selenites and selenates that plants accumulate and convert to organic forms, mostly selenocysteine and selenomethionine and their methylated derivatives.



Figure 2.11: Selenium salt

Selenium plays a critical roles in reproduction of thyroid hormone metabolism, DNA synthesis, and protection from oxidative damage and infection [30,114]. Selenium as antioxidant partakes in chemical reactions that stop free radicals from damaging cells. Free radicals are unstable molecules from environmental toxins, or byproducts from human body's metabolism. Antioxidant supplements, including selenium, are

often advertised to help prevent to heart disease, cancer and vision loss [13]. The level of selenium drop with age, it's claimed that selenium can slow the aging process, cognitive decline and dementia. It can also slow the progression of HIV [115]. However, low selenium levels are also implicated in depression, male infertility, weak immune systems and thyroid problems. Selenium supplements are mostly used by asthmatic patient, which help to reduce the risk of rheumatoid arthritis and cardiovascular disease [15].

Selenium supplements for cancer

Evidence from various studies found that people eating selenium enriched food have a lower risk of some cancers, specifically bladder cancer, prostate cancer, lung cancer and some gastrointestinal cancers [30]. Regions with selenium-rich soil tend to have lower death rates from cancer compared to regions with low-selenium soil, particularly for lung, esophagus, bladder, breast, colon, rectum, pancreas, ovary and cervical cancer [9]. But these trends do not prove selenium is an underlying factor in cancer survival.

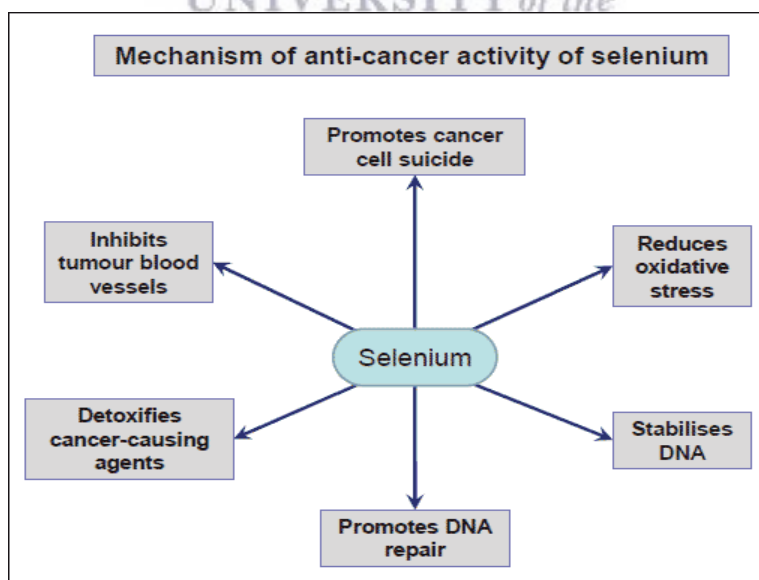


Figure 2.12: Mechanism of anti-cancer activity of selenium

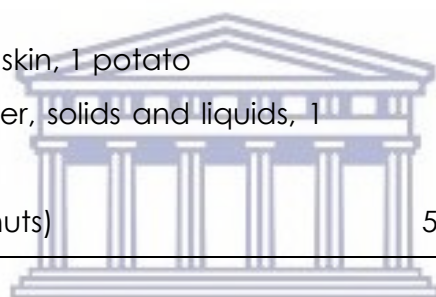
2.8. RECOMMENDED INTAKES

Table 3.1 lists the current RDAs for selenium in μg . For infants from birth to 12 months, the Food and Nutrition Board (FNB) established an upper limit for selenium that is equivalent to the mean intake of selenium in healthy, breastfed infants [9].

Table 2.3: Summary of most source of selenium [59].

Food	Micrograms (μg) per serving	Percent DV*
Brazil nuts, 1 ounce (6–8 nuts)	544	777
Tuna, yellowfin, cooked, dry heat, 3 ounces	92	131
Halibut, cooked, dry heat, 3 ounces	47	67
Sardines, canned in oil, drained solids with bone, 3 ounces	45	64
Ham, roasted, 3 ounces	42	60
Shrimp, canned, 3 ounces	40	57
Macaroni, enriched, cooked, 1 cup	37	53
Beef steak, bottom round, roasted, 3 ounces	33	47
Turkey, boneless, roasted, 3 ounces	31	44
Beef liver, pan fried, 3 ounces	28	40
Chicken, light meat, roasted, 3 ounces	22	31
Cottage cheese, 1% milkfat, 1 cup	20	29
Rice, brown, long-grain, cooked, 1 cup	19	27
Beef, ground, 25% fat, broiled, 3 ounces	18	26
Egg, hard-boiled, 1 large	15	21
Puffed wheat ready-to-eat cereal, fortified, 1 cup	15	21
Bread, whole-wheat, 1 slice	13	19
Baked beans, canned, plain or vegetarian, 1 cup	13	19

Oatmeal, regular and quick, unenriched, cooked with water, 1 cup	13	19
Spinach, frozen, boiled, 1 cup	11	16
Milk, 1% fat, 1 cup	8	11
Yogurt, plain, low fat, 1 cup	8	11
Lentils, boiled, 1 cup	6	9
Bread, white, 1 slice	6	9
Spaghetti sauce, marinara, 1 cup	4	6
Cashew nuts, dry roasted, 1 ounce	3	4
Corn flakes, 1 cup	2	3
Green peas, frozen, boiled, 1 cup	2	3
Bananas, sliced, 1 cup	2	3
Potato, baked, flesh and skin, 1 potato	1	1
Peaches, canned in water, solids and liquids, 1 cup	1	1
Brazil nuts, 1 ounce (6–8 nuts)	544	777



UNIVERSITY of the
WESTERN CAPE

Table 2.4: Tolerable upper intake levels (ULs) for selenium[9]

Age	Male	Female	Pregnancy	Lactation
Birth to 6 months	45 µg	45 µg		
7–12 months	60 µg	60 µg		
1–3 years	90 µg	90 µg		
4–8 years	150 µg	150 µg		
9–13 years	280 µg	280 µg		
14–18 years	400 µg	400 µg	400 µg	400 µg
19+ years	400 µg	400 µg	400 µg	

2.9. CHEMICAL SENSORS

Today, electrochemical sensors are tightly integrated and hyphenated with sampling, fluidic handling, separation and other detection principles [116]. This device consists of a transducer, which transforms the response into a detectable signal, and a chemically selective layer, which isolates the response of the analyte from its immediate environment. They are classified according to the property that is being determined such as; electrical (biosensor, immunosensor), optical, mass or thermal properties and are designed to detect and respond to an analyte in the gaseous, liquid or solid state. Compared to optical, mass and thermal sensors, electrochemical sensors are highly attractive because of their remarkable detection capability, experimental simplicity and low cost. Therefore in the current work we will be focusing on the electrochemical (biosensor and immunosensor)[116,117].

Biosensor/immunosensor are analytical devices, used for the detection of biological analyte. Therefore it is impossible to talk about biosensor without bio-recognition component such as enzymes and antibodies. These recognition component are also called bioreceptors, uses biomolecules from organisms or receptors modeled after biological systems to interact with the analyte of interest. This interaction is measured by the biotransducer which outputs a measurable signal proportional to the presence of the target analyte in the sample. The biological component used in the current work based on their compatibility with respect to the analyte was alkaline phosphatases and selenoprotein p antibodies.

Alkaline phosphatases

Alkaline Phosphatases (ALP) can be classified as a group of enzymes found primarily in the liver (isoenzyme ALP-1) and bone (isoenzyme ALP-2). They can also be defined as a small amounts of enzymes produced by cells lining the intestines (isoenzyme ALP-3), the placenta, and the kidney (in the proximal convoluted tubules)[118,119]. These enzymes are measured in the blood as the total amount of alkaline phosphatases released from these tissues into the blood[118]. The optimum working condition of these enzymes are best at an alkaline pH (a pH of 10), and thus the enzyme itself is inactive in the blood. Alkaline phosphatases act by splitting off phosphorus (an acidic mineral) creating an alkaline pH[119,120]. The choice of ALP bio-recognition element in this biosensor is its ability to catalyze reactions, and the potential detection of the analyte by controlling its catalytic activity. Notably, since enzymes are not consumed in reactions, the biosensor can easily be used continuously. The catalytic activity of enzymes also allows lower limits of detection compared to common binding techniques. However, the sensor's lifetime would be limited by the stability of the alkaline phosphatase (ALP).



Figure 2.13: *Ribbon diagram (rainbow-color, N-terminus = blue, C-terminus = red) of the 3D structure of bacterial alkaline phosphatase.*

Selenoprotein P antibody

Selenoprotein P antibody is commonly known as eukaryotic selenoprotein that contained numerous selenocysteine residues [121]. It was also identified as a secreted glycoprotein, often found in the plasma. The chain of this protein contains two main functional groups or terminal N and C. The N-terminal domain is larger than the C-terminal and the N-terminal is believed to be glycosylated. The N-terminal domain is used for conservation of selenium in the body and appears to supply selenium to the kidney. The C-terminal participates in the transport and storage of selenium in the body. Selenoprotein P (SePP) was found to be unique due to the fact that it contains multiple selenocysteine residues which can be used for the transportation of selenium [121–123].



Figure 2.14: Rainbow-color of the 3D structure of Selenoprotein p antibody.

Chapter 3

Materials and Methodology

This chapter gives a synopsis of the different analytical techniques employed, in this work. The research methodology and general experimental procedures for the chemical and electrochemical experiments, are presented. Aspects of the hydrogel synthesis, characterization and sensory properties of polysulfone hydrogel for electro-analytical profiling of vanadium and selenium in aqueous solutions has been peer reviewed and published in the Journal of Surface Engineering and Journal of Nano Research respectively.

F. N. Muya, L. Phelane, P. G. L. Baker, and E. I. Iwuoha, "Synthesis and Characterization of Polysulfone Hydrogels," J. Surf. Eng. Mater. Adv. Technol., vol. 4, no. 4, pp. 227–236, Jun. 2014.

F. N. Muya, X. T. Ngema, P. G. L. Baker, E. I. I. "Sensory Properties of Polysulfone Hydrogel for Electro-Analytical Profiling of vanadium and selenium in Aqueous Solutions," J. Nano Res., vol. 44, pp. 142–157, 2016

3. REAGENTS

All chemicals used were of analytical grade and purchased from Sigma Aldrich. Purified water from a Millipore Mill Q system was used in the preparation of all solutions. Analytical grade Argon gas was used to purge the system. Polysulfone (Sigma Aldrich, 182443) was purchased as beads. The vanadium was purchased as the yellow powder of vanadium pentoxide (Sigma Aldrich, 223794, 98% purity) and selenium as the white salt of selenium dioxide (Sigma Aldrich, 200107, 98% purity).

3.1. PREPARATION OF SOLUTION AND HYDROGEL SYNTHESIS

Vanadium powder and selenium salt have good solubility in water i.e. 8 g/L and 38.4g/100 mL respectively. The commercial vanadium and selenium powders were dissolved in deionized water to yield a concentration of 0.01 M in each case and was sonicated subsequently, for one hour to produce homogeneous solutions.

Polysulfone hydrogel (PSF/HGL) was synthesized by dissolving 0,442g of polysulfone beads in 50 mL of N,N-dimethyl acetamide (DMAC). The solution was sonicated for 1 hour to produce 0.05 M PSF solution. 5 mL of 0.05 M of PSF solution was transferred to a round bottom flask, followed by the addition of 2,590g of PVA powder. To this reflux mixture, 1 mL glutaraldehyde cross-linker was added, followed by 1 mL of 2 M HCl as catalyst. The mixture was allowed to stand for 3 hours at 75°C with constant stirring using a magnetic stirring bar. After three hours, the mixture was stored at room temperature for 10 days in order for the cross-linking to reach completion [33]. The synthesized polysulfone material (hydrogel) was characterized by electrochemical methods, spectroscopy and morphology. The PSF/HGL was also used to prepare hydrogel electrodes.

UNIVERSITY of the
WESTERN CAPE

3.2. ANALYTICAL TECHNIQUES USED FOR THIS STUDIES

Various electro-analytical techniques were used in this study namely, cyclic voltammetry (CV), Osteryoung square wave voltammetry (OSWV), and electrochemical impedance spectroscopy (EIS). Spectroscopic techniques such as ultra violet-visible spectroscopy (UV-vis), Raman spectroscopy as well as scanning electron microscopy (SEM) and atomic force microscopy (AFM) were used for morphological evaluation of hydrogel materials.

3.2.1 Electrochemical techniques

Cyclic voltammetry technique (CV)

In cyclic voltammetry (CV), a potential is applied to the system, and the Faradaic current response resulting from a redox reaction, is measured. The potential is cycled between a pre-determined potential window from an initial potential, E_i , to a final (switching) potential, E_f , at a constant scan rate (from 1-2000 mV/s). By varying the potential limits, the reactivity of the electrochemical system is probed over a large range of potentials in a single sweep. Also by varying the sweep rate, the kinetics of the reactions or mass transfer processes may be evaluated [124]. The cycling may be done two ways oxidatively (increasing positive potential) or reductively (decreasing negative potential) [124,125]. When the potential is scanned in a positive direction, the electroactive species at the surface of the electrode are oxidized and if it is scanned in the negative direction, they are reduced. The oxidation/reduction generates a current response that is proportional to the concentration of depleted of species at the electrode surface.

The plot of the applied potential vs. the resulting current produces a voltammogram with characteristic peak potentials for both oxidation ($E_{p,a}$) and reduction ($E_{p,c}$). This characteristic feature of the voltammograms provides information about the redox (formal) potential of a system denoted as E° [126]. The formal reduction potential (E°) for a reversible or quasi-reversible couple is at the mid-point of $E_{p,a}$ and $E_{p,c}$ on the voltammograms and it is commonly determined from equation 3.1 [124–126]

$$E^{\circ} = (E_{p,a} + E_{p,c}) / 2 \quad \text{Equation 3.1}$$

From cyclic voltammetry analysis, important parameters can be obtained such as peak potential (E_{pc} , E_{pa}), and peak current (I_{pc} , I_{pa}) of the cathodic and anodic peaks. These peaks provide information about the type of system (reversible,

irreversible or quasi-reversible), electron movement, mass transfer and diffusion coefficient. The number of electrons transferred (n) can be determined from the separation between $E_{p,a}$ and $E_{p,c}$ using equation 3.2

$$\Delta E_p = (E_{p,a} - E_{p,c}) = 0.059 / n \quad \text{Equation 3.2}$$

Cyclic voltammetry can also provide information about the rate of electron transfer between the electrode and the analyte, and the stability of the analyte in the electrolyzed oxidation states (e.g., do they undergo any chemical reactions). For a thin layer of adsorbed electro active material at the electrode surface undergoing Nernstian reaction, the plot of peak current versus scan rate for both cathodic and anodic peaks respectively show linear dependence. This is in accordance with Brown-Anson model, from which the surface concentration of the various redox states could be estimated. [124–126]

$$I_p = n^2 F^2 \Gamma^* A v / 4RT \quad \text{Equation 3.3}$$

I_p = Peak current for either the oxidation or reduction peak being considered

n = Number of electrons transferred

F = Faraday constant (96584 C mol⁻¹)

Γ^* = Surface concentration of the electroactive film bound to the working electrode

A = Surface area

v = Scan rate (Vs⁻¹)

R = Gas constant (8.314Jmol⁻¹K⁻¹)

T = Temperature of the system (K).

By varying the scan rates (Vs⁻¹) of the process, the diffusion coefficient, D_e (which tells how rapidly the electroactive species is diffusing through the solution to and from the surface of the working electrode) can be calculated using the Randles-Sevcik equation [125]

$$I_p = 2.686 \times 10^5 n^{3/2} A \Gamma^* D^{1/2} v^{1/2} \quad \text{Equation 3.4}$$

A plot of I_p versus $v^{1/2}$ should give a straight line from which D_e can be evaluated. For a reversible system, the values of I_{pa} and I_{pc} should be identical for a simple reversible (fast) couple. However, the ratio of the peak currents can be significantly influenced by chemical reactions coupled to the electrode process [124–126].

In this work CV was used to understand the electrochemical properties of the hydrogel electrodes. From the peak current response we could derive information about the type of system, electron mobility, surface concentration and mass transfer. The formal potential and peak separation of vanadium and selenium in solution was determined at hydrogel electrodes.

Osteryoung square wave spectroscopy (OSWV)

The technique involves the application of square wave modulation to a constant or nearly constant DC potential, and the current generated is sampled at the end of successive half cycles of the square wave. Three currents are generated, viz: forward current, the reverse current from the reverse pulse (i_r) and that for the net current (I_d) vs. the potential on the corresponding staircase tread [127]. The net current is larger than that for the forward and reverse current since it is the difference between the two [124]. The net current is used for analytical evaluation because any residual charging current has been subtracted. Figure 3.1 shows the OSWV containing the forward, reverse and reverse currents. The peak height is directly proportional to the concentration of the electroactive species and direct detection limits as low as 1×10^{-8} M is possible compared to 5×10^{-8} M with differential pulse voltammetry and 1×10^{-5} M with cyclic voltammetry [126][127].

OSWV has many advantages over other differential techniques such as faster scan times, excellent sensitivity, the rejection of background current, high signal to noise ratio and applicability to a wide range of electrode materials and systems. Osteryoung square wave voltammetry plays a very important role in the

characterization of electroactive species with poor, overlapping or ill-formed redox signals in cyclic voltammetry by producing individual, sharp peaks [127].

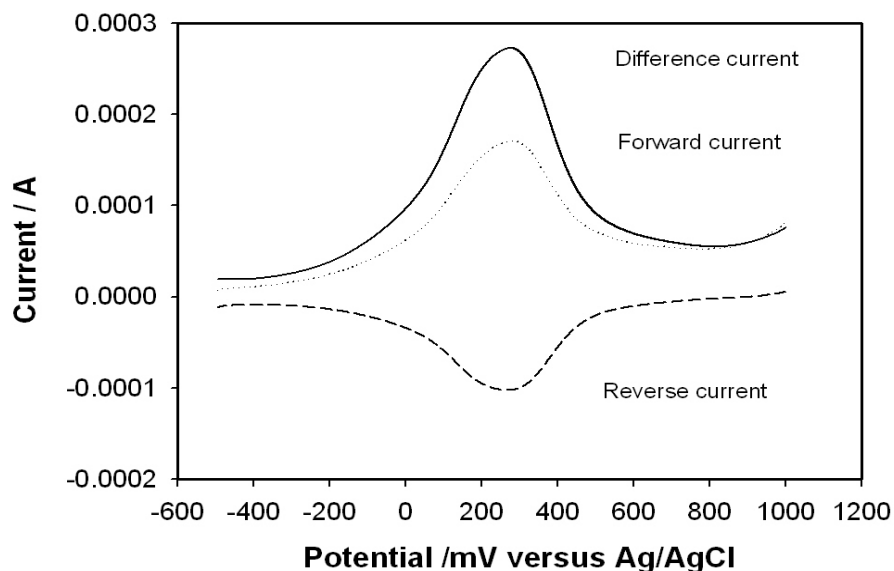


Figure 3.1: Typical OSWV for film containing the forward, reverse and reverse currents.

The hydrogel material has been characterized to have multiple redox peaks. OSWV was used to determine formal potential for hydrogel material as well as formal potential associated with vanadium and selenium redox chemistry at hydrogel electrode. OSWV was also employed in the evaluation of alkaline phosphatase (ALP) biosensor and selenoprotein (SePP) immunosensor electrochemical response to the analyte species in solution.

Electrochemical impedance spectroscopy

The term impedance is a measure of the ability of a circuit to resist the flow of an alternating current (AC). It is analogous to resistance (R) used in direct current (DC), which is defined by Ohm's law (equation 3.6) as the ratio between voltage (E) and current (I) [128].

$$R = E/I$$

Equation 3.5

In impedance a small perturbing potential is applied across a cell that changes in a sinusoidal manner and generates a current resulting from the over potential (η) which is caused by the small displacement of the potential from the equilibrium value. The induced current alternates because the voltage changes in a cyclic manner, and hence the term alternating current (AC). A small amplitude (5–10 mV) AC wave form superimposed on the DC potential in the electrochemical cell (EC) to generate a response to the applied perturbation, which can differ in phase and amplitude from the applied signal. This response is measured in terms of the AC impedance or the complex impedance, Z , of the system. The complex impedance permits analysis of electrode process in relation to diffusion, kinetics, double layer and coupled homogeneous reactions. [128].

The ratio of the applied voltage (E) over measured current (I) is the impedance of the system ($Z = E/I$). Since an AC potential is applied to the cell, there will probably be a phase shift by an angle (ϕ) between the applied AC potential waveform and the AC current response. Therefore, the impedance can be represented using a vector diagram (Figure 3.3) displaying the in-phase and out-of-phase impedances, the total impedance, and the phase angle (ϕ).

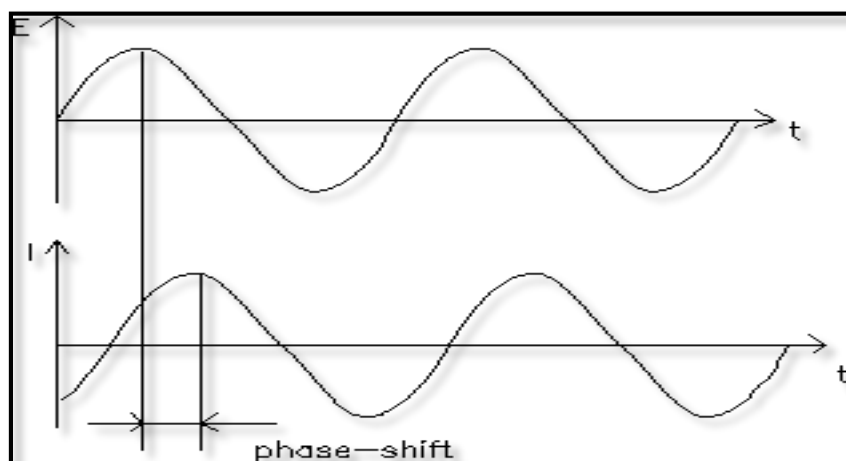


Figure 3.3: Sinusoidal current response to potential perturbation as a function of time.

The data collected from impedance experiments may be presented as Nyquist or Bode plot. In Nyquist we plot Z' versus Z'' , over a wide frequency range (normally 100 kHz to 0.1 Hz) and in Bode plot the logarithm of the absolute value of Z' and the phase (ϕ) are plotted against the logarithm of the frequency (f) [128]. Impedance data is usually evaluated by fitting it to an equivalent circuit model. The frequently used circuit, is the Randles equivalent circuit which represents solution resistance, double layer capacitance and transfer resistance of a typical EC cell.

Electrochemical Impedance may contain several time constants, but often only a portion of one of their semicircles is seen. The shape varies depending on dominant electrochemical processes taking place.

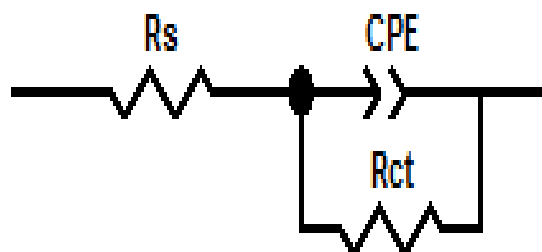


Figure 3.4: Randles equivalent circuit

Electrical circuit elements

Solution resistance (R_s): Can be defined as the resistance between the working electrode and the reference electrode. This is indicated by a small change in the real impedance axis. It is measured at high frequency intercept near the origin of the Nyquist plot. The resistance of an ionic solution depends on the ionic concentration and type of ions the electrolyte is made up, temperature and the geometry of the area in which current is carried.

Charge transfer resistance (R_{ct})

R_{ct} is a measure of the resistance to electron transfer at the electrode interface. It is deduced from the kinetically controlled electrochemical reaction at low overpotentials. The charge transfer resistance is estimated from the diameter of the semicircular region on the real impedance axis of the Nyquist plot. When the chemical system is kinetically sluggish, the R_{ct} will be very large and may display a limited frequency region where mass transfer is a significant factor. However, if the system is so kinetically facile the semicircular region is well formed [128].

Warburg Impedance

Warburg resistance is associated with the diffusion of ions across the electrode/electrolyte interface. This impedance is associated with the difficulty of mass transport of electroactive species [128]. Layers of ions at the electrode interface behave like an RC element (i.e. a resistor and a capacitor in parallel) and this produces infinite sum of RC elements called the Warburg impedance. It is characterized as a linear portion at an angle of 45° and slope of unity on the Nyquist plot and a slope of -0.5 on the Bode plot [128].

Capacitor (C)

The capacitance (C) is the ability of an electrochemical system to store or retain charge. An electrical double layer exists on the interface between any electrode and its surrounding electrolyte. This double layer is formed as ions from the solution adhere onto the electrode surface. The potential at the terminals of this double layer (capacitor) is proportional to its charge.

Often, a CPE is used to model non-homogeneity of a system. The non-homogeneity may arise from irregular surface coating or physico-chemical imbalances at the electrodes interface. During circuit fitting, the CPE is defined by two values, i.e., the capacitance, C, and the CPE exponent, α , which has a value between 0.5 and 1 for a non-ideal capacitor. If α equals 1, the equation is identical to that of a capacitor and smaller values can be related to surface roughness and inhomogeneities, which lead to frequency dispersion.

Impedance spectra are often modeled using an electrical circuit which produces a similar spectrum as that from the experimental data. The electrical components (resistors, capacitors, inductors, etc.) and some 'components' that have no electrical analogue (constant phase elements, Warburg impedances, etc.) are then matched to physical characteristics of the measured cell. In this work, EIS was used for characterization of hydrogel electrode, and detection of vanadium at ALP biosensor.

3.2.2. Spectroscopic techniques

Raman spectroscopy

The Raman scattering is a spectroscopic technique used to measure the vibrational molecular derivatives from an inelastic light scattering process[129]. With Raman spectroscopy, a laser photon is scattered by a sample molecule and loses (or gains) energy during the process. The amount of energy lost is considered to be a change in energy (wavelength) of the irradiating photon. The loss of energy is characteristic of a particular bond in the molecule. Raman spectroscopy is similar to FT-IR spectroscopy, however there are a distinct number of advantages when using Raman than FTIR [129,130]. Raman can be used to analyze aqueous solutions since it does not suffer from the large water absorption effects found with FTIR techniques. The intensity of spectral features in solution is directly proportional to the concentration of the particular species. Raman spectra are generally robust to temperature changes. It also requires little or no sample preparation. It does not need the use of Nujol, or KBr matrices and is largely unaffected sample cell materials such as glass. The use of a Raman microscope such as the LabRAM provides very high level of spatial resolution and depth discrimination, not found with the FTIR methods of analysis

These advantages and its highly specific nature, has made Raman a very powerful tool for analysis and chemical monitoring [130,131]. Depending upon instrumentation, it is a technique which can be used for the analysis of solids, liquids and solutions and can even provide information on physical characteristics such as crystalline phase and orientation, polymorphic forms, and intrinsic stress. Raman spectroscopy was used throughout the construction of the biosensors and will be presented as separate chapter to highlight the surface future such as surface modification.

Fourier transformer infrared spectroscopy (FTIR)

The term Fourier Transform Infrared Spectroscopic (FTIR) refers to a development in the manner in which the data is collected and converted from an interference pattern to a spectrum. The expected functional group stretching vibrations for the starting materials and synthesis product have been identified from literature [132–134]. FTIR was used to confirm chemical crosslinking of the hydrogel by comparing to starting material and product spectra.

Ultra-violet-visible spectroscopy

UV/Vis is a spectroscopic technique that involves the spectroscopy of photons in the UV/visible region. It uses light visible and adjacent (ultraviolet (UV) and near infrared (NIR) ranges) [135]. UV-visible spectroscopy monitors the intensity of color of a material and the wavelength of absorption simultaneously. The monitored color is the wavelength at maximum absorption (λ_{max}). In some cases more than one color might be present, therefore the absorption peak will be associated with energy of transitions within the molecule [135,136].

The absorption spectrum provides information about conjugation within molecules and energy transitions due to excitation by UV light. UV/Vis is widely used in the quantitative determination of solutions of transition metal ions and highly conjugated compounds. For a material that absorbs UV-visible light, we can monitor its concentration using Beer- Lambert relationship. UV/Vis analysis was used to evaluate oxidation state of vanadium and selenium, also to verify the enzymatic activity of ALP.

3.2.3. Morphological techniques

These techniques involve the use of microscopes to visualize the area of an object at micro and nano range which cannot be seen with the naked eye. There are three well-known branches of microscopy: optical, electron, and scanning probe microscopy. However in this work we will be focusing on SEM and AFM which were used for characterization of hydrogel after synthesis.

Scanning electron microscopy

Scanning electron microscopy (SEM) can be classified as a microscope imaging technique used to study surface morphology, topography of material composition when coupled to EDS. The study can be performed by scanning the sample to be analyzed with a high-energy beam of electron in raster scan pattern[137]. SEM analysis requires a conductive platform for generation of electrons that will interact with atom for signal generation. The signal being generated by SEM is based on the collection of back scattered electrons, characteristic of X-rays, light, transmitted electrons or secondary electron[138,139].

In SEM analysis, the electron beam is thermionically emitted from electron gun fitted with a metal filament cathode (tungsten). Once the first electromagnetic wave interacts with the sample the electrons lose energy by continual random scattering and absorption among a teardrop-shaped volume of the specimen. The energy exchange between the electromagnetic wave and the sample ends up in the reflection of high-energy electrons by elastic scattering. Emission of secondary electrons is detected by specialized detectors. The energy-dispersive x-ray spectroscopy (EDS or EDX) was coupled to Zeiss Auriga for elementary analysis and morphological characterization. The hydrogel sample was prepared by drop coating 10 μ L at screen printed carbon electrode (SPCE). The hydrogel electrode was further coated with gold to enhance the signal for viewing. The coating was necessary for preventing the accumulation of electrostatic charge at the surface.

Atomic force microscopy

Atomic force microscope (**AFM**) is another type of scanning probe microscope, which was designed to measure local properties of a material, such as height, with a probe. In order to generate an image, the probe should be scanned over a specific small area of the sample while measuring the local property simultaneously [140,141].

AFM is composed of a sharp tip cantilever which is used to scan the surface of specimen. The cantilever is made of silicon or silicon nitride with a tip radius of curvature in nanometers range. The image is generated when the tip of the cantilever is brought close to the sample, the forces between the tip and the sample lead to a deflection of the cantilever according to Hooke's law [142]. The forces being measured are mechanical contact force, capillary force, van der Waals, electrostatic forces, chemical bonding, electrostatic forces, and magnetic forces, [143],[144–148]. Depending on the application various operational mode such as contact, non-contact and tapping mode can be applied. In these modes we measure the cantilever vibration at a specific frequency [149,150]. In this work a contact mode cantilever was used and AFM images were recorded for the morphological evaluation of synthesized hydrogel, construction of ALP and SePP biosensors.

3.3. RESEARCH METHODOLOGY

A screen printed carbon electrode (SPCE) is a combined electrode containing a carbon working electrode, silver/silver chloride (Ag/AgCl) as reference electrode and a platinum wire (Pt) as counter electrode all in one. The working electrode area of the SPCE was modified with hydrogel to prepare a SPCE/HGL electrode.

SPCE/HGL was evaluated in HCl medium for the oxidation reduction behaviour of vanadium and selenium. It was also characterized by Raman, AFM and SEM. The

immobilization of hydrogel onto SPCE was through physical adsorption onto the electrode surface after drop coating. A second transducer namely gold micro electrode (1.6 mm) was used for the electrochemical attachment of the hydrogel to produces Au/HGL. This electrode (Au/HGL) was used to evaluate the electrochemical behaviour or attachment of hydrogel at AuE interface by CV, SWV AFM and Raman. Au/HGL was further evaluated in Tris-buffer solution for the redox behaviour of alkaline phosphatase (ALP). It also was used as suitable transducer for the immobilization of ALP to produced Au/HGL-ALP biosensor. This Au/HGL-ALP was used for the detection of vanadium in aqueous medium by SWV, amperometry and electrochemical impedance spectroscopy (EIS).

Au/HGL was evaluated in phosphate buffer for the immobilization of selenoprotein p antibody (SePP) to yield Au/HGL-SePP immunosensor. Au/HGL-SePP was used to monitor the concentration of selenium in aqueous solution by SWV and amperometry.

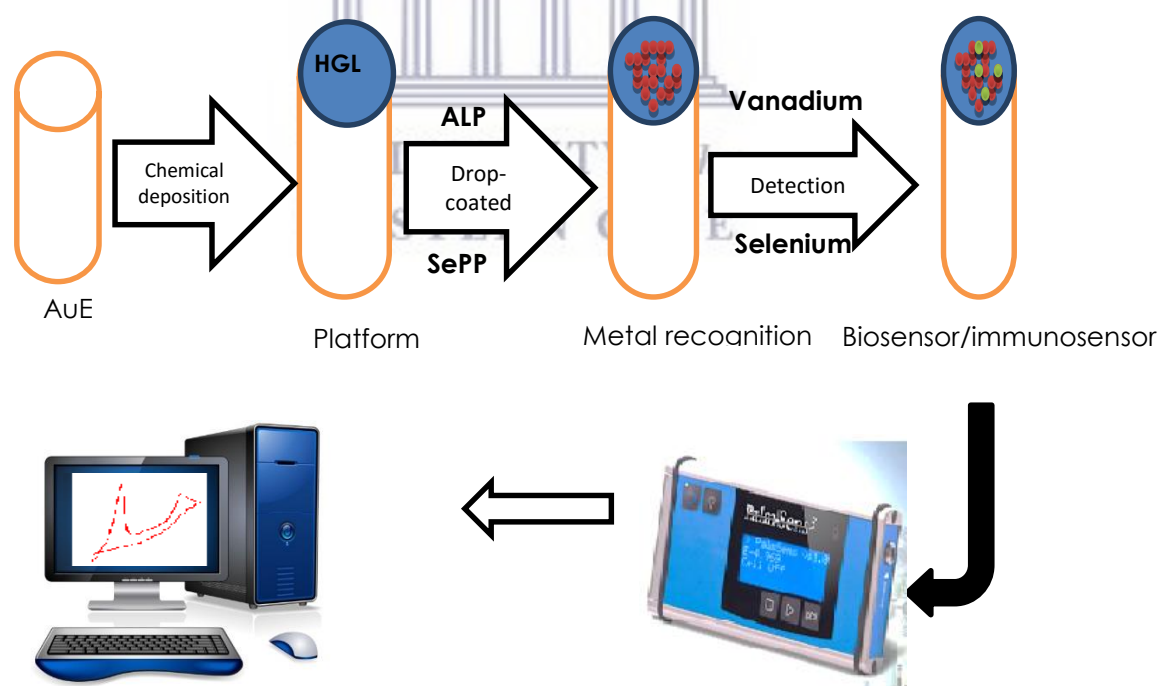


Figure 3.5: construction of biosensors

It is impossible to talk about biosensor without the bio-recognition component such as enzymes and antibodies. These two recognition components are also called bioreceptors. In this work the bioreceptors used were alkaline phosphatase and selenoprotein p antibodies in the construction of appropriate biosensors. Alkaline phosphatase is an enzyme found in your bloodstream with a phosphate group that is involved in the complex formation with metals. ALP helps break down proteins in the body and exists in different forms, depending on where it originates. It is mostly produced in your liver, but some is also produced in your bones, intestines, and kidneys. Abnormal levels of ALP in your blood most often indicates a problem with your liver, gall bladder, or bones. However, they may also indicate malnutrition, kidney tumors, or a serious infection.

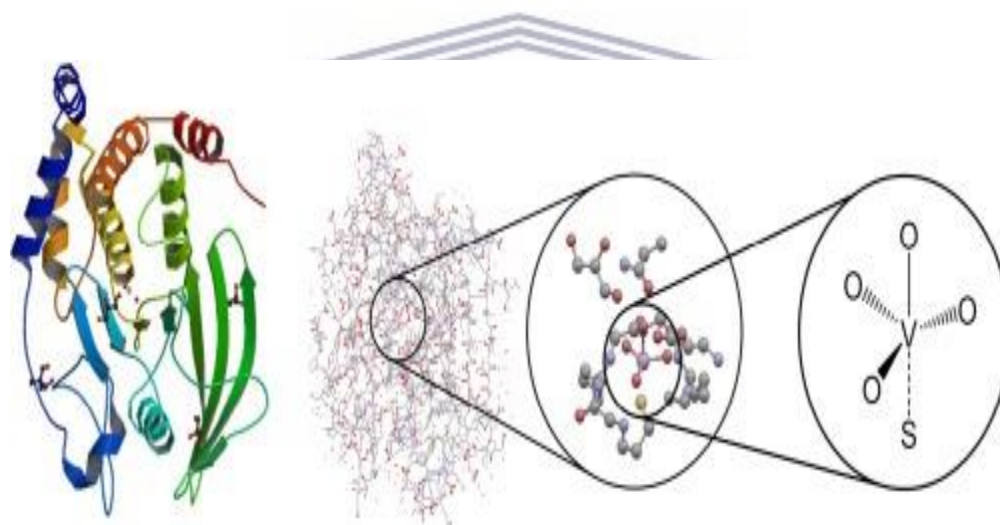


Figure 3.6: ALP biochemistry: Ribbon diagram (rainbow-color, N-terminus = blue, C-terminus = red) of the 3D structure of bacterial alkaline phosphatase.

Selenoproteins are proteins containing selenium in the form of amino acid. Selenium is incorporated into proteins not simply through ionic association, as most metals are, but is covalently bonded within the amino acid (selenocysteine). Selenocysteine has a structure that is nearly identical with that of cysteine, except with selenium in place of sulfur. Selenoprotein contained two terminals C and N. The function of the

C-terminal domain is known to be vital for maintaining levels of selenium in brain and testis but not for the maintenance of whole body selenium.

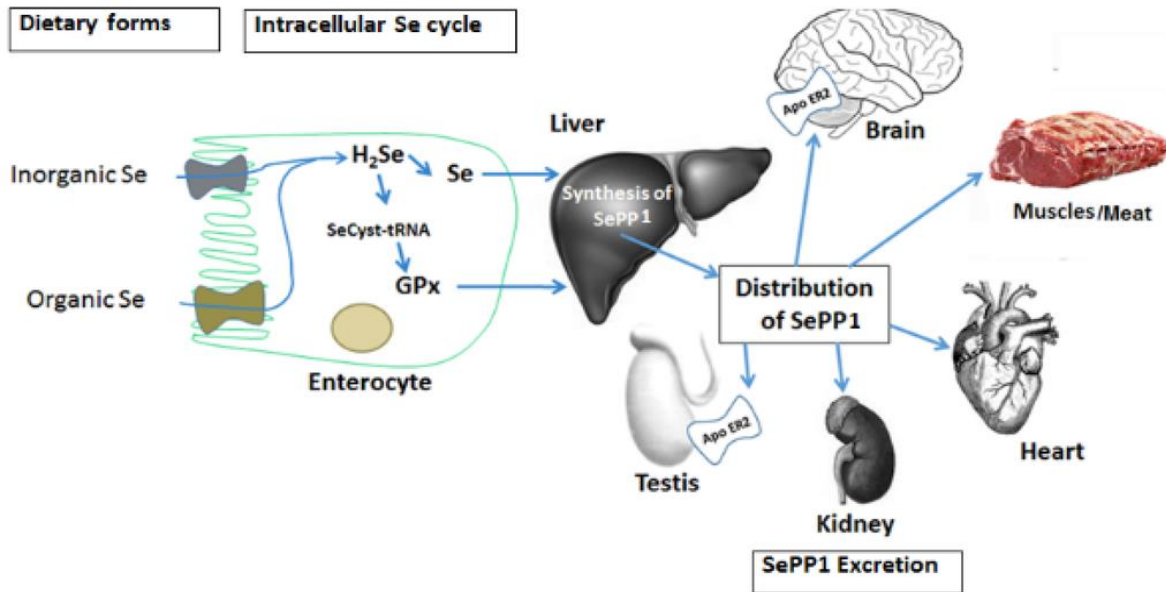


Figure 3.7: SePP-biochemistry/SePP in selenium homeostasis and transport of the testis, brain and kidney

UNIVERSITY of the
WESTERN CAPE

Chapter 4

Hydrogel sensors for vanadium and selenium in aqueous solutions

ABSTRACT

This chapter deals with synthesis and characterization of polysulfone-hydrogel. Physical properties were interrogated using techniques such as FTIR, SEM, AFM and swelling. Whereas, electrochemical properties of the material was also investigated using CV and OSWV. The electron diffusion and ionic transport properties of the hydrogels as immobilized thin films in aqueous solutions were evaluated by CV. Aspects of sensory properties of polysulfone hydrogel for electro-analytical profiling of vanadium and selenium in aqueous solutions has been published in the Journal of Nano Research.

F. N. Muya, X. T. Ngema, P. G. L. Baker, E. I. I. "Sensory Properties of Polysulfone Hydrogel for Electro-Analytical Profiling of vanadium and selenium in Aqueous Solutions," *J. Nano Res.*, vol. 44, pp. 142–157, 2016

4. INTRODUCTION

Hydrogels may be defined as a three dimensional crosslinked polymer materials capable of absorbing a large amount of water without being dissolved. Many techniques have been used to synthesize hydrogels including physical and chemical crosslinking [33]. Hydrogels have also been used in drugs delivery system due to it swelling capability, entrapment and control release of drugs [151]. The entrapment and release can be triggered by a change in oxidation state. These

properties attest to hydrogels being suitable materials in the design of programmable devices. In this work we have synthesized hydrogel based on chemically crosslinked PSF and PVA. The synthesized hydrogel was characterized by (CV, and SWV), High resolution scanning electron microscopy (HR-SEM), and atomic force microscopy (AFM)), FTIR and drop shape analyzer. Synthesis and characterization of hydrogel has been peer reviewed and published in the Journal of Water Science and Technology [33,152].

4.2. EXPERIMENTAL METHODS

The commercial polysulfone beads (PSF) and polyvinyl alcohol (PVA) with molecular weight of 35,000 and 26,000 - 30,000 respectively was crosslinked using glutaraldehyde. Polysulfone beads (PSF) were dissolved in N,N-dimethyl acetamide (DMAc) to yield a concentration of 0.05 M to which a specific amount of (PVA) was added in a 1:1 ratio. The mixture was refluxed for three hours at 75°C to yield hydrogel with final concentration of 0.5M [33]. A thin film was prepared by drop coating 10 μ L of hydrogel solution onto the surface of a working SPCE electrode.

4.3. ELECTROCHEMICAL CHARACTERIZATION OF SYNTHESIZED POLYSULFONE HYDROGEL

Cyclic voltammetry was used to evaluate the interfacial kinetics of PSF, PVA and hydrogel thin films in aqueous. These materials were evaluated in a three electrochemical cell system, to which 3 mL of 1 M HCl as the electrolyte was added. The experiments were recorded with BAS 100B electrochemical work station (100B, 1526) within the potential window ranging from -1 V to 1.5 V vs (Ag/AgCl). SPCE working (4 mm diameter) and counter electrodes (DRP-C110) was used as working,

reference and counter electrodes. The voltammogram of polysulfone deposited at SPCE is presented here (Figure 4.1).

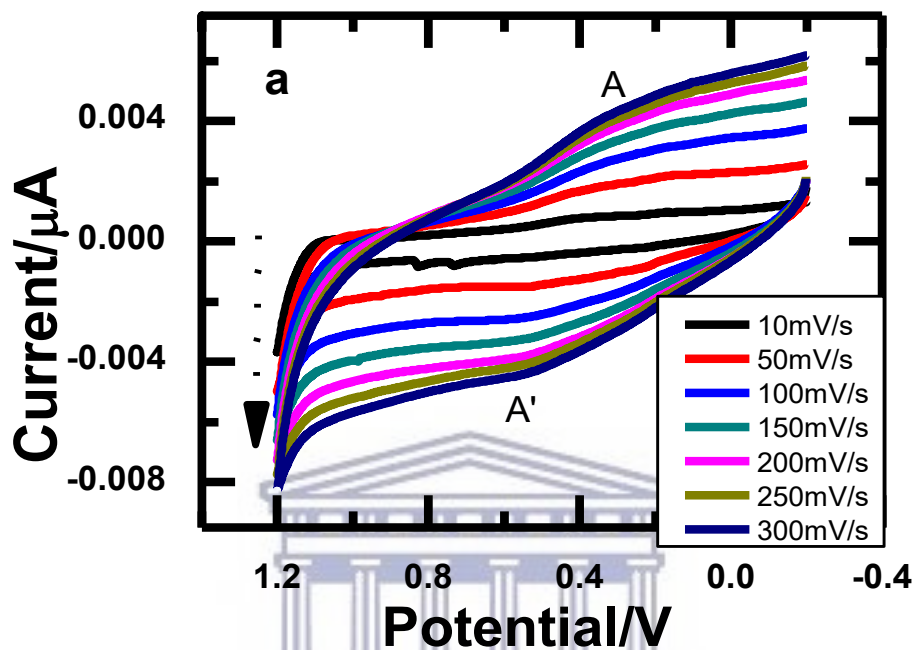


Figure 4.1: Cyclic voltammometry of PSF at SPCE in 1 M HCl vs Ag/AgCl

Cyclic voltammometry of PSF and PVA in solution, were electrochemically characterized at SPCE in 1 M HCl. Scan rate depended studies of PSF showed no peaks associated with PFS, except an increase in residual capacitance. This results from electron delocalization and the increase in current response of polysulfone film on the electrode as a function of scan rates. The separation of oxidation and reduction current showed a near square shaped voltammograms indicative of the capacitive nature of polysulfone (Figure 4.1). The electrochemistry of PVA showed 2 redox pairs a redox peaks A, A' and B, B' (Figure 4.2) and their formal potential are presented in (Table 4.1). The observed peak at B and B' are associated with the protonation of the alcoholic oxygen and secondary carbanion cation in PVA [33].

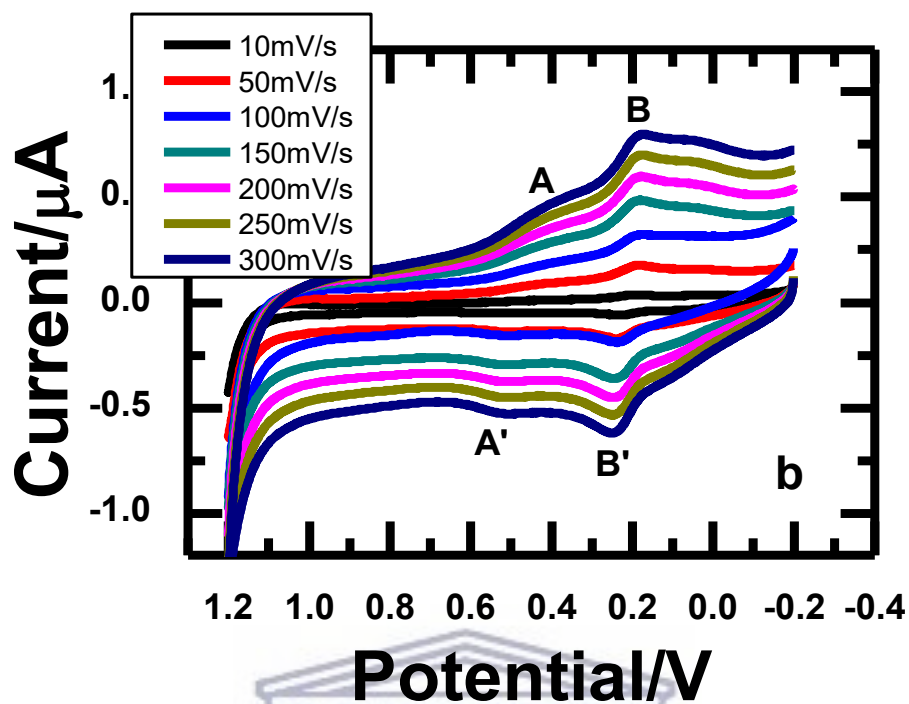
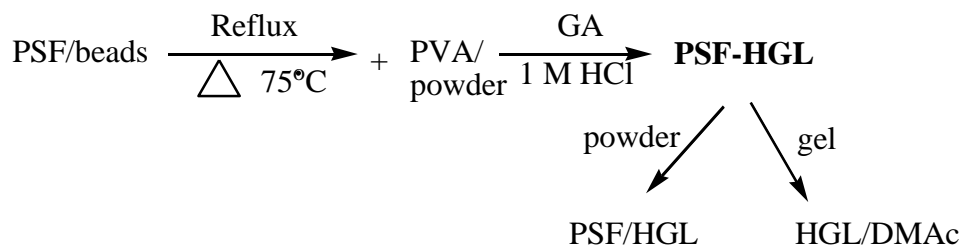


Figure 4.2: Cyclic voltammetry of PVA and at SPCE in 1 M HCl vs Ag/AgCl

CV of synthesized hydrogel showed a strong electrochemical response at screen printed electrode. Scan rate dependent studies of hydrogel was used to calculate diffusion coefficient. Three redox couples peaks A, A', B, B' and C, C' were identified in the hydrogel voltammograms (Figure 4.3) and their formal potentials are reported in (Table 4.1). The redox peaks B and B' were associated with the delocalization of the double bond within the benzene ring structure of the hydrogel [153].



Scheme 4.1: Schematic representation of hydrogel synthesis

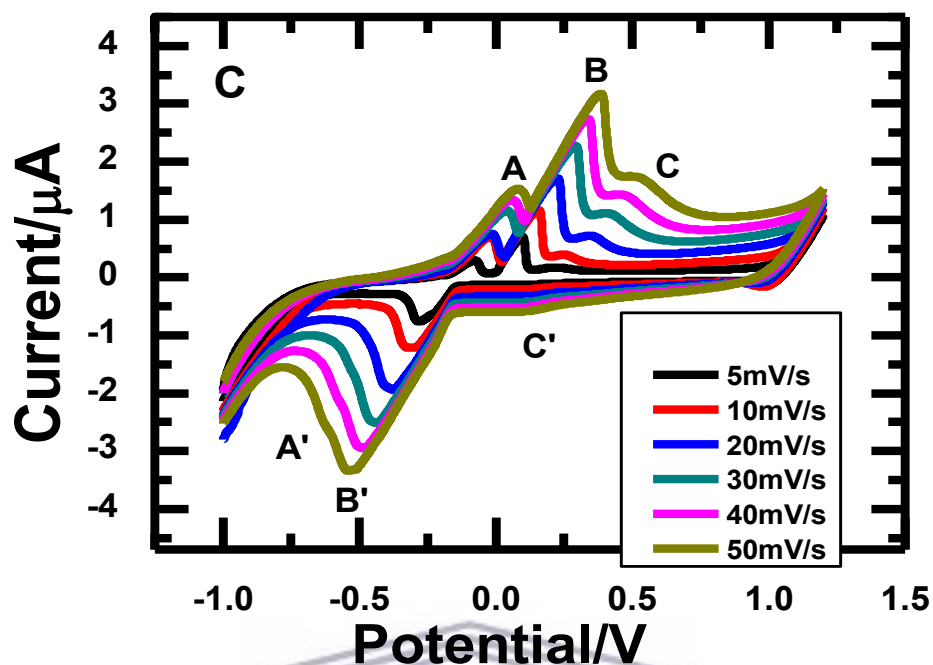


Figure 4.3: Cyclic voltammery of hydrogel at SPCE in 1 M HCl vs Ag/AgCl

Diffusion coefficient can be related to the molar flux due to molecular diffusion across the gradient in the concentration of the species as a proportional constant. Diffusion coefficient is related to the efficient transport of ions, electrons and small molecules (under mass transport control) to and through a membrane. The redox pairs B and B' were used to calculate the diffusion coefficient and surface concentration. Diffusion in the absence of an analyte molecule was used to assess the electron mobility to the hydrogel interface in aqueous solution. The diffusion coefficient for the hydrogel thin film electrodes in aqueous medium was calculated to be $9.06 \times 10^{-9} \text{ cm}^2/\text{s}$ favoring the reduced state.

Table 4.1: Summary table of peak potential

	A	B	C	A'	B'	C'
PVA	0.439 V	0.201 V	-	0.526 V	0.241 V	-
PSF	0.340 V	-	-	0.557 V	-	-
PSF-PVA	0.075 V	0.491 V	0.549 V	-0.0663 V	-0.512 V	0.113 V

4.4. SPECTROSCOPY CHARACTERIZATION

FTIR was used to confirm the formation of a new hydrogel due to chemical crosslinking of PSF and PVA. The two possibilities were identified for the position at which carbocation attachment could occur i.e. either at the ester oxygen, or sulphur oxygen.

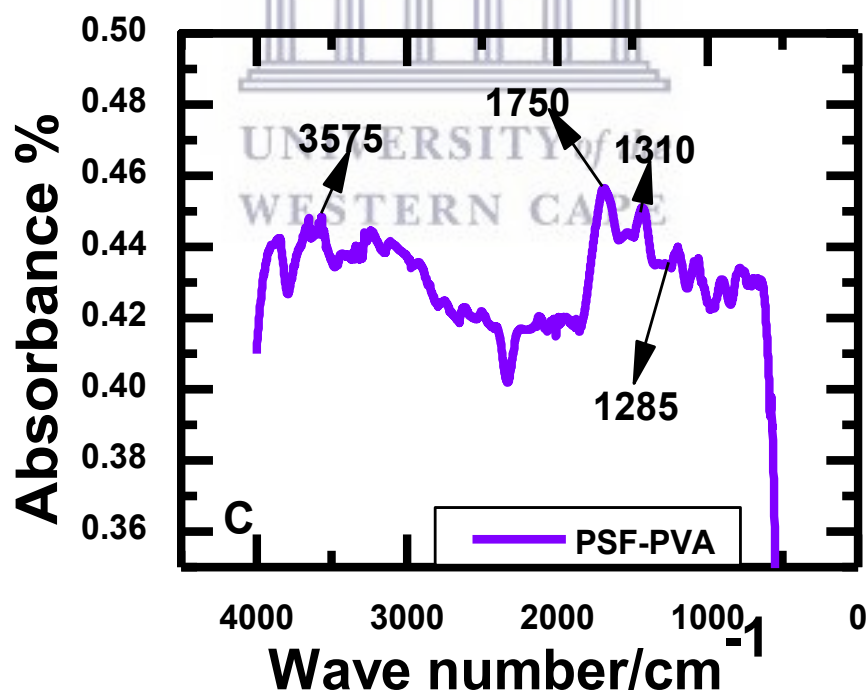


Figure 4.4: FTIR spectra of hydrogel powder at SPCE

Table 4.2: PSF-PVA hydrogel functional group identification

Functional group	Wave number (cm ⁻¹)
CH	3575
C=C	1750
S=O=S	1310
C-O-C	1285

Fourier transform infrared spectra of the (PSF-PVA) hydrogel confirmed the cross-linking of the ester side by the absence C-O-C which is involved in crosslinking. This indicates that the ester oxygen was consider to be the crosslinking side in the formation of hydrogel. The sulphone oxygen vibrations were still visible in the spectrum of the hydrogel products (Figure 4.4) and (Table 4.2) [33].

4.5. PHYSICAL TESTING OF SYNTHESIZED HYDROGEL

Hydrogel can be classified into two category; powder or gelatin however, for any hydrogel it is a mandatory for it to able to absorb up to 20% of its body weight, in water. Therefore, in order to prove that a swelling testing was required. The **swelling capacity** of hydrogel can be determined by the amount of liquid material that can be absorbed. This test was evaluated by a beaker methods.

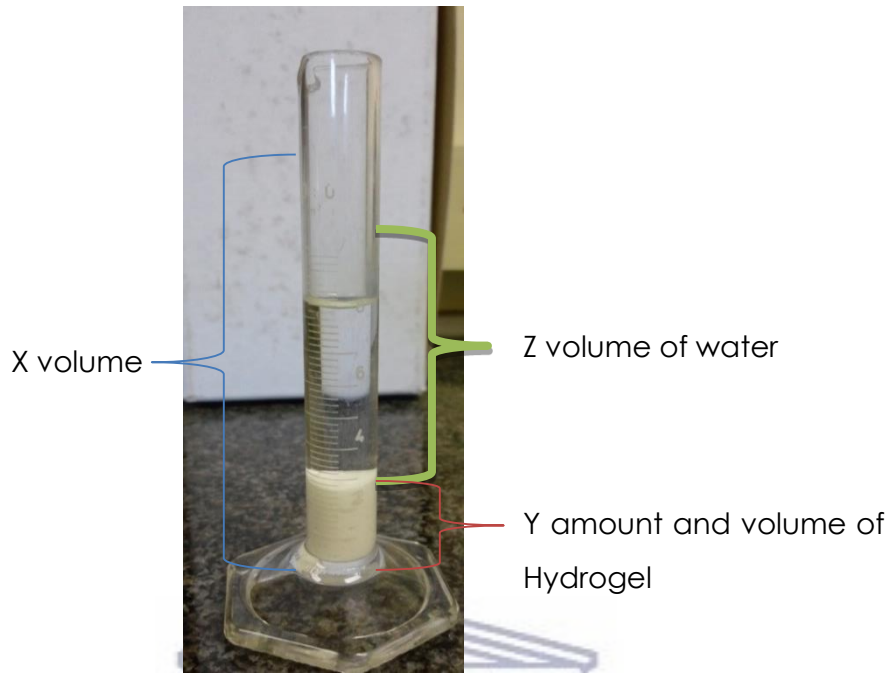


Figure 4.5: Swelling capacity of hydrogel

The beaker method was assessed by weighing a specific amount of dry hydrogel and compact it into a cylinder. The mass and volume of the dry hydrogel in the cylinder was recorded. A specific volume of different solvents such as H₂O, HCl, PBS, and NaOH was measured and poured into the cylinder and allow the swelling. After swelling the volume of the wet hydrogel was recorded and swelling capacity was calculated by the following equation:

$$\text{Uptake water by Volume} = \frac{\text{Volume of dry hydrogel}}{\text{Volume of wait hydrogel}} \times 100$$

From literature a good hydrogel should adsorbed a minimum of 15 to 20% (V/V) or (g/g) of it body weight [154]. However PSF-hydrogel showed a swelling capacity of 48% in water 33% (v/v) in HCl 28% (v/v) in NaOH and 26% (v/v) in PBS. The results

obtained confirmed that the synthesized PSF-PVA material as a new class of hydrogel. This can be used for various application i.e. adsorbent for heavy metal remediation and loading material for drug delivery.

Table 4.3 Swelling capacity of hydrogel in various electrolyte

pH	Solvent	Swelling (V/V)	Swelling (g/g)
7	Water	48%	43%
3	Hydrochloric acid	33%	30%
12	Sodium hydroxide	28%	25%
7.2	Phosphate buffer	26%	26%

The results tabulated above (Table 4.3) showed that molecular size plays a major factor in adsorption. Water showed a higher adsorptive capacity compare to the other solvent due to the fact that it's more polar, with a smaller molecular size, bond length and electronegativity. This mean water molecule can easily be absorbed into the pore of the hydrogel than other solvent. Nevertheless the synthesized hydrogel showed an adsorption capacity of greater than 20% in all the solvents.

4.6. HYDROGEL STABILITY

Hydrogel stability was evaluated based on the diffusion coefficient and was found to be stable for more than a year [33]. The adsorption capacity or swelling behavior was electrochemically evaluated by using a fixed concentration of free metal ions solution at SPCE/HGL (Figure 4.6). Here 10 μ L of hydrogel was drop coated onto SPCE to produce SPCE/HGL electrode and the electrode was connecting to BAS system.

To this SPCE/HGL electrode a fixed concentration of free metal ion (selenium) was added, and the potential was scanned every 10 mins within a potential window ranging from -1.5V to 1.5V at a scan rate of 50mV/s.

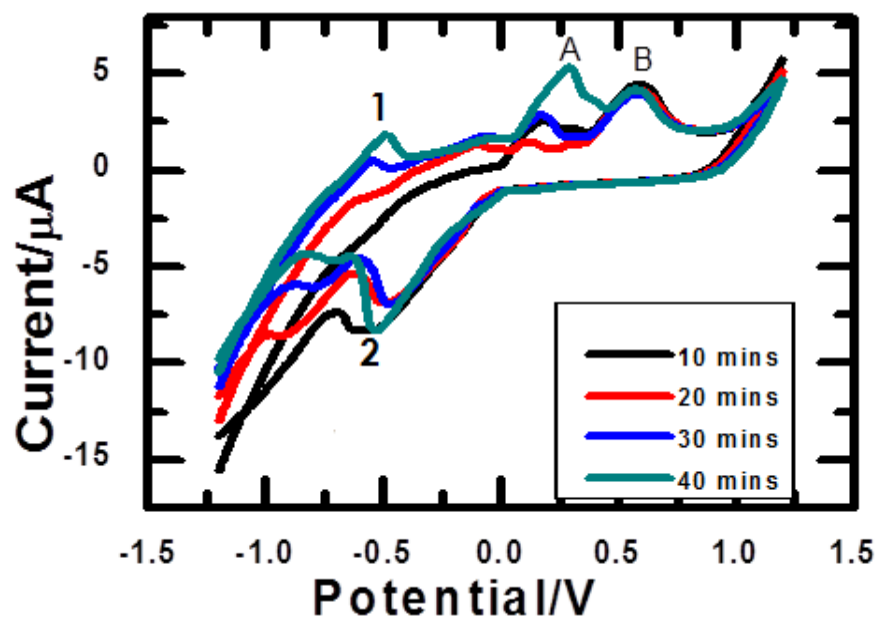


Figure 4.6: CV of time interval studies of selenium at hydrogel interface in 1 M HCl vs Ag/AgCl

The voltammograms in (Figure 4.6) shows the current response at different time intervals for a fixed concentration of metal. The results revealed that from t_1 to t_{20} minutes hydrogel electrochemistry was dominant, meaning that the adsorption process of metal into the hydrogel had not reached completion. The redox (1 and 2) chemistry of metal became visibly superimposed onto the hydrogel matrix and continued to give a stable response as a function of time. The oxidation states of selenium observed at 1 and 2 agrees with the standard redox potential of Se^{4+} and Se^0 respectively (Table 4.7). It was concluded that maximum potential response at peak 1 was observed at t_{40} minutes (Figure 4.6).

4.7. MICROSCOPIC CHARACTERIZATION OF HYDROGEL

Scanning electron microscopy (SEM)

The electrodes were prepared by drop coating a specific amount of PSF and HGL onto separate SPCE to produce SPCE/PSF and SPCE/HGL electrodes. The modified electrodes were allowed to dry overnight and coated with gold nanoparticle for surface enhancement. SPCE/PSF and SPCE/HGL morphology were evaluated by High resolution scanning microscopy (HRSEM).

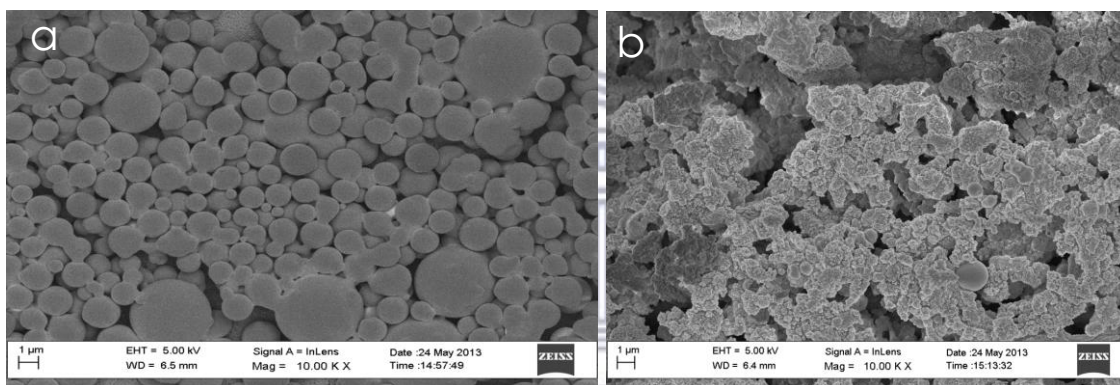


Figure 4.7: HR-SEM spectrum of a) PSF and b) PSF-hydrogel at SPCE at 10 x magnification with EHT 5 W

Scanning electron microscopic image on (Figure 4.7a) shows that polysulfone has a spherical shape with fairly uniform size distribution of spheres in the order of 1 μm. The uniformity in color of the image indicated the absence of charging due to interaction with the incident electron beam[32]. When compared to polysulfone on its own, a change in morphology was observed due to the integration of both PVA and PSF. Polyvinyl alcohol introduction resulted in a decrease in size of the surface morphology features. Very little PSF spheres were visible, it was evident that PSF spheres directed the growth of PVA polymer, which is consistent with expectation for efficient crosslinking (Figure 4.8b)[33].

Atomic Force Microscopy (AFM)

AFM was used for characterization of hydrogel. For this kind of work, surface roughness can be regarded as one of the most important surface properties. It plays an important role in membrane permeability and fouling behavior. Various parameters can be derived from surface roughness (S_a) including average roughness (R_a), and root mean square roughness (R_{rms}). The electrode was prepared by drop coating 10 μL of hydrogel onto SPCE to produce SPCE/HGL electrode. The SPCE/HGL electrode was allowed to dry overnight and subjected to the Nanosurf easyScan 2 (Wirsam) for imaging and surface roughness measurement (Figure 4.8).

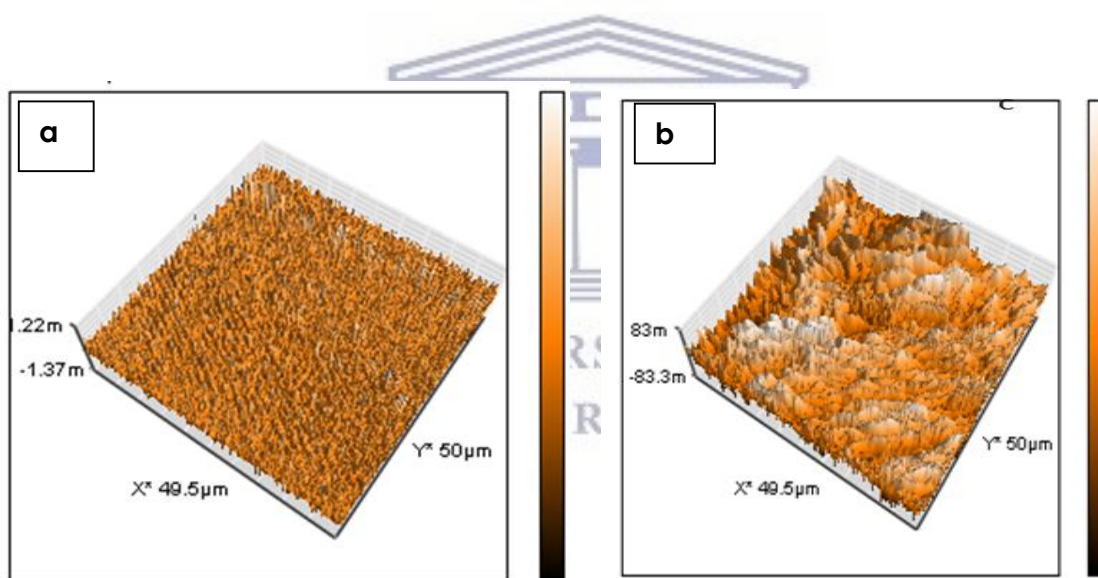


Figure 4.8: AFM images of a) PSF and b) PSF-hydrogel at SPCE

The hydrogel showed a higher surface roughness of 8.900 nm compared to PSF 4.021 nm (Figure 4.8). The surface roughness and height distribution were in good agreement with the observed surface features of the polymers from SEM. The S_a and R_a values show a clear distribution of roughness associated with PSF contribution respectively. And a clear decrease in hydrophobicity trend upon modification with PVA was observed [33].

4.8. HYDROGEL APPLICATION

The synthesized polysulfone-hydrogel material was used for the following application:

- Hydrogel as a sensor for detection of metal ions of biological significant (vanadium and selenium).
- Hydrogel as an encapsulating agent for alkaline phosphatases based on its swelling behavior for the detection of vanadium in real sample.
- Hydrogel as a transducer for the construction of immunosensor based on selenoprotein p antibody for the detection of selenium in real sample.

Hydrogel as sensor for the detection of vanadium

The chemical sensor for the detection of vanadium was constructed by immobilizing a specific amount of hydrogel solution at SPCE to produce SPCE/HGL sensor. The SPCE/HGL electrode was connected to the SPCE box connector and the electrode was suspended at the SPCE box connector and analyzed. To understand the electrochemistry of the analytes each one was analyzed at unmodified SPCE electrodes and the peak produced was used as the analytical signal.

Electrochemistry of vanadium at unmodified SPCE

Cyclic voltammetry (CV) and Osteryoung square waves (OSVW) of increasing vanadium concentration at bare electrode were investigated in order to study redox behaviors and multiple oxidation states of vanadium at unmodified electrode. The potential was cycled from -1.5 V to 1.0 V, and then back to -1.5 V. Vanadium showed multiple redox peaks which were associated with various oxidation states. Here we used V_2O_5 at the start of the sweep. V^{5+} is reduced to V^0 and progressively oxidized to V^{4+} , V^{3+} and V^{2+} at 0.890 V, 0.301 V and -0.260 V respectively.

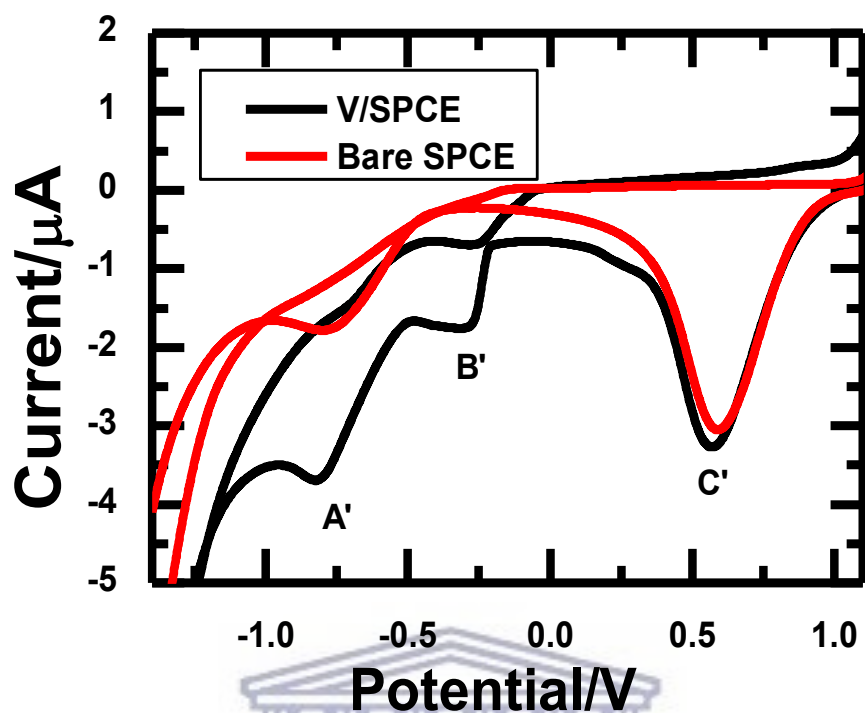


Figure 4.9: CV of bare SPCE in solution and vanadium at unmodified SPCE In 1M HCl vs Ag/AgCl

In CV three reductions peaks A', B' and C' were observed, however only one transition B' which was attributed to the transition of V^{3+}/V^{2+} (Figure 4.9) according to standard redox potential (Table 4.4). The intermediate transition state was not observed by CV due to high and fast kinetic. The OSWV of vanadium at unmodified electrode depicted multiple oxidation state which was associated with several transitions in solution. Initial oxidation state was 5+ in solution, the V^{5+} gain an electron and reduced to V^{4+} which was observed at a potential of 0.890 V (Figure 5.10a), same applied for V^{4+}/V^{3+} at 0.301V and V^{3+}/V^{2+} at - 0.290 V (Table 4.3).

Metal ion such as vanadium interact with a transducer (carbon electrode) by forming a complex. From the voltammograms obtained in (Figure 4.10a and 10b) various peaks where observed. The redox peaks at ± 0.850 V was associated to the complex formation.

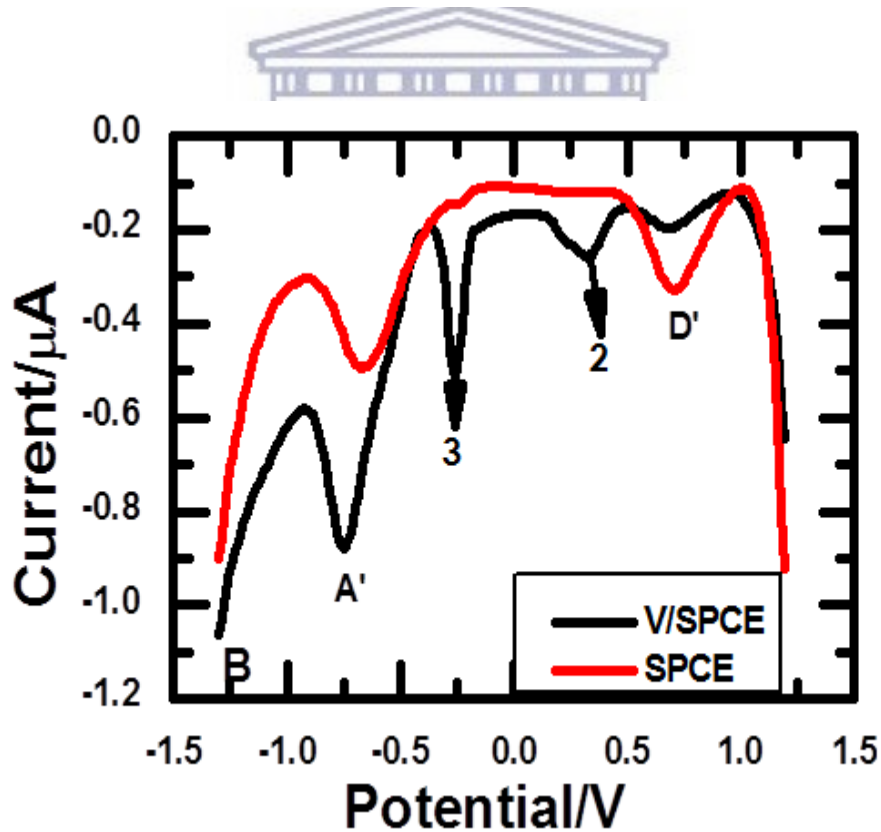
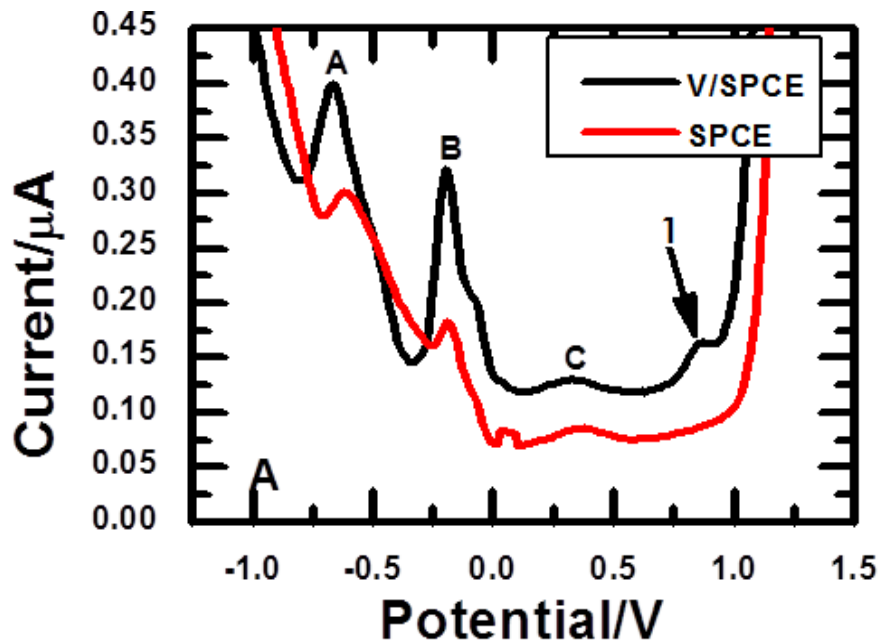
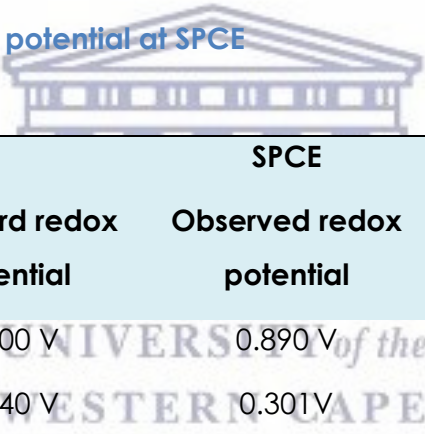


Figure 4.10: SWV A) Oxidation and B) Reduction of bare electrode and vanadium at unmodified SPCE in 1 M HCl vs Ag/AgCl

OSW provide three additional peaks A, B and C at -0.668 V, -0.203 V and 0.331 V respectively (Figure 4.10). According to literature peaks B and C are direct interaction (complex) between the transducer and the free metal. However the peak A was assigned to metal hydride (MH) hence free metals bonds strongly to hydrogen. Same applied to (Figure 4.10b) two additional peaks were observed A' and D' at -0.743 V and 0.699 V. The peak D' showed a decrease in peak intensity as the concentration increases which showed a decreased in background. However the peak at A' increased as the concentration increases which is also associated with metal complex formation. The peaks 1, 2 and 3 were associated with V^{4+} , V^{3+} and V^{2+} in solution respectively based on standard redox potential (Table 4.4). The peak 2 and 3 were the most dominant peaks and was used for quantification.

Table 4.4: Vanadium redox potential at SPCE



Oxidation state	Standard redox potential	SPCE	SPCE/HGL
		Observed redox potential	Observed redox potential
(1) V^{4+}	1.000 V	0.890 V	-
(2) V^{3+}	0.340 V	0.301 V	0.270 V
(3) V^{2+}	-0.260 V	-0.260 V	-0.270 V

4.8.1. HYDROGEL SENSOR FOR DETECTION OF Vanadium

Electrochemical studies of vanadium at hydrogel interface

The SPCE/HGL electrode was used for the detection of vanadium in solution. The results of hydrogel at SPCE electrode and vanadium at hydrogel interface for comparison purposes are presented in (Figure 4.11). The peaks 4 and 5 at the

potential - 0.270 V, and 0.270 V, respectively were attributed to V^{3+} and V^{2+} based on standard reduction potential (Table 4.4). The electrochemical behavior of vanadium is a complex process and strongly depends on the nature of the transducer [43]. The remaining peaks were attributed to the intermediary redox states.

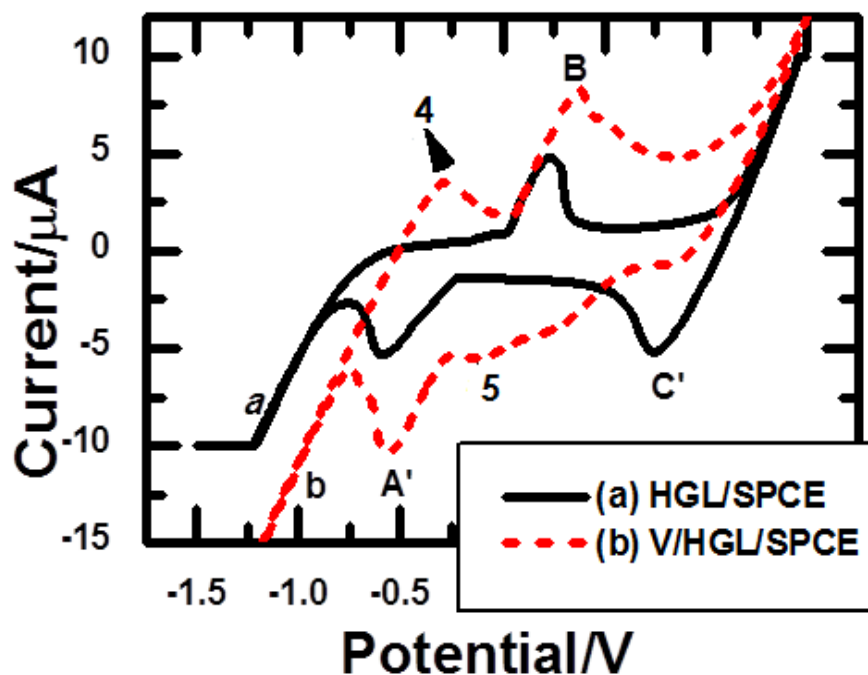


Figure 4.11: Cyclic voltammetry of (a) Vanadium at hydrogel interface and (b) vanadium at Hydrogel immobilized at electrode in 1 M HCl vs Ag/AgCl

The current response for peak 4 and 5 were used to plot the calibration curves (Figure 4.12). The concentration dependent study of vanadium at hydrogel interface was done in the concentration range from 0.1 mM to 0.6 mM. These studies showed an increase in peak current of 4 and 5 as the concentration increases which revealed the catalytic behavior of the analyte at the hydrogel interface.

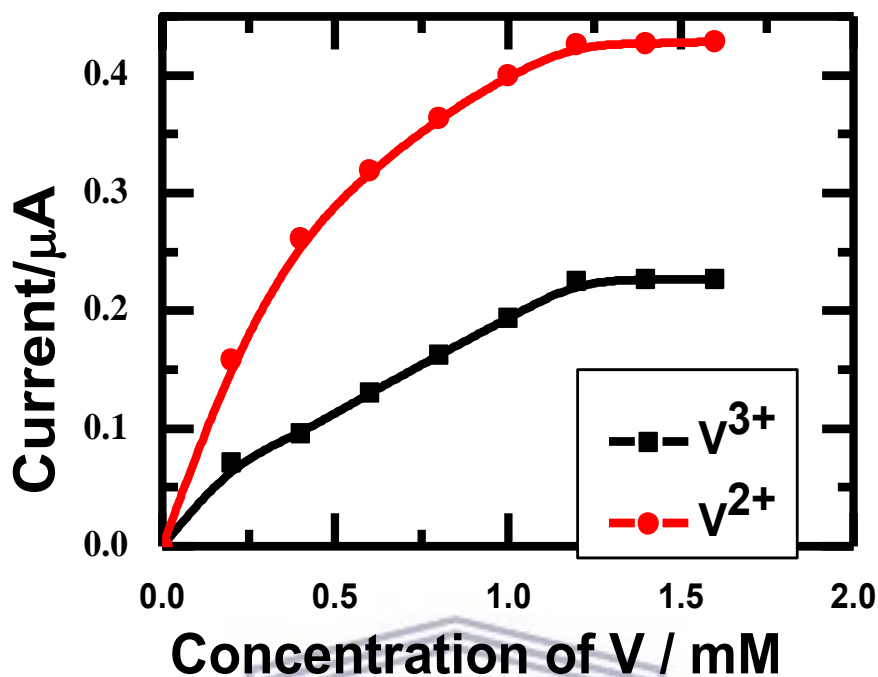


Figure 4.12: calibration curves plot based on the influence of concentration of vanadium on the peak current response at hydrogel interface in 1 M HCl vs Ag/AgCl.

Table 4.5: Summary of hydrogel performance sensor in the presence of vanadium

	Peak 5 (V ²⁺)	Peak 4 (V ³⁺)
De	9.148 e ⁻³ Cm ² /s	3.860 e ⁻⁵ Cm ² /s
LOD	0.223 mM	0.087 mM
Sensitivity	2.192 e ⁻³ μA/mM	1.424 e ⁻⁴ μA/mM

Vanadium redox behavior was influenced by the nature of the transducer and is hampered by multiple redox peaks which are traditionally difficult to resolve. However guided by standard redox potential Tables as well as a detailed stepwise analytical protocol, unambiguous quantification is possible. The calibration plot of SPCE/HGL sensor response to vanadium are shown in (Figure 4.12). The results shows a higher sensitivity for peak 5 than 4 with LOD and LOQ of 0.2231 mM and 0.474 mM

respectively (Table 4.5). The peak 5 showed highest sensitivity to vanadium at hydrogel electrode. Therefore peak 5 was used for vanadium detection in general.

Hydrogel as adsorbent for vanadium remediation

Analysis of adsorption process is very important for the design of adsorbents because the kinetics can provide essential information on the adsorption mechanism and the metal ion adsorption rate [15, 28]. To investigate such properties, a pre-weighed 0.5 g of hydrogel sample was allowed to swell in 40 mL of 0.05 M of vanadium solutions. The adsorption capacities were determined at desired time intervals. The UV-vis absorbance of 1 mL of vanadium solution, collected at 5 minute intervals was measured until the absorbance reading stabilized.

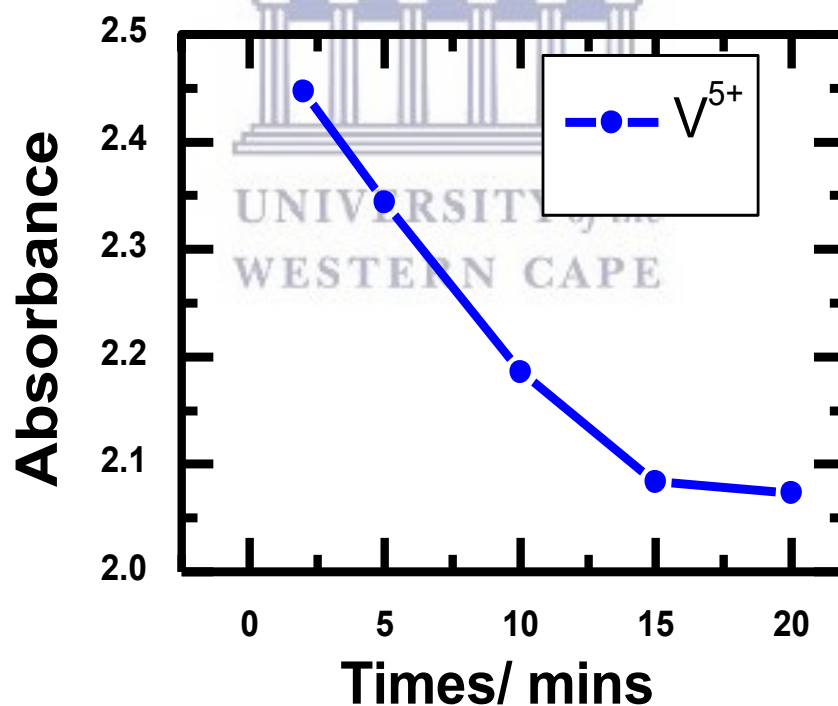


Figure 4.13: Effect of time on heavy-metal ions adsorption ($C_0 = 100 \text{ mg/L}$, $m = 0.5000 \text{ g}$, $V = 40 \text{ mL}$, $\text{pH}=6$, $T = 25^\circ\text{C}$)

Figure 4.13 confirmed that high adsorption rates are observed at the beginning (t_1), then slow and finally levels off after (t_{20}) minutes, implying that hydrogel have quite fast adsorption rate. The adsorption capacity (Q) was calculated to be 0.189 mg/g by the following equation

$$Q = [(C_i - C_f) \times V] / m \quad (1)$$

where Q is the adsorption capacity of heavy-metal ions (mg/g), C_i and C_f are the concentrations of the heavy metal ions in the aqueous phase before and after the adsorption, respectively (mg/L); V is the volume of the aqueous phase [35] and m is the amount of the dry hydrogel used (g).

Adsorption behavior was also investigated by SEM after electrochemical analysis where by, the modified electrode was collected and dried at room temperature for 24hours. The modified electrode was imaged using the Zeiss Auriga, high resolution (fegsem) field emission gun scanning electron microscope. Vanadium at (SPCE) showed particles sized 1-2 μm with cuboid shape (Figure 4.14a) which appeared to sit on the surface of the hydrogel (Figure 4.14b) rather than move into the pores due to size restriction. Hydrogel seems to aggregate in large particles in the form of large globules. This was due to an increase in chain interaction compared to its stabilized particles. In which the polymeric surfactant chains act as a limiting factor for such an interaction[1-2]. Energy Dispersive Spectrometry (EDS) with an accelerating voltage of 5.00 KV and an energy resolution of 18 keV, was employed to identify the elements present in the hydrogel before and after adsorption of the respective metals species. No significant trace of vanadium was found in the hydrogel imaging before electrochemical analysis (Figure 4.7b). However, the EDS analysis of hydrogel sensor after electrochemical analysis of vanadium (Figure 4.14b), revealed that vanadium was entrapped and adsorbed onto the hydrogel matrix by 8.3%.

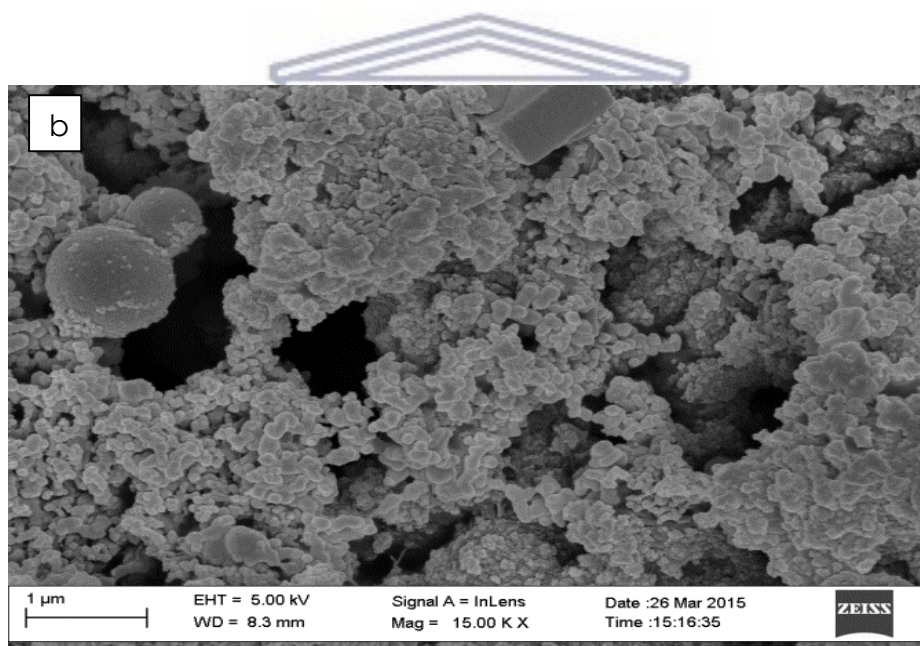
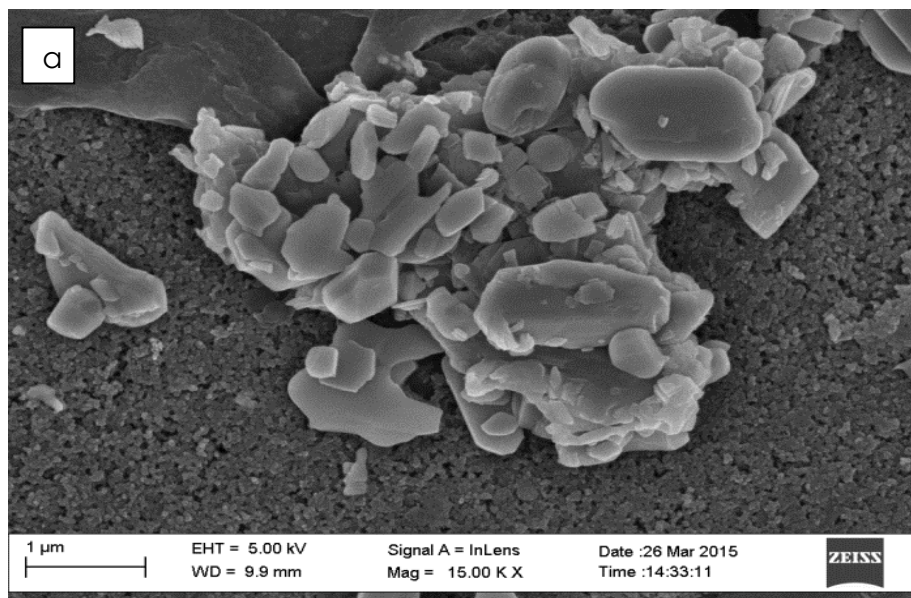


Figure 4.14: HR-SEM image of (a) Vanadium at SPCE, (b) Vanadium at hydrogel interface after electrochemical analysis and dried for 24 hrs.

Table 4.6: Adsorption capacity of various hydrogels systems

Adsorbent	Metal ions	Metal concentration	pH	Adsorption capacity (mg/g)	References
PVA/AAC	Cu ²⁺	300 mg/l	4.5	13	[25]
Poly(EGDMA-VIM) hydrogel	Cd ²⁺	300 mg/l	3-5	69	[27]
	Pb ²⁺	300 mg/l	3-5	112	[30]
	Hg ²⁺	300 mg/l	3-5	162	[31]
Alginate beads	Cd ²⁺	200-300 mg/l	6.5	182	[32]
	Pd ²⁺	100 mg/l	6.0	165	[32]
AMPS/PVAcCopolymer hydrogel	Ni ²⁺	200 mg/l	6.5	230	[33]
	Mn ²⁺	350 mg/l	5.5	160	[33]
PAA hydrogel	Pb ²⁺	150 mg/l	6.5	113	[34]
Chitosan nanofibril	Cd ²⁺	300 mg/l	6.0	140	[35]
	Cu ³⁺	250 mg/l	5.5	169	[35]
	V ⁵⁺	100mg/l	0-2	0.189	[155]
Polysulfone hydrogel	Se ⁴⁺	100mg/l	0-2	0.559	[155]

The use of hydrogels in adsorption or detection of vanadium has not been reported. Polysulfone hydrogel adsorbent shows low adsorption capacity (mg/g) compared to commonly used adsorbents (Table 4.6) [25, 27-29, 36-40]. Adsorption capacity is strongly affected by various parameters as temperature, ion concentration and in particular pH of a solution [41]. The low values for adsorption capacity reported here are directly impacted by the low pH of the measurement. However further pH dependence was not evaluated here. Hence improving adsorption capacity was not primarily the main objective of this work, therefore improving adsorption could be attend in future work.

In conclusion SPCE/HGL was used as chemical sensor for the detection of vanadium, in terms of sensitivity, diffusion coefficient, and LOD. A higher preference for detection of V^{2+} compared to V^{3+} was also demonstrated. Vanadium in its second state (V^{2+}) was used to quantify vanadium at hydrogel interface in aqueous systems. The results reported here provides evidence of the hydrogel being used as an excellent sensor compare to literature [156]. However a poor performance in adsorbent for heavy metals was observed 0.189 mg/g compare to others (Table 4.6) [157]. Vanadium redox behaviour was influenced by the nature of the transducer and is hampered by multiple redox peaks which are traditionally difficult to resolve. However guided by standard redox potential Tables as well as a detailed stepwise analytical protocol, unambiguous quantification is possible. In literature various chemical sensors have reported vanadium response in milligrams per liter (mg/L)[156], however SPCE/HGL showed a response within micrograms per liter ($\mu\text{g/L}$). Which is in the range of WHO guidelines for these species vanadium in aqueous systems [155].



4.8.2. HYDROGEL SENSOR FOR DETECTION OF SELENIUM

Electrochemical studies of selenium at unmodified SPCE

Preliminary cycling voltammetry (CV) experiments were performed in order to study the behaviour of bare screen printed carbon electrode (SPCE) and selenium at bare SPCE. Electrode activation was done first by cycling the bare SPCE electrode in an electrochemical cell containing 1 M HCl. The electrochemical response are observed in (Figure 4.15). This Figure despite CVs for selenium solutions obtained at bare and modified electrodes.

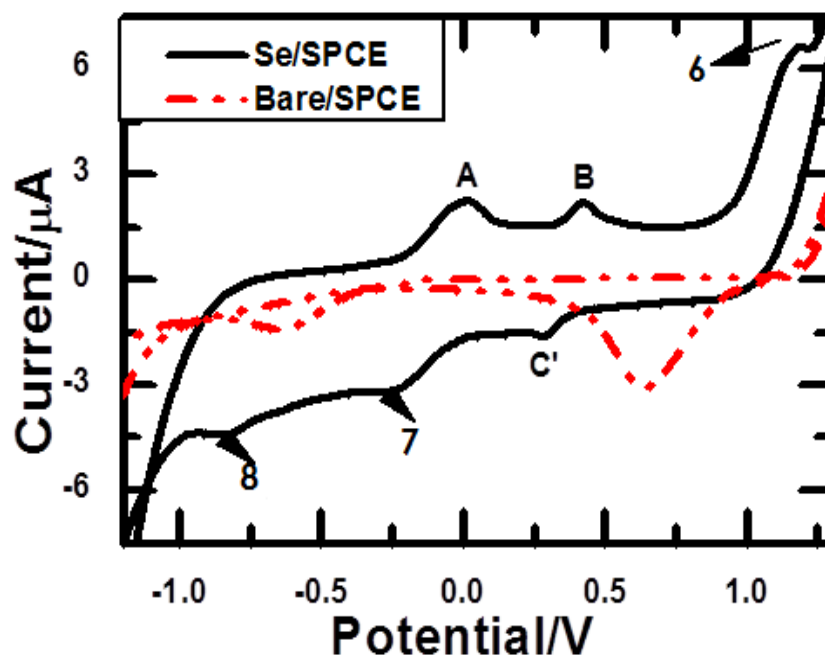


Figure 4.15: CV of bare SPCE and selenium at SPCE in 1 M HCl vs Ag/AgCl

Voltammogram of selenium exhibited one oxidation peak and two reduction peaks. The peak 6 observed at 1.160 V was attributed to Se^{4+} and peaks 7 and 8 which were associated with the transition from Se^{4+} to Se^0 and from Se^0 to Se^{2-} respectively [42]. And this was in agreement with standard redox potential of selenium (Table 4.7). The electrochemical behaviour of selenium is reported in literature as a very complex process which is strongly dependent on the nature of the substrate [43].

Table 4.7: Selenium redox at bare SPCE

Oxidation state	Standard redox potential	SPCE Observed redox potential	SPCE/HGL Observed redox potential
(6) Se ⁶⁺ to Se ⁴⁺	1.150 V	1.160 V	-0.431 V
(7) Se ⁴⁺ to Se ⁰	-0.370 V	-0.260 V	-0.450 V
(8) Se ⁰ to Se ²⁻	0.920 V	0.900 V	-
Se ⁶⁺ to Se ⁴⁺	-0.420 V	-	-

Electrochemical studies of selenium at hydrogel interface

Here we are investigating the detection of selenium at hydrogel interface. Physical immobilization of hydrogel at SPCE was used as platform for detection of selenium. Figure 4.16 provides voltammograms of (1) hydrogel at SPCE and (2) selenium solutions at hydrogel interface. It was observed that both hydrogel and selenium have multiple peaks, however monitoring a complex peaks can be an option if no new peaks were observed.

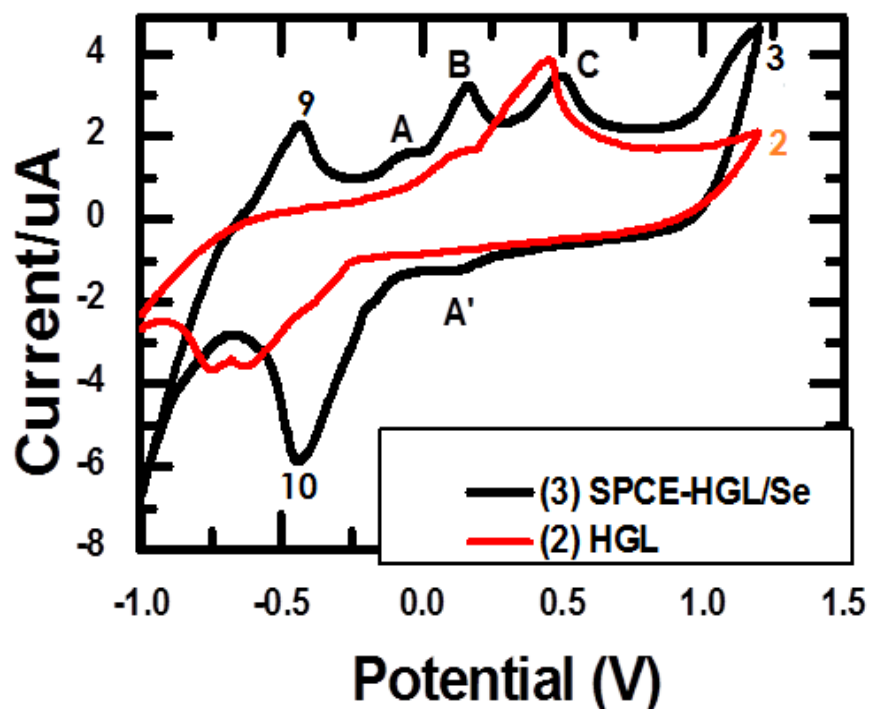


Figure 4.16: CV of unmodified electrode, Hydrogel at SPCE and selenium at hydrogel SPCE interface in 1 M HCl vs Ag/AgCl

The peak B and C in Figure 4.16 (3) was associated to the hydrogel, which is present in the voltammograms (2). Nevertheless the reduced peak 10 at -0.430 V was allocated to the transition of Se^{4+} to Se^0 which normally occurs at -0.370 V [42]. The redox couple A and A' observed respectively are associated with complex formation at hydrogel interface, hence selenium tend to form a complex with the transducer [43]. The interaction of selenium ions with the transducer was investigated and confirmed by scan rate dependent studies. Two concepts can be derived from migration of peak potential by investigating scan rate dependence. Peak potential might shift or no increased as the function of scan rates. A shift is mainly depending upon reduction of rate constant (and also the voltage scan rate). This occurs because the current takes more time to respond to the applied voltage.

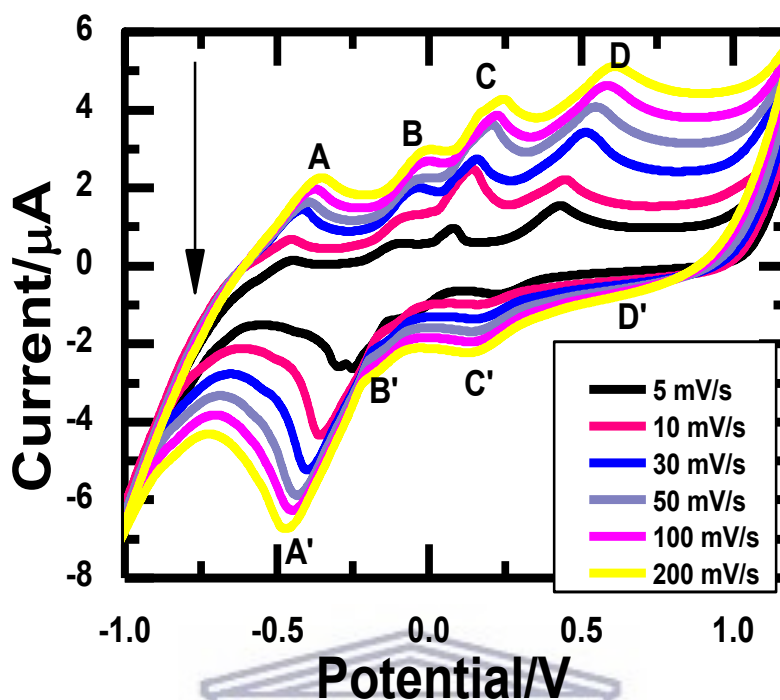


Figure 4.17: Series of CV recorded at different scan rates for the same solution containing only Se^{4+} at hydrogel interface in 1 M HCl vs Ag/AgCl

Scan rate dependence studies was investigated by increasing the scan rate of the system. A series of voltammograms recorded at different scan rates for the same solution containing a fixed concentration of selenium are presented in (Figure 4.17). Each curve has the same form but it is apparent that the total current increases with increasing scan rate. This again can be rationalized by considering the size of the diffusion layer and the time taken to record the scan. A final point to note from the (Figure 4.17) is the position of the current maximum which does not occurs at the same voltage there is a slight shift within the potential range. This is a characteristic of electrode reactions which have rapid electron transfer kinetics. This occurs because the current takes more time to respond to the applied voltage at hydrogel interface.

Concentration dependence study of selenium at hydrogel interface was evaluated in a concentration range 0.1 mM to 0.6 mM (Figure 4.18). The current response of peaks 9 and 10 corresponding to Se^{4+} and Se^0 were used to plot the calibration

curves. Other peaks in the selenium voltammograms relates to intermediary redox states was also observed.

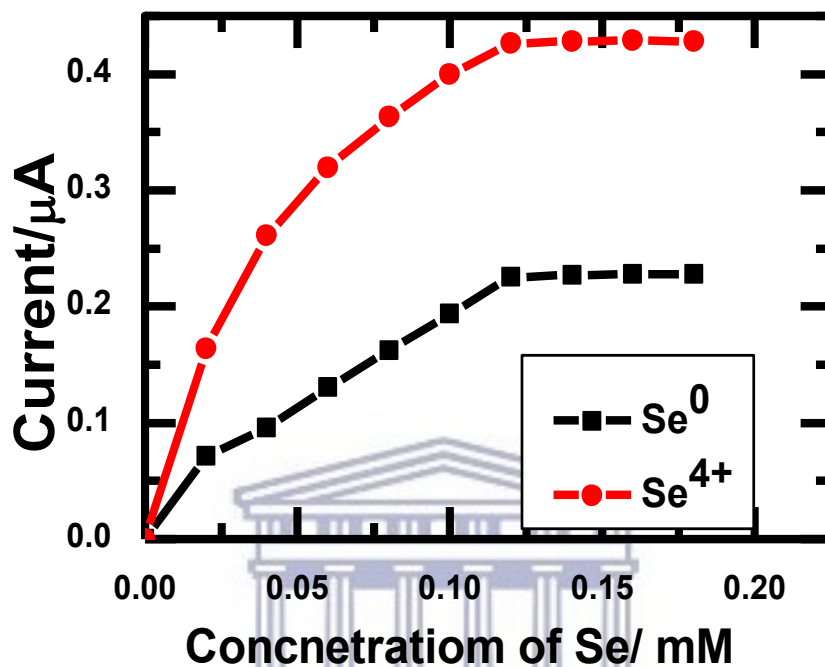


Figure 4.18: Influence of concentration of selenium on the peak current response at hydrogel interface in 1 M HCl vs Ag/AgCl

Various parameters were calculated from the plot including diffusion coefficient (D_e), limit of detection (LOD), and sensitivity (Table 4.8). The calibration plots confirmed higher sensitivity for selenium in the labile Se^{4+} state, with LOD and LOQ of 0.144 mM Se^{4+} and 0.433 mM Se^{4+} respectively.

Table 4.8: Summary of hydrogel performance sensor in the presence of selenium

	Peak 9 (Se^{4+})	Peak 10 (Se^0)
De	$3.028 \text{ e}^{-4} \text{ Cm}^2/\text{s}$	$1.869 \text{ e}^{-4} \text{ Cm}^2/\text{s}$
LOD	0.144 mM	0.097 mM
Sensitivity	$1.994 \text{ e}^{-4} \text{ } \mu\text{A}/\text{mM}$	$1.566 \text{ e}^{-4} \text{ } \mu\text{A}/\text{mM}$

Comparing Tables 4.5 and 4.8 it clear that vanadium detection is more sensitive to SPCE/HGL sensor than selenium. Vanadium mobility (diffusion coefficient) is three times faster than that of selenium. This can be due to size of the molecule also vanadium have two electrons in it out shell whereas selenium have six electrons. Therefore in terms of electron mobility vanadium will be the most favour because of it instability in the d orbital with only 3 electrons $[\text{Ar}] 3d^34s^2$. Whereas selenium's d and s orbital are filled $[\text{Ar}] 3d^{10}4s^24p^4$.

Hydrogel as adsorbent for selenium remediation

The adsorption capacities were determined at desired time intervals. Here a well know specific amount of hydrogel was place into a container containing a specific volume of selenium solution. An aliquot amount of selenium solution were collected every 5 minutes and analyzed by UV/Vis. A high adsorption rates are observed at the beginning (t_1), then slow and finally levels off after (t_{15}) minutes, implying that hydrogel have quite fast adsorption rate (Figure 4.19). Low value of adsorption capacity calculated here 0.559 mg/g was directly impacted by the low pH of the measurement. However further pH dependence was not evaluated here.

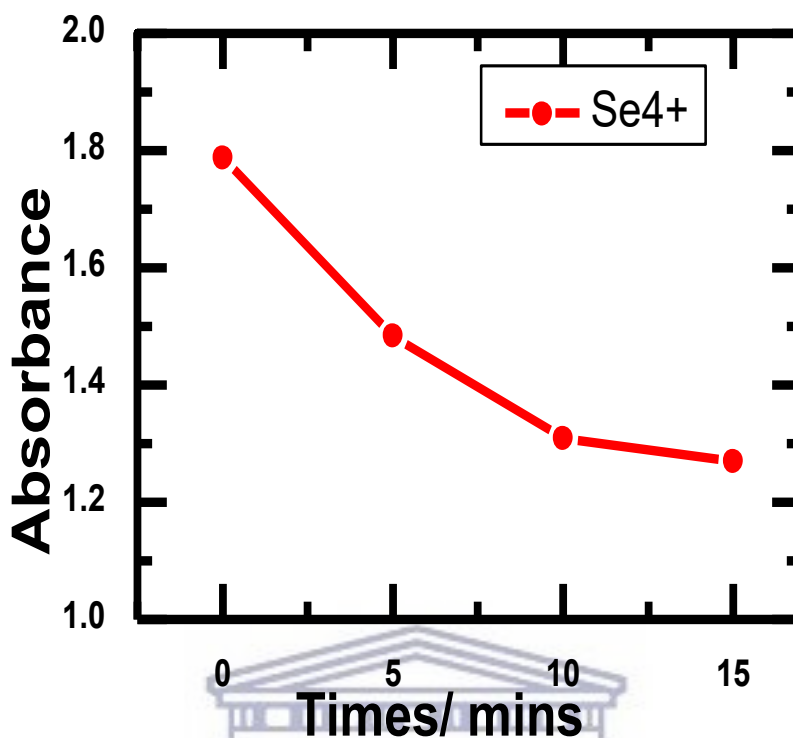


Figure 4.19: Effect of time on heavy-metal ions adsorption ($C_0 = 100 \text{ mg/L}$, $m = 0.5000 \text{ g}$, $V = 40 \text{ mL}$, $\text{pH}=6$, $T = 25^\circ\text{C}$)

Adsorption behaviour was also observed by SEM after electrochemical analysis, where by the selenium nanoparticles were not clearly distinguishable from the SPCE background signal in SEM (Figure 4.20a). However the EDS compositional analysis based on the detection of backscattered electrons, confirmed the presence of selenium as 10% weight percentage. Selenium proved to have small particles in a range of 100 - 200 nm which can be absorbed into the pore sized of hydrogel (Figure 4.21b). Hydrogel was seen to aggregate in large particles in the form of large globules. This was due to an increase in chain interaction compared to its stabilized particles in which the polymeric surfactant chains act as a limiting factor for such an interaction[1-2]. However no significant trace of selenium was found in the hydrogel imaging before electrochemical analysis (Figure 4.7b). However, the EDS analysis of hydrogel sensor after electrochemical response to selenium (Figure 5.20), revealed that selenium were entrapped and adsorbed onto the hydrogel matrix by 10%. This is an indication of hydrogel being an excellent adsorbent for selenium.

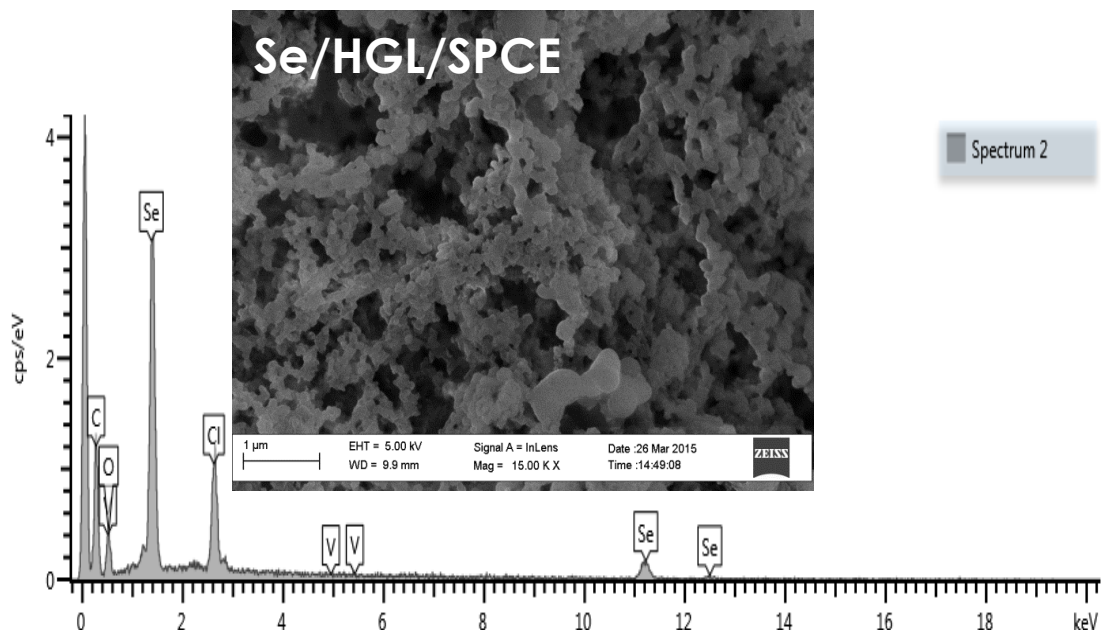


Figure 4.20: HR-SEM EDS image of (a) Selenium at SPCE, (b) Selenium at hydrogel interface after electrochemical analysis and dried for 24 hrs.

In conclusion polysulfone hydrogel was characterized by 2 well resolved redox peaks with a formal potential of 0.490 V and -0.510 V (vs Ag/AgCl). The diffusion coefficient for the hydrogel thin film electrodes in aqueous medium was calculated as 9.061×10^{-9} cm^2/s . Due to these superior properties, the hydrogel was applied as a sensor for the detection of vanadium and selenium. The chemical sensor favored Se^{4+} compared to Se^0 , in terms of sensitivity, diffusion coefficient, and LOD. A higher preference for detection of V^{2+} compared to V^{3+} was also demonstrated. Therefore, it is recommended that the V^{2+} and Se^{4+} species are used for quantitative determination at the hydrogel interface in aqueous systems. The results reported in this chapter provide evidence of the hydrogel being used as an excellent chemical sensor and excellent adsorbent for heavy metals. Vanadium and selenium redox behaviour are influenced by the nature of the transducer and are hampered by multiple redox peaks which are traditionally difficult to resolve. However guided by standard reduction potential Tables as well as a detailed stepwise analytical protocol,

unambiguous quantification is possible. The hydrogel can be used as a chemical sensor for direct detection of V^{2+} and Se^{4+} species at 0.189 mg/g and 0.559 mg/g respectively.



UNIVERSITY *of the*
WESTERN CAPE

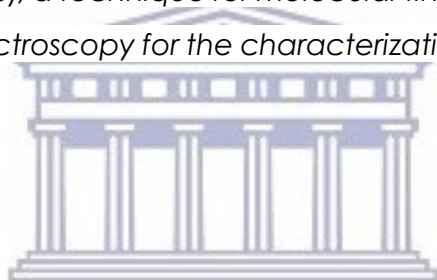
Chapter 5

Raman spectra of hydrogel biosensors

ABSTRACT

Raman spectroscopy has emerged as a useful tool for sensor and biosensor characterization. Characterization was based on the principle of surface-enhanced Raman spectroscopy (SERS), a technique for molecular fingerprinting. In this chapter we have used Raman spectroscopy for the characterization of the various stages of biosensors development.

5. INTRODUCTION



UNIVERSITY of the
WESTERN CAPE

Raman spectroscopy is used for observation of vibrational, rotational, and other low-frequency modes in a given system [158,159]. It is useful for characterization of molecular composition and sample structure [160,161]. Raman spectroscopy has been widely used in the study of biological samples to provide information regarding living cells over the last two decades [162]. A modified Raman spectroscopy called surface enhanced Raman spectroscopy (SERS) has been intensively reported as the way forward for nano-molecular analysis [159,160]. The difference between the conventional Raman (RS) spectroscopy and SERS is, in RS molecules are detected by their characteristic scattering of laser light but with low sensitivity. However, in SERS molecules are adsorbed through metal surfaces allowing the detection of single molecules [163]. Unfortunately, the mechanism of enhancement is strongly dependent on the combination of surface and target

molecule. In this chapter we demonstrate the use of Raman spectroscopy to characterize and follow the steps of the biosensor construction.

5.1. PRINCIPLE OF RAMAN

Raman can be classified as a non-destructive technique used to study the interaction of the photons of a monochromatic source of light (laser) with molecules of the sample. Raman spectroscopy measures the adsorbed light and part of the light are diffuse and the diffused light can be classified into two categories such as: Rayleigh diffusion and Raman diffusion. Rayleigh diffusion is an approximation of scattering of light off of the molecules. Which can be extended to scattering from 1 to 100000 photons without a change in energy of particles. Raman diffusion is defined as an inelastic scattering of a photon by molecules which are excited to higher vibrational or rotational energy levels from 1 to 1000000 photons with a little loss of energy. Raman diffusion can be classified into two subcategories called stokes and anti-stokes scattering (Figure 5.1).

- **Stokes scattering:** is if the energy of the diffused photons is weaker than the incident photon or material absorbs energy and the emitted photon has a lower energy than the absorbed photon.
- **Anti-stokes scattering:** is if the energy of the diffused photon is greater than the incident photon or material loses energy and the emitted photon has a higher energy than the absorbed photon.

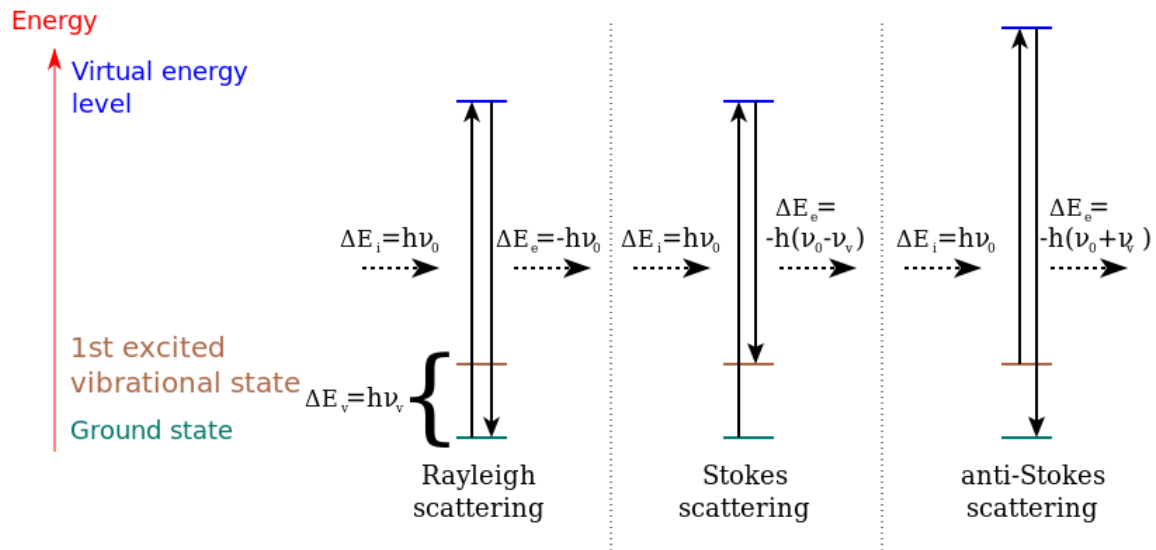


Figure 5.1: Different possibilities of light scattering

5.2. PARTS OF RAMAN SPECTROMETER

A typical Raman spectrometer has three main components: an excitation source, a sampling apparatus and a detector. However over the years the components came in different forms. The modernized Raman instrument uses a laser as source of light, spectrometer as detector and microscope for sample analysis. For sample analysis the laser beam goes through a channel called travel in Raman spectrometer. The laser beams goes through two filters interferential and density filters. Interferential filters were used to clean the laser beam at $\pm 2\text{nm}$ and density filters to decrease the power of the laser beam going through the sample and prevent sample degradation. The beam will now reach the microscope which is used for focal changing and examination of the working distance. The beam reached the sample and generate secondary electrons. The electrons will be collected by the objects and sent to the edge filters (beam splitter) allowing the separation of the Raman part and the laser part. This it will further pass through the focusing lens and spectrograph which are used to separate the different

wavelengths of the Raman signal and finally it will reach the charged coupled device (CCD) (Figure 5.2).

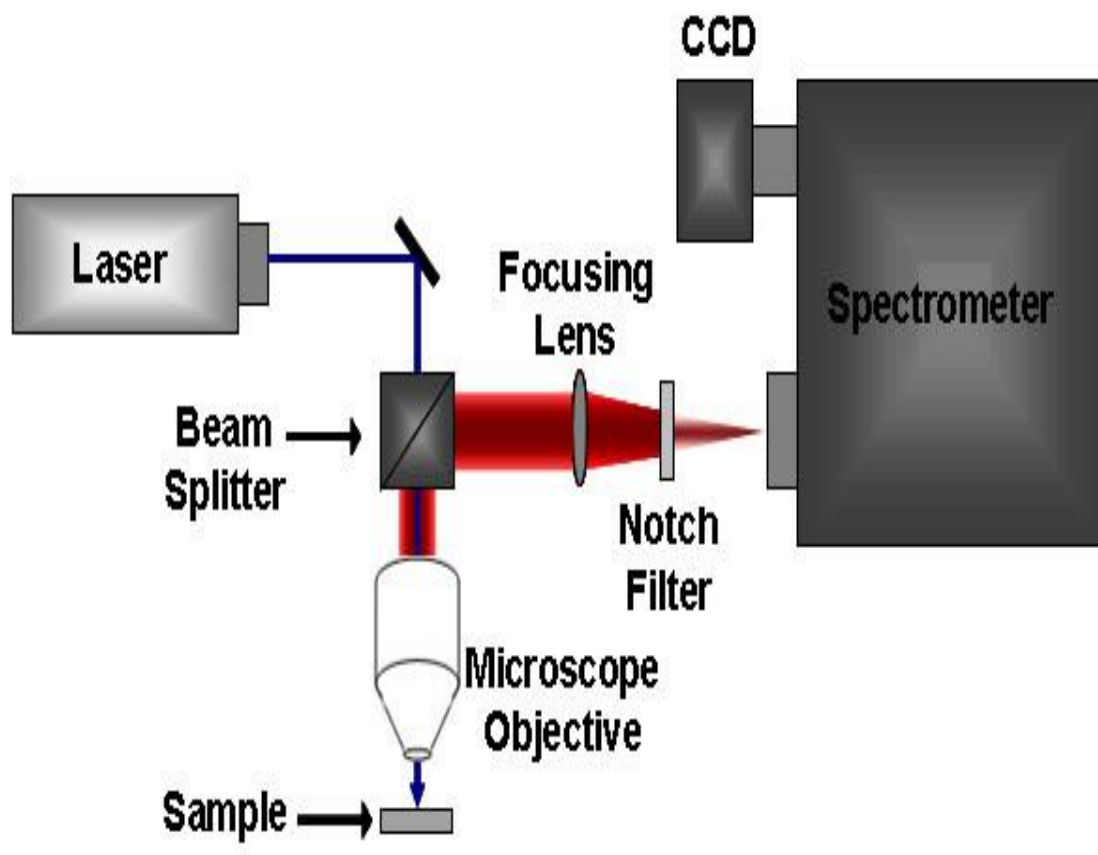


Figure 5.2: travel in the Raman spectrometer

5.3. EXPERIMENTAL

The experiments were performed by using the XploRA HORIBA model Edge filter with a gratings 600 - 2400 lines/mm. Backscattering geometry wavelengths were 532 nm and 676 nm. Raman spectrometer was coupled to a confocal microscope (adjustable pinhole) and motorized XYZ Table (0.1 μm steps). In this work parameters were adjusted based on the type of material used.

System parameters

All samples were analyzed at 523 nm laser, interference and density filters were set at 100% and slit at 100. The gratings were also set at 1200T and the acquisition time varied from time to time depending on sample. In order to select an appropriate area of the sample to be analyzed the video camera and white lamp reflection were used. Initially the 10x magnification object was used for positioning, followed by second 100x Olympus objective having the same focus. The point of focus was optimized by using the reflected white light (WL). The spectra were recorded by measuring the reflection of secondary electrons generated by the laser.



Figure 5.3: Image of XploRA HORIBA Raman spectroscopy

Sample preparation

Two different electrodes were used screen printed carbon electrode (SPCE) and gold electrode (AuE) in the development of the final biosensors. SPCE was used for the characterization of polysulfone and polysulfone hydrogel. Au electrode was used for the construction of the biosensors. The hydrogel was also prepared at the Au electrode to draw on the benefit of surface enhancement from Au material in Raman spectroscopy. The hydrogel electrode (SPCE/HGL) and polysulfone electrode (SPCE/PFS) were prepared by drop coating 10 μL of PSF and HGL respectively at SPCE. Au/HGL electrode was then further modified with alkaline phosphatase (ALP) and selenoprotein p (SePP) respectively to produce Au-HGL/ALP biosensor and Au-HGL/SePP immunosensor. These biosensors were allowed to dry for 24 hrs before Raman analysis.

5.4. RESULTS AND DISCUSSIONS

Polysulfone structure is made of 6 carbon atoms joined together, methyl, ester and sulfonate group. The Raman spectrum of PSF showed no peaks associated with sulphone, however; G and D band (1405 cm^{-1} and 1544 cm^{-1}) associated with C-bond was observed. The peak at 500 cm^{-1} was associated with the silicon of the glass slide which was used as sample holder. The G band in the spectrum is due to the bond stretching of all pairs of sp^2 atoms in both rings. And the D band peak is due to the breathing modes of sp^2 atoms in rings. Incorporation of a conductive polymer such as polyvinyl alcohol (PVA) could only enhance the conductivity of the PSF. The synthesized PSF-hydrogel showed an increased in peak intensity which was associated with PVA incorporation and enhance PSF signal (Figure 5.4).

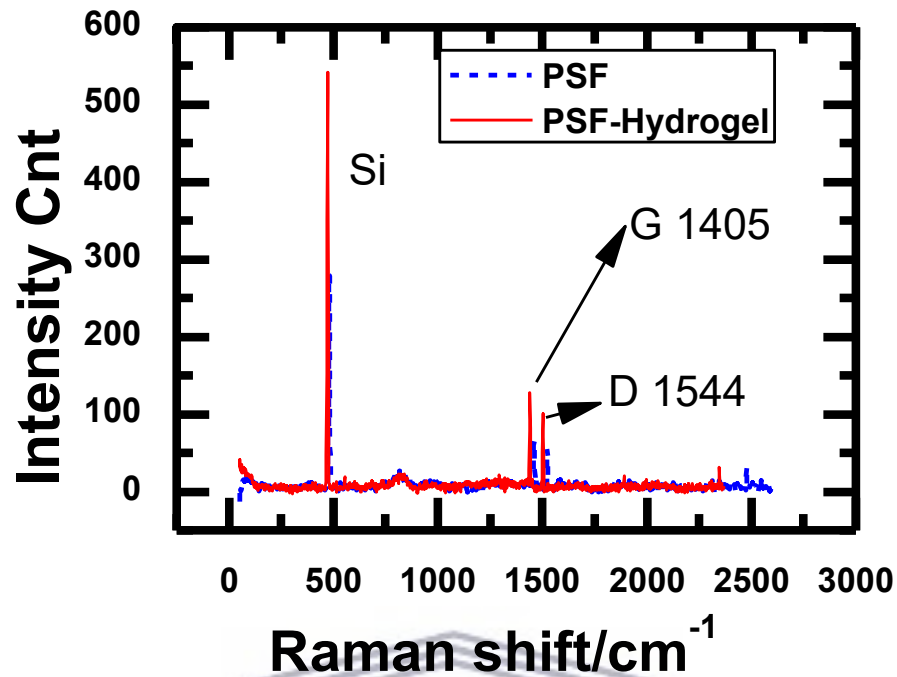


Figure 5.4: Raman spectrum of PSF and PSF-hydrogel at SPCE

5.5. CHARACTERIZATION OF AU-HGL/ALP BY RAMAN SPECTROSCOPY

The Raman spectra of Au-HGL sensor and Au-HGL/ALP biosensor are represented in (Figure 5.5). The spectrum of Au-bare electrode provided no peaks associated with the gold metal (Figure 5.5). Most metals are Raman inactive except for some metal nanoparticles which enhance the Raman scattering signal e.g. (gold, silver and nickel) [130,164]. Modifying the Au electrode with hydrogel produced two broad peaks within the region 1000-1800 cm⁻¹ and 2400-3000 cm⁻¹ which were associated with C-C in aromatic ring chain vibrations and C-H and S-H respectively [164].

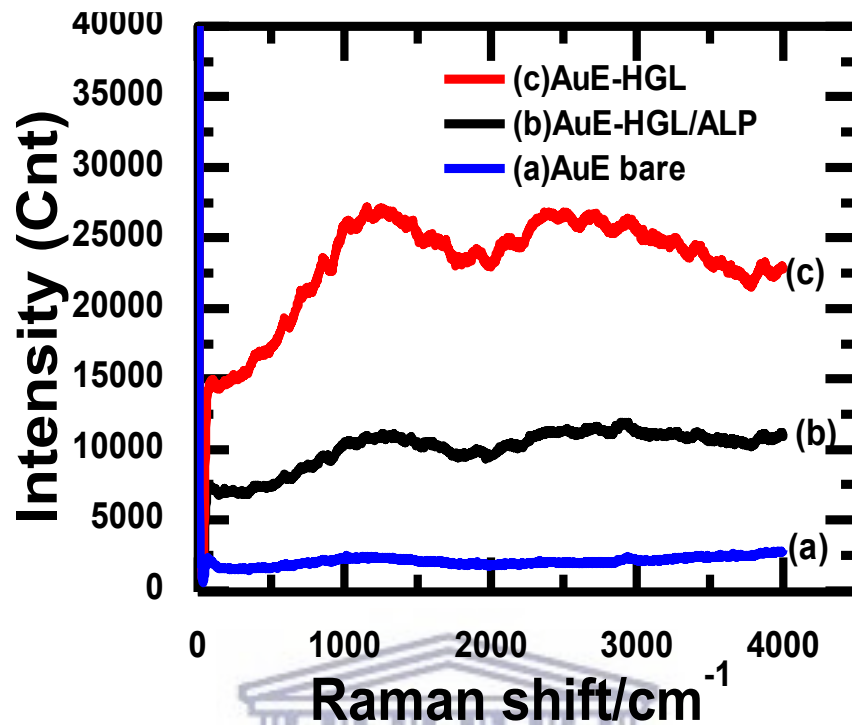


Figure 5.5: Raman spectra of (a) Au-electrode, (b) hydrogel electrochemical deposited at gold electrode (AuE-HGL) and alkaline phosphatase incubated to the hydrogel interface (AuE-HGL-ALP)

The spectrum associated with incorporation of ALP onto the Au-HGL showed no peak associated with ALP but a decrease in AuE-HGL spectrum was observed. The decrease was due to the presence of ALP within the hydrogel structure by suppressing the hydrogel matrix spectrum [129]. No chemical interaction between the ALP and the gold surface was expected, since the HGL forms an encapsulating layer around the ALP. The reduction in peak intensity in the spectrum of Au-HGL/ALP compared to Au-HGL spectrum, in consistence with a densified HGL/ALP layer is due to incorporation of enzyme within hydrogel matrix (Figure 5.6).

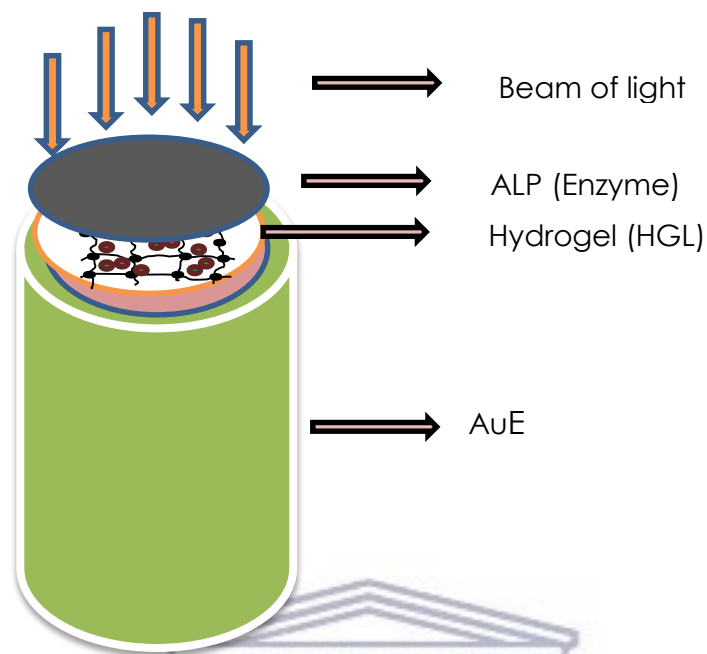


Figure 5.6: Representation of electrode modification

5.6. CHARACTERIZATION OF AU-HGL/SePP BY RAMAN SPECTROSCOPY

The immunosensor prepared by incubation of Au-HGL electrode in selenoprotein p antibody solution was very difficult to dry (chapter 7 p163). Au-HGL/SePP sample showed a peak at 850 cm^{-1} which was associated with C-O-H in glycerol present in the antibody (Figure 5.7). The result also showed a decrease in Raman signal intensity of the AuE-HGL spectrum, as observed with ALP incorporation.

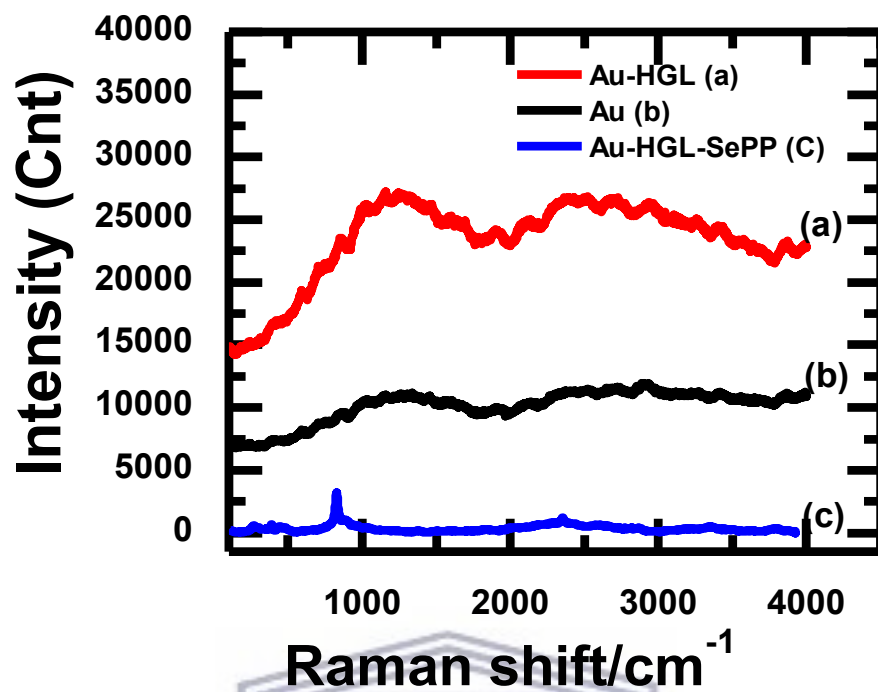


Figure 5.7: Raman spectra of (a) hydrogel electrochemical deposited at gold electrode (AuE-HGL), (b) Au-electrode, and (c) Selenoprotein p antibody incubated to the hydrogel interface (AuE-HGL-SePP)

5.7. CONCLUSION

Raman spectroscopy (RS) has shown some advantages for the characterization of biosensors constructed in this work. The use of Au electrode in sample analysis amplified the observed Raman signal significantly up to 250 times comparing SPCE/HGL and Au-HGL. The spectra for the presence and composition of the hydrogel was characterized by a broad peak associated with the delocalized double bond within the ring of the hydrogel. As well as a second broad peak for CH and SH out of the ring structure. The introduction of the bio-element in both cases, produced no new peaks but effectively suppressed the hydrogel spectrum due to carbon network densification.

Chapter 6

Au-HGL/ALP biosensor for vanadium detection

ABSTRACT

A biosensor is an electroanalytical device used for selective qualification and quantification of an analyte in aqueous medium. The Au-HGL/ALP biosensor for the detection of vanadium was based on alkaline phosphatases (ALP) inhibition. The sensor was evaluated using electrochemical techniques such as voltammetry, amperometry, and electrochemical impedance spectroscopy. ALP showed a strong electrochemical response at both GCE and AuE modified with hydrogel.

Muya, F.N, Phelane, L. Baker P and Iwuoha E (2016), selectively functionalized polysulfone hydrogel biosensors for vanadium and selenium detection. Paper presented at the international society of electrochemistry (ISE) 67th conference, The Hague Netherlands 21-27 August 2016, Viewed on the 22 august 2016.

6. INTRODUCTION

The enzymatic electrochemical biosensors for detection of vanadium based on the inhibition principle has been applied for a wide range of toxic analytes such as derivatives of insecticides [165], glycoalkaloids [165,166] and heavy metals [167]. The analytical detection was based on their excellent performance capabilities in terms of selectivity and sensitivity of the biosensor [168]. ALP is widely used as a conjugated enzyme for inhibition processes due to its high turnover number and range of application [169]. The direct electron transfer between an electrode and a redox enzyme is very crucial for the fundamental studies and the construction of

biosensors. However, because of the unfavorable orientation of the ALP on a bare gold electrode surface and adsorption of impurity that denature it. Surface modification using a suitable compatible matrix such hydrogel are known to provide a favorable micro-environment for the protein to exchange electrons directly with gold electrode. Biosensor was developed by electrode deposition of hydrogel polymer onto the gold electrode surface (Au-HGL), followed by incubation of the ALP to the hydrogel layer resulting in Au-HGL/ALP biosensor. The Au-HGL/ALP biosensor were studied, optimized and applied to vanadium and Centrum for electrochemical evaluation.

6.1. EXPERIMENT

The commercialized bovine intestinal mucosa alkaline phosphatase, buffered in aqueous glycerol solution $\geq 5,500$ DEA units/mg protein was purchased from Sigma Aldrich and diluted to a molar ratio of 1:10 in 10 mM Tris-buffer-1% BSA. The UV-vis spectra were recorded on Nicolet Evolution 100 Spectrometer (Thermo Elctron Corporation, UK). Aliquots 10 μ L of Alkaline phosphatase solution (ALP) was placed in 4 cm³ quartz cuvettes containing 3 mL of 10 mM Tris buffer solution pH 7.2 and It UV-vis spectra were recorded. The spectra were recorded in a region of 200 nm to 500 nm. Spectra showed an absorbance peak at 240 nm (Figure 6.1) which was associated with ALP in solution based on literature [170]. Also an increase in the absorbed peak was observed as ALP concentration increases.

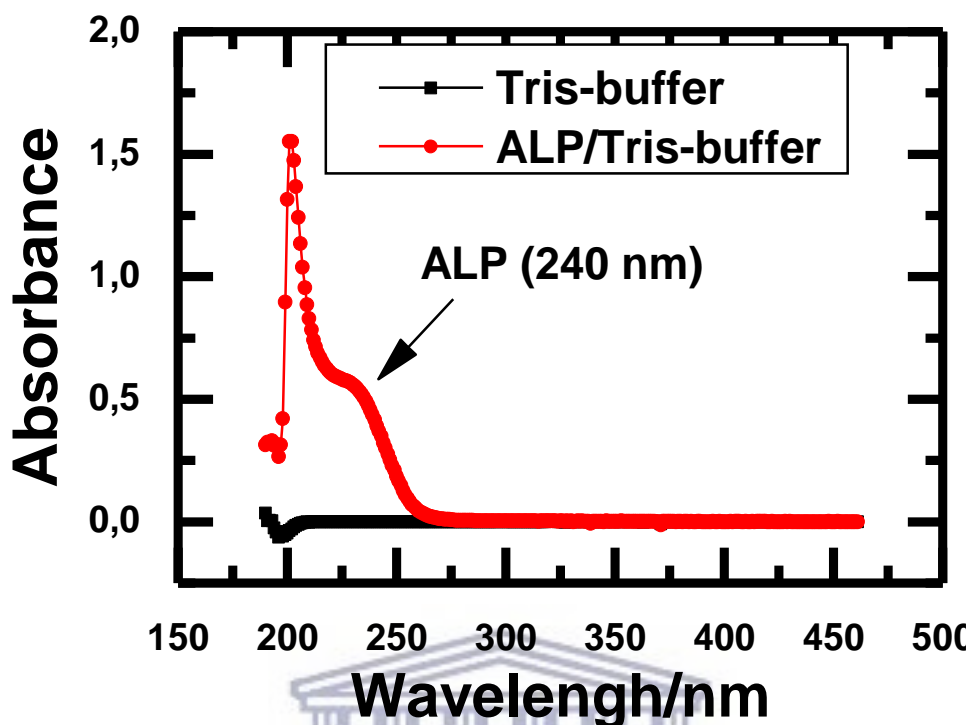


Figure 6.1: UV-vis of ALP in 10mM Tris-buffer solution

6.2. ELECTROCHEMICAL RESPONSE OF ALKALINE PHOSPHATASE AT GLASSY CARBON ELECTRODE

The electrochemical activity of ALP at glassy carbon electrode (GCE) was investigated by cyclic voltammetry in a three electrodes cell. GCE was connected as working electrode, with Ag/AgCl as reference and 1 mm Pt wire as counter electrode. The electrolyte used was 3 mL of 10 mM Tris buffer solution to which 10 μ L of ALP was added once off. The characterization was done by cyclic voltammetry and the electrode was scanned from -1.500 V to 1.000 V at scan rates of 50 mV/s. CV of ALP in solution showed a strong electrochemical affinity with GCE represented by a reduction peak A' at -0.854 V (Figure 6.2). The peak was irreversible and grew in peak intensity with successive addition of ALP.

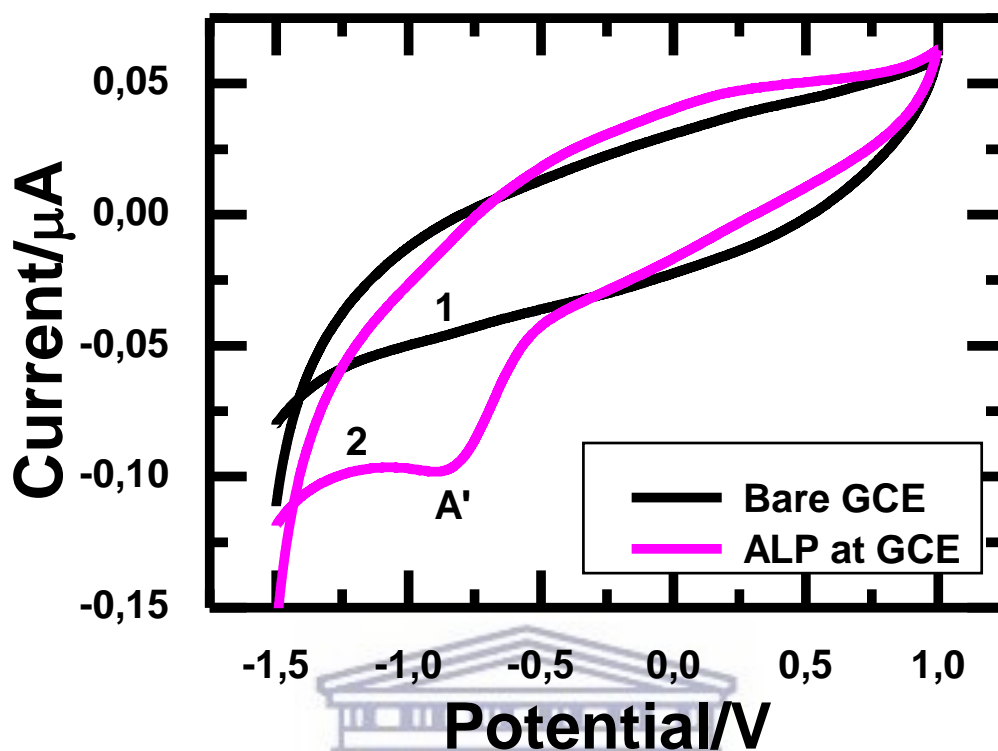


Figure 6.2: CV of (1) bare GCE in Tris-Buffer pH 7.9 at scan rate of 50 mV/s and (2) with 10 μ L ALP added to the buffer at GCE.

6.3. ELECTROCHEMICAL DEPOSITION OF HYDROGEL AT GOLD ELECTRODE

A gold electrode (Au) has proven to have a strong affinity with polysulfone hydrogel compared to a carbon electrode. Polysulfone hydrogel are sulfonate based polymer material. The electrochemical deposition was done in three electrodes cell system. Au electrode was connected as working electrode, with Ag/AgCl as reference and 1 mm Pt wire as counter electrode. The electrolyte used was 4 mL of 2 M HCl solution to which 1 mL of HGL solution was added once off. The deposition was achieved by cycling the potential repeatedly (10 cycles) within a window ranging from -0.2 to 0.8 V at 50 mV/s. The cyclic voltammograms for the deposited hydrogel film on Au electrode surface (Au-HGL) are presented in (Figure 6.3).

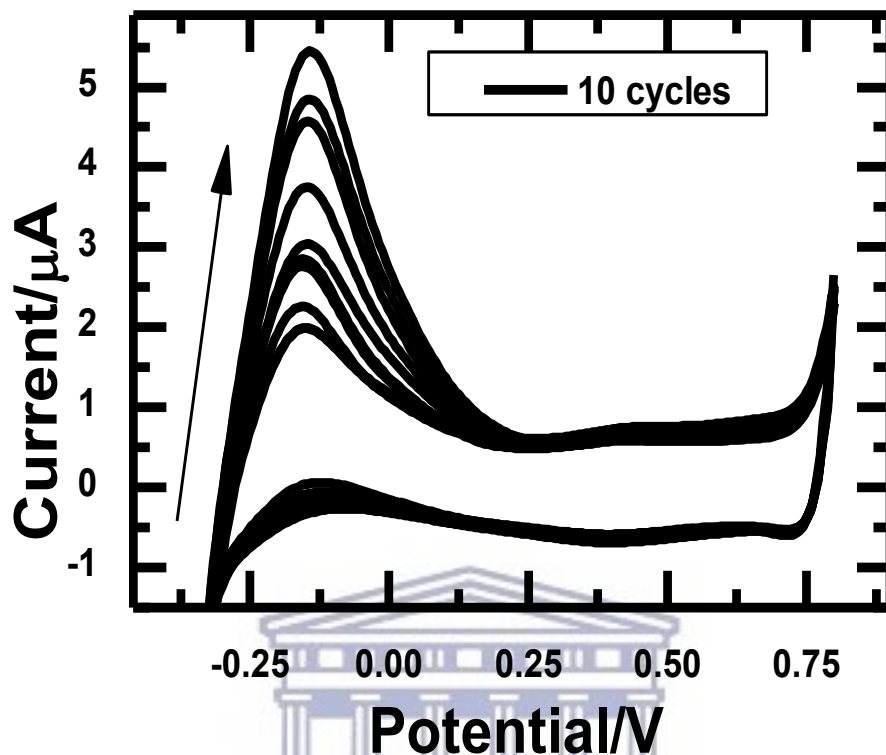


Figure 6.3: Electrochemical deposition of Hydrogel onto Au (10 cycles) in 0.2 M HCl vs Ag/AgCl

Sulfonate affinity to Au was observed at -0.150 V (Figure 6.3), which showed a growth in polymer as a function of number of scan. This was an evidence of HGL being electrochemically deposited at Au electrode to produce Au-HGL electrode based on chemical bond formation between gold and Sulfur.

Electrochemical characterization of hydrogel thin film in hydrochloric acid

Scan rate dependence was used to characterize the deposited hydrogel at the gold electrode. After the deposition the hydrogel electrode was removed rinsed and returned to a fresh HCl solution and then investigated by CV within the potential window ranging from -0.5 V to 1 V at scan rates varying from 50 mV/s to 500 mV/s.

The change in scan rate showed an increase in amplitude of the reduction peak B at -0.150 V with repeated potential scans (Figure 6.4).

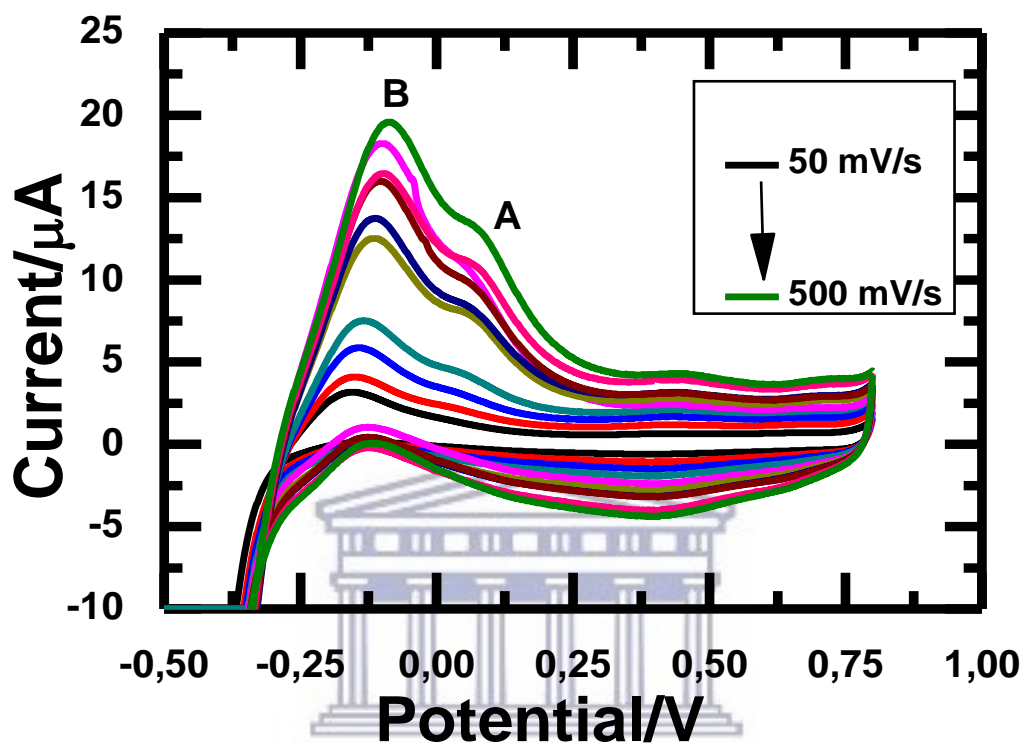


Figure 6.4: Characterization of the deposited polysulfone Hydrogel unto Au electrode in fresh 0.2 M HCl vs Ag/AgCl

This electrochemically deposited film played two important roles in the biosensor system. Firstly, it behaved as an electron mediator, transferring electrons between the immobilized enzyme and Au electrode surface. Secondly, it served as a point of attachment for the enzyme (alkaline phosphatase). Moreover, this increase in the amplitude of the peak B confirms that the diffusion of the electrons was taking place within the hydrogel thin film matrix. The scan rate dependent behavior supports the conclusion of electron mobility and diffusion within a surface bond thin film. Randle Sevčik plot was used to calculate electron mobility as electron diffusion. The plot of the cathodic current (I_{pc}) as a function of the square root ($v^{1/2}$) showed an increase in peak current with an increase in scan rate (Figure 6.5).

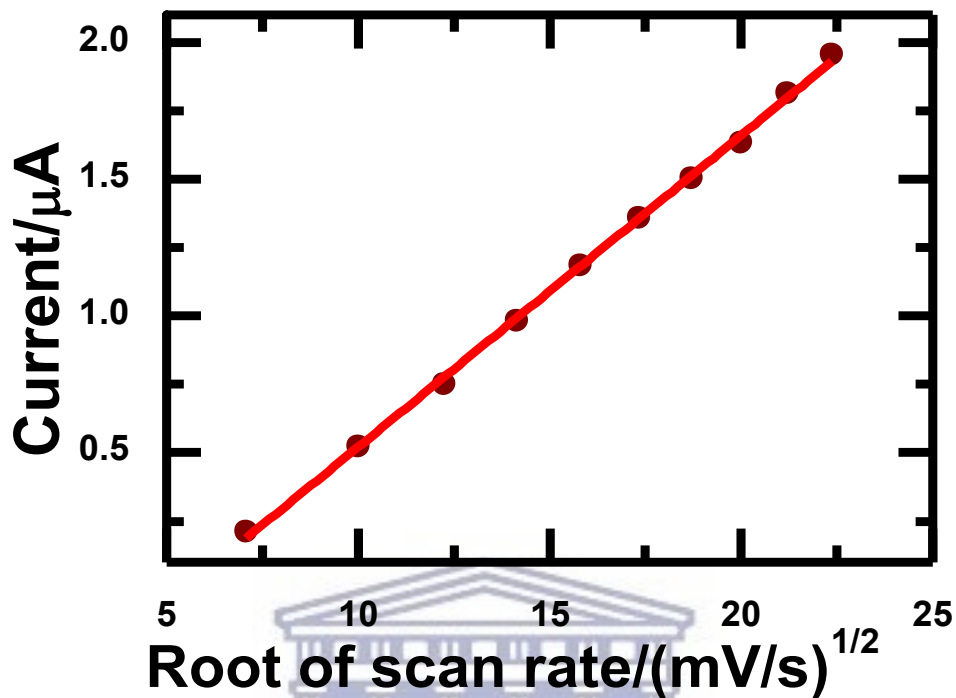


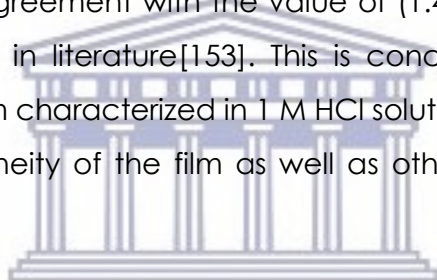
Figure 6.5: Randle Sevcik plot of peak current versus root of scan rate in 0.2M HCl Ag/AgCl obtained after electrochemical characterization of HGL/Au

A straight line was observed for the peak current plot as a function of square root of scan rate. This confirmed that the cathodic peak current arising from the electron propagation at hydrogel interface was diffusion controlled at $1.549 \times 10^{-4} \text{ cm}^2/\text{s}$. The surface concentration of the adsorbed electroactive hydrogel film was estimated from the plot of the peak current as function of scan rate using Brown-Anson model and was calculated to be $7.281 \times 10^{-10} \text{ M}$. The Randle-Sevcik equation was used to determine the rate of electron transport within the hydrogel matrix. Diffusion coefficient (D_e) was evaluated from the slope of the straight line obtained from the $i_{p,a}$ vs $v^{1/2}$ plot (Figure 6.5). The calculated results are shown in (Table 6.1).

Table 6.1: Kinetic parameters of Polysulfone hydrogel film deposited at Au electrode in 0.2M HCl

	Value	Deviation from linearity
Intercept	-0.618	0.021
Slope	0.114	0.001
R ²	0.999	
Diffusion coefficient (De)	1.549 x 10 ⁻⁴ cm ² /s	
Surface concentration	7.281×10 ⁻¹⁰ M	

De value obtained is in agreement with the value of (1.425 x 10⁻⁴ cm²/s) that has been reported previously in literature[153]. This is concerning a similarity of the electroactive hydrogel film characterized in 1 M HCl solution. De value depends on the density and homogeneity of the film as well as other conditions for growing polymer.



UNIVERSITY of the
WESTERN CAPE
pH 7.9

Electrochemical characterization of hydrogel thin films in 1% BSA-Tris buffer

Tris-buffer is an organic compound with the formula (HOCH₂)₃CNH₂ used for biosensor investigation due to its biological compatibility and physical properties [171,172]. The characterization of the Au-HGL in different electrolyte (HCl and Tris-buffer BSA) showed two completely different voltammograms. The difference in voltammogram was due to the ionic size and ion mobility of the two solutions. After the electrochemical deposition of hydrogel onto the Au electrode (Au-HGL). The Au-HGL electrode was rinsed and placed into a 3 mL of 10 mM Tris buffer solution pH 7.2 solution and connected as working electrode in a three electrodes cell, with Ag/AgCl as reference and 1 mm Pt wire as counter electrode. Cyclic voltammetry

was applied to the Au-HGL electrode by scanning the potential from -0.5 V to 1 V at scan rates varying from 10 mV/s to 400 mV/s (Figure 6.6).

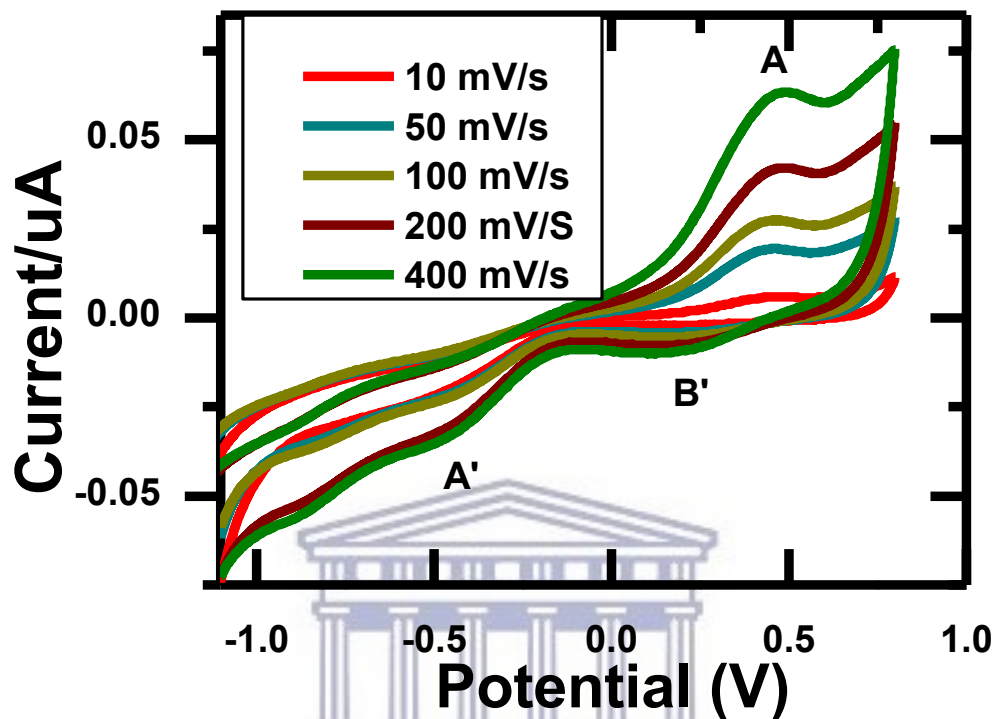


Figure 6.6: Characterization of Au-HGL in 1%BSA, 10mM Tris-buffer pH 7.9 vs Ag/AgCl

A well-defined voltammogram was observed in 1% BSA, 10 mM Tris buffer solution (Figure 6.6). Au-HGL electrode in 0.2 M HCl presented one reduction peak at -0.150 V whereas in the BSA/Tris-buffer a reversible couple peaks A/A' at 0.475 V and -0.495 V respectively was observed. The redox process observed depends on charge density and molecular size of the buffer solution. BSA/Tris-buffer contains large molecules that act as tiny conductive centers facilitating the transfer of more electrons to the hydrogel interface (Figure 6.6). Whereas the monovalent HCl (one electron transfer) displays a single peak at the Au/HGL interface (Figure 6.3).

6.4. IMMOBILIZATION AND CHARACTERIZATION OF ALKALINE PHOSPHATASE (ALP) ONTO AU/HGL ELECTRODE.

Detection of ALP in solution at AuE-Hydrogel

The direct electron transfer between an electrode and redox enzyme is very important for the fundamental studies and the construction of biosensors. An enzyme often exhibits sluggish electron transfer at conventional electrode surface. Therefore electrode surface modification using suitable compatible matrices would provide a favorable micro-environment for the protein to exchange electrons directly with the electrode. Here the electrochemical response of ALP to Au-HGL electrode was investigated by cyclic voltammetry in a three electrodes cell. The Au-HGL electrode was placed in 3 mL of 10mM Tris buffer solution and connected as working electrode, with Ag/AgCl as reference and 1mm Pt wire as counter electrode. Cyclic voltammetry was applied to the Au-HGL electrode by scanning the potential from -1.2 V to 0.8V at 50 mV/s (Figure 6.7).

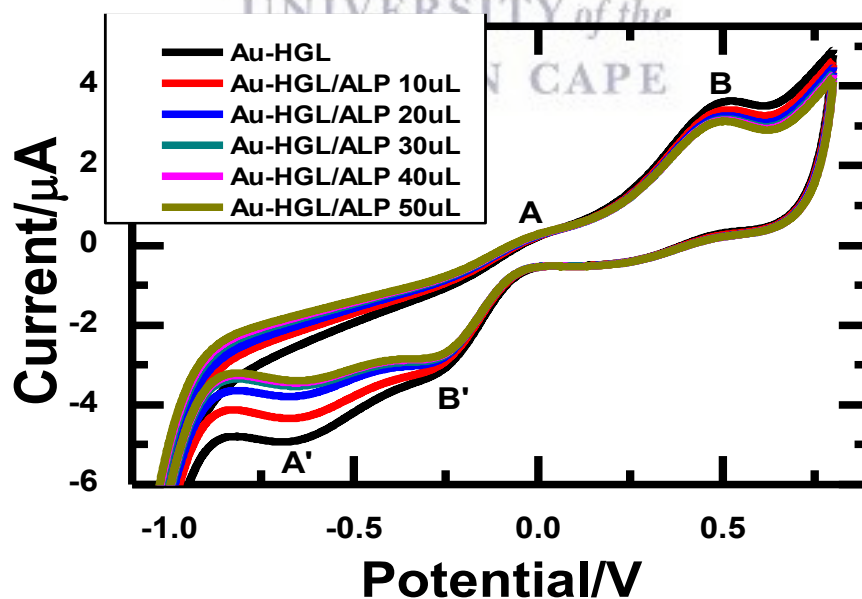


Figure 6.7: Au-HGL response to ALP in solution

Aliquots amount of ALP was added to the solution until the peak current associated with ALP at -0.650 V reached a maximum and stabilized. CV of ALP at Au-HGL electrode showed two irreversible redox couples A/A' and B/B' at -0.046 V/ 0.485 V and -0.673 V/0.240 V respectively (Figure 6.7). Irreversibility was confirmed by a peak separation according to equation 3.2. The redox couple at A/A' was associated with ALP affinity at hydrogel interface and the redox couple at B/B' was associated with hydrogel film.

Immobilization of ALP onto the Au-hydrogel by Incubation

Various methods have been reported for immobilization of enzymes onto transducers such as adsorption, covalent binding, incubation, entrapment and membrane confinement [173]. Incubation requires a material with surface density of binding sites together with the volumetric surface area sterically available to the enzyme to determine the maximum binding capacity. The actual capacity will be affected by the number of potential coupling sites in the enzyme molecules and the electrostatic charge distribution and surface polarity (i.e. the hydrophobic-hydrophilic balance) on both ALP and hydrogel. The nature of hydrogel has showed considerable effect on ALP which is expressed in terms of activity and kinetics. The incubation time was investigated by SWV in order to predict the optimum time required for ALP immobilization (Figure 6.8).

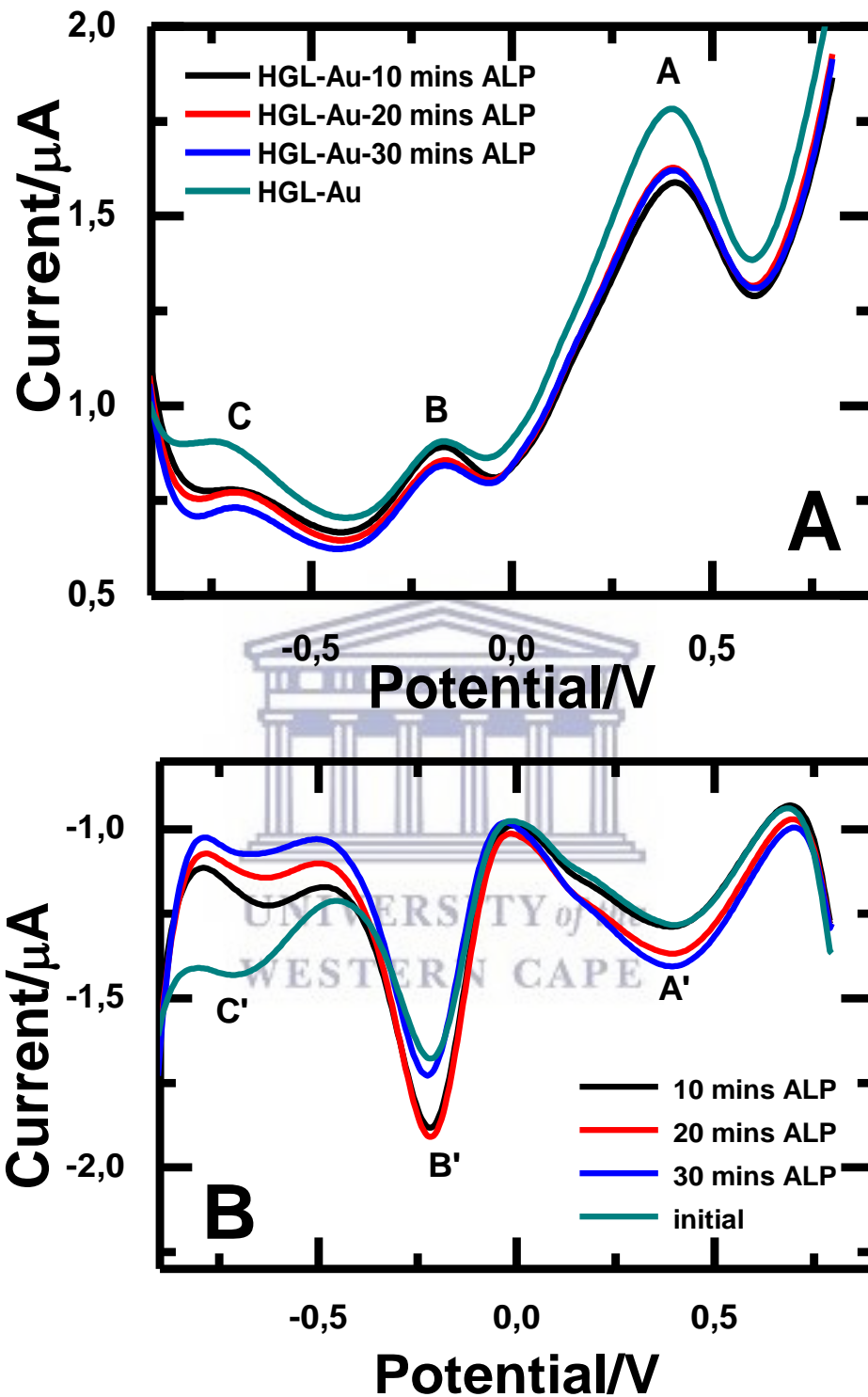


Figure 6.8: SWV of Au-HGL/ALP biosensor at different incubation time interval by (A) oxidation and (B) reduction

SWV showed two major redox couples peaks A/A' and B/B' observed at 0.450 V and -0.200 V. The redox couples A/A' and B/B' are characteristic of hydrogel material. The redox couple C/C' with formal potential of -0.850 V was observed at each addition of ALP solution (Figure 6.7). A small deviation in peak current as a function of time was observed (RSD=7.12%, Table 6.2). Finally 30 minutes incubation time was selected to ensure effective incubation and minimum physical interference effects in the preparation of Au-HGL/ALP biosensors.

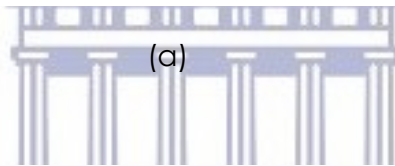
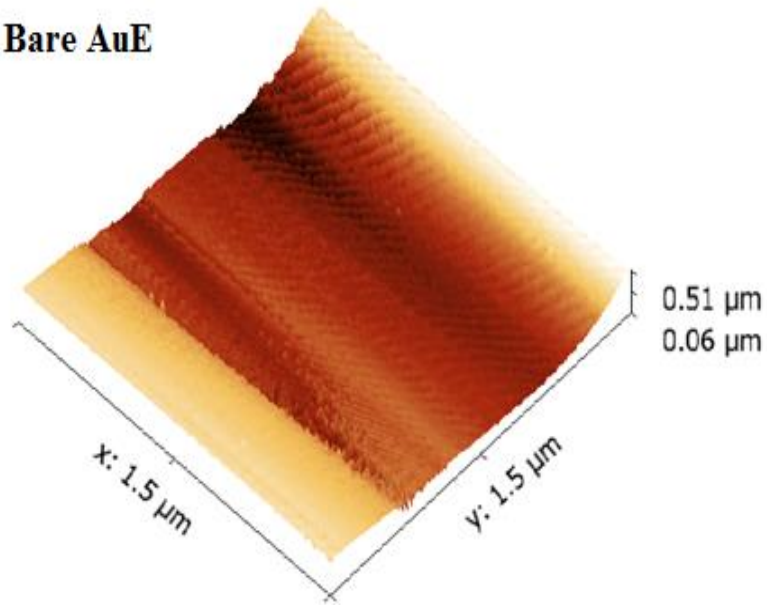
Table 6.2: Analytical parameters of ALP incubation time

Incubation time (minutes)	Current response (μA)	STD (μA)	% RSD
10	1.227	0.067	7.12
20	1.151		
30	1.064		

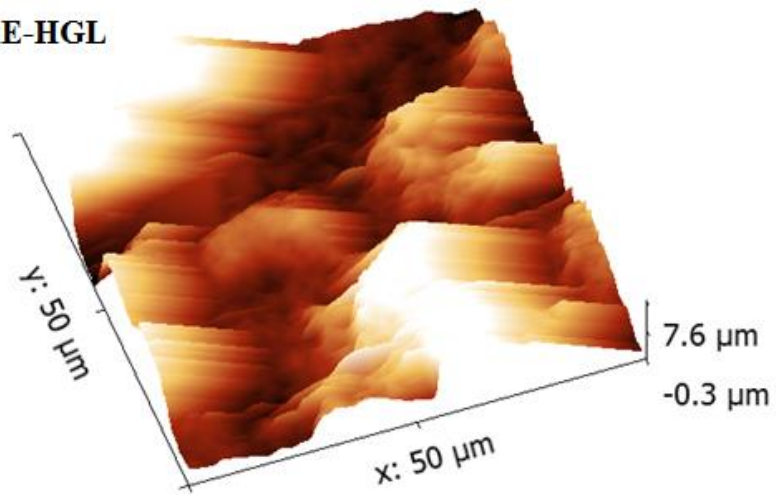
6.5. MICROSCOPIC CHARACTERIZATION OF ALP-HGL BIOSENSOR BY ATOMIC FORCE MICROSCOPY (AFM)

The atomic force microscopy (AFM) is a microscopic technique dedicated to nanoscale surface characterization [174–176]. In this work AFM was used to characterize the topographic behaviour of Au electrode, Au-HGL and Au-HGL/ALP film. The obtained topography image links to the measured height values, for a given area. The results were analyzed using Gwydion software and reported in terms of topographic image, surface roughness and height distributions. The AFM images below (Figure 6.9) show a smooth surface for the Au electrode, globular clustering for HGL and smoother surface topographic after incubation with ALP (Figure 6.9).

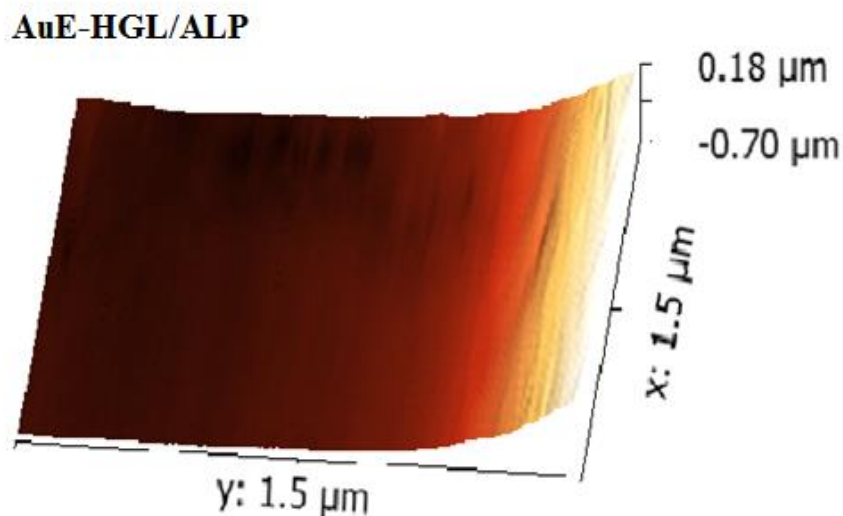
Bare AuE



AuE-HGL



(b)



(c)

Figure 6.9: AFM images of (a) Bare AuE, (b) AuE-HGL and (c) AuE-HGL/ALP

The amplitude parameters such as average surface roughness (Ra), mean square roughness (Rq) and surface area are the principal parameters generated by the surface in characterizing the surface topography (Table 6.3). The average surface roughness (Ra) and the root mean square roughness (Rq) were used to study the changes in electrode modifications.

Table 6.3: Analytical parameters of AuE, HGL and ALP derived from AFM image

Parameters	Bare AuE	AuE-HGL	AuE-HGL/ALP
Average value	271.7 nm	3.468 μm	498.9 nm
Ra	79.0 nm	1.910 μm	152.6 nm
Rms /Rq	92.7 nm	2.260 μm	204 nm
Surface area	6.081 μm ²	3.956 μm ²	3.308 μm ²

The trends in calculated values for Ra, Rq and surface area are consistent with the observed topography trends and provides a quantitative measure of the effect of the stepwise modification. The surface area of the Au electrode is significantly increased by modification with hydrogel material and the increased surface area of the Au-HGL electrode provides an efficient and biocompatible counterface for enzyme entrapment (Figure 6.10). This trends is in agreement with electrochemical results obtained from cyclic voltammetry as well as Raman spectroscopy.

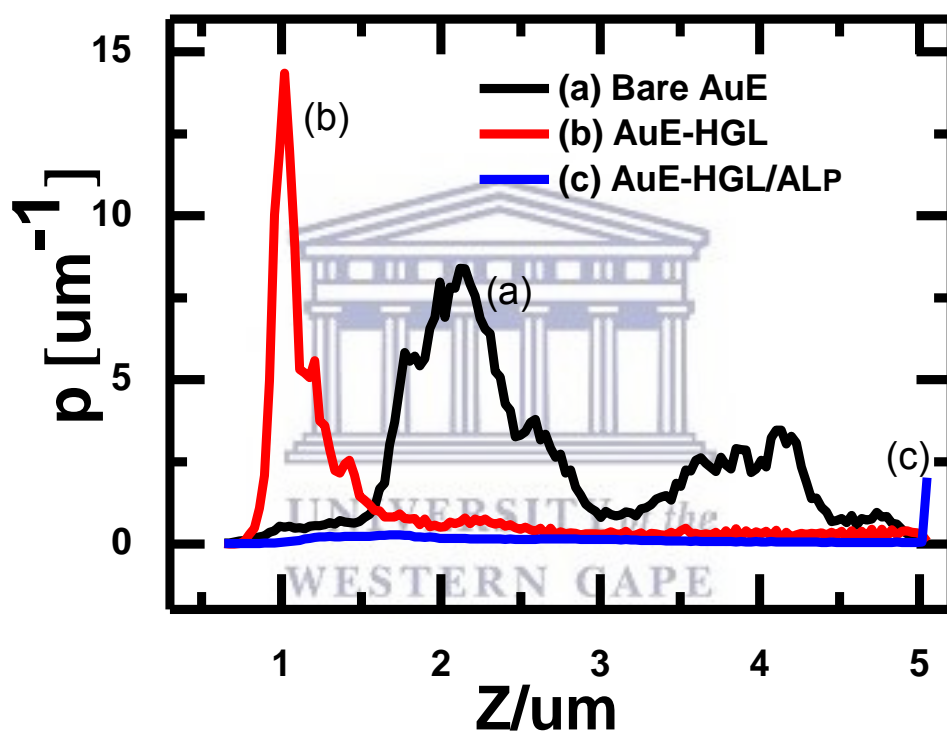


Figure 6.10: AFM height distribution of (a) Bare AuE, (b) AuE-HGL and (c) AuE-HGL/ALP

6.6. OSTERYOUNG SQUARE WAVE SPECTROSCOPY OF AUE-HGL/ALP BIOSENSOR RESPONSE TO VANADIUM

The response of AuE-HGL/ALP biosensor to vanadium concentration was investigated by SWV. The Au-HGL/ALP biosensor was placed in 3 mL of 10 mM Tris buffer and connected as working electrode in a 3 electrodes cell, with Ag/AgCl as reference and 1 mm Pt as counter electrode. Single sweep oxidative and reductive SWV was applied to the Au-HGL/ALP biosensor respectively by scanning the potential from -1 V to 1 V at scan rate of 50 mV/s and 5 mHz frequency step potential (Figure 6.11). Aliquots 5 μ M of vanadium solution was added successively after each run and the recorded voltammograms are presented in (Figure 6.11).

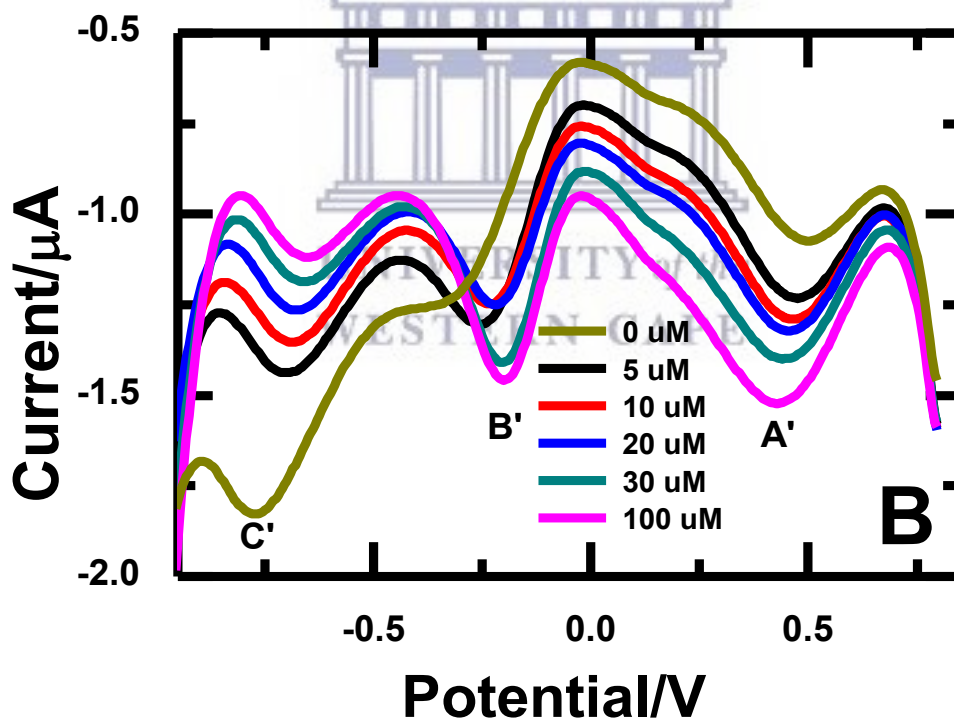


Figure 6.11: SWV of vanadium (A) oxidation and (B) reduction in Tris-buffer 1% BSA, scan at 50 mV/s.

The SWV showed multiples redox couple peaks A/A', B/B' at 0.467 V and -0.201 V respectively. The redox couple peaks C/C' observed at -0.850 V was previously identified as characteristic of ALP. Upon successive addition of vanadium a decrease in both oxidative and reductive peak current was observed at -0.850 V (Figure 6.11). The decrease in peak current at -0.850 V was indicative of the inhibition of ALP by vanadium added to the solution. However at a high concentration the peak at -0.850 V plateaued and an increase was observed at A/A' (0.467 V). This demonstrate an effective electro catalytic oxidation of vanadium to the Au-HGL/ALP with an increase in peak current A/A' as concentration increases. The peak C/C' was modelled as Michaelis-Menten kinetics [177,178] and used to plot a calibration curve of vanadium concentration vs peak current (Figure 6.12).

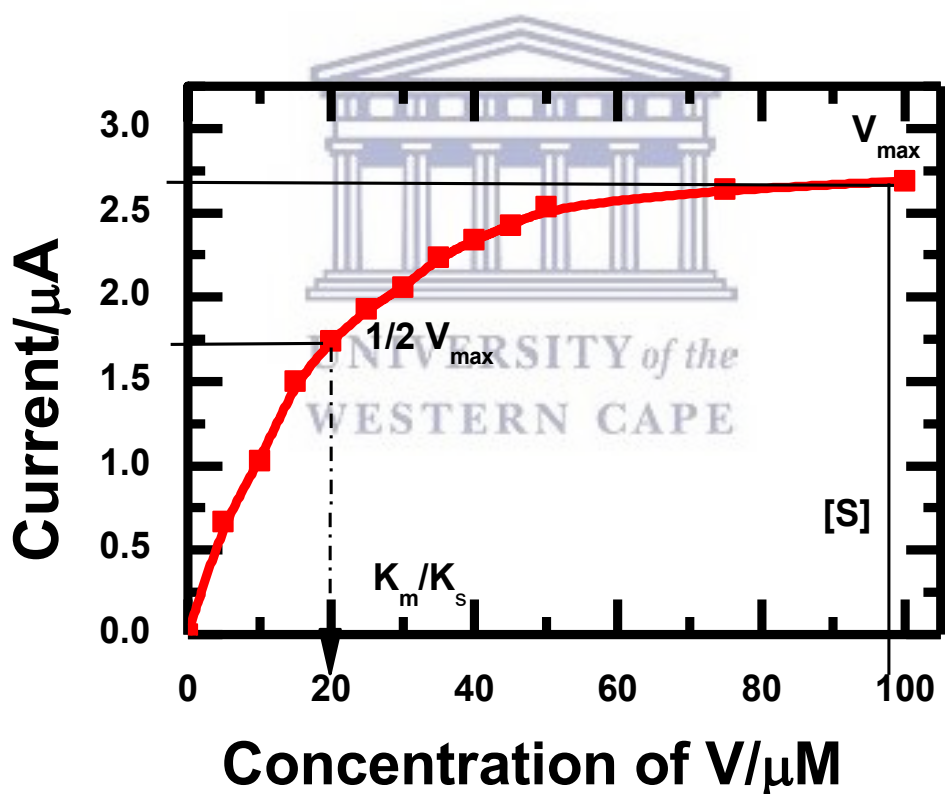


Figure 6.12 Michaelis-Menten plots of the AuE-HGL/ALP biosensor response to vanadium

From Michaelis-Menten calibration plot various parameters were derived such as (V_{max} , K_m and rate of reaction). Where K_m is the substrate concentration at which the reaction velocity is at 50 % and it was find to be 20 μM . V_{max} is the concentration of the substrate at the maximum velocity and the rate of the reaction was calculated by using Michaelis-Menten equation below;

$$V = \frac{V_{max} [S]}{K_m + [S]}$$

Where V is the rate of the reaction and V_{max} is the concentration of the substrate at the maximum velocity, K_m is constant or concentration at which the reaction velocity is half. The rate constant of the immobilized ALP at AuE-HGL was calculated for the anodic and cathodic peak and find to be 0.002 $\mu\text{A}/\mu\text{M}$ and 0.059 $\mu\text{A}/\mu\text{M}$ respectively. K_m and V_{max} values obtained were low compared to other ALP biosensors reported in literature [170,179]. According to (Robe L. Dean 2002) higher values of V_{max} and K_m in the presence of the inhibitor are characteristic of competitive inhibition [180]. Competitive inhibition occurs when substrate (S) and inhibitor (I) both bind to the same site on the enzyme. Or the inhibitory molecule is thought to bind reversibly at the substrate-binding site on the enzyme consequently preventing the substrate from binding. Therefore the low value obtained was attributed to non-competitive inhibition of vanadium in solution.

From Michaelis-Menten equation, an evaluation of a linear range and limit of detection for the biosensors was established (Figure 6.13). The linearity, coefficient correlation, limit of detection (LOD) and limit of quantification (LOQ) of the biosensors were calculated and tabulated in (Table 6.4).

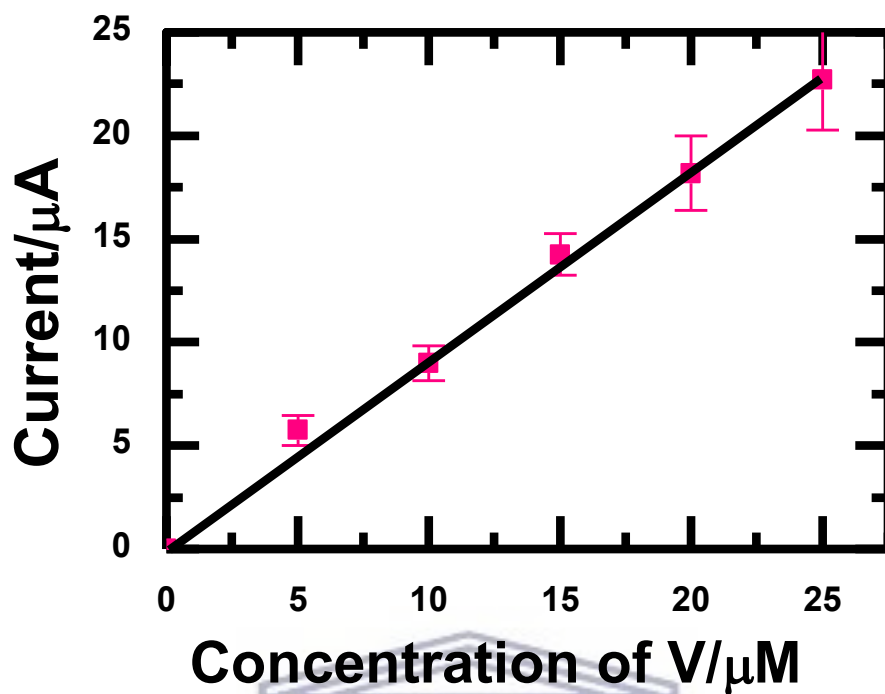


Figure 6.13. Calibration plot for the AuE-HGL/ALP biosensor response to vanadium in the linear range between 0-25 μM ($n=4$).

The reproducibility of this method was very good and evaluated by plotting different calibration curves using their slopes to determine the relative standard deviation (RSD). The low RSD of 9% (triplicate measurement) obtained for the biosensors demonstrate that its response was highly reproducible.

Table 6.4: Analytical performance of Au-HGL/ALP response to vanadium.

Linear range	R ²	LOD	LOQ	n	RSD
0-25 μM	0.998	0.227 μM	0.758 μM	4	9%

Effect of ALP enzyme in the Au-HGL/ALP biosensor

Hydrogel as an adsorbent can easily adsorb vanadium and produced a signal directly proportional to adsorptive capacity. On the other hand ALP is a vanadium

inhibitor therefore, the effect of enzyme in biosensor construction is critical. The experiment was conducted by developing an Au-HGL sensor in the absence of ALP following the same protocol in the presence of vanadium. The effect of ALP enzyme in the construction of the biosensor was investigated by monitoring Au-HGL sensor chip reaction in the presence and absence of ALP by SWV and amperometry. The hydrogel sensor calibration curve was based on the oxidation peak C observed at -0.850 V corresponding to vanadium in solution.

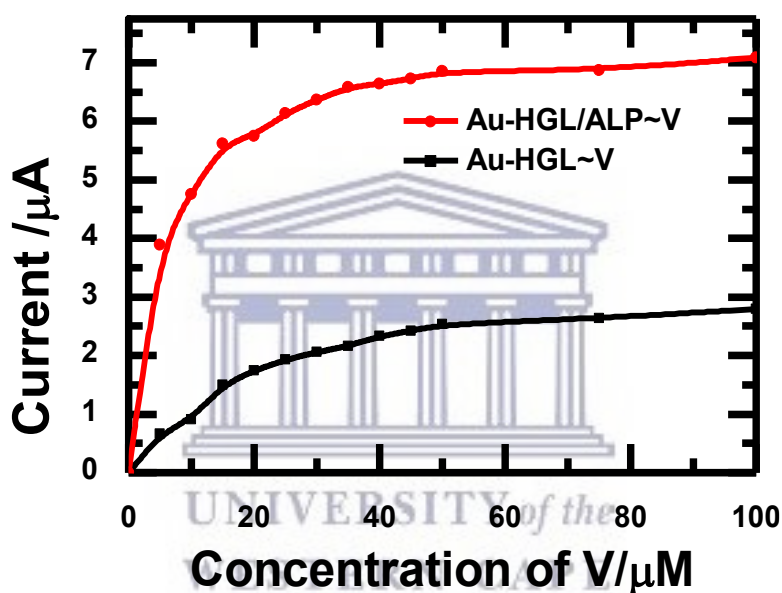
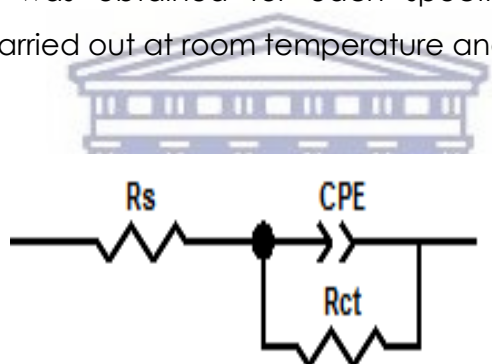


Figure 6.14: Effect of ALP in the biosensor construction

Based on the results obtained vanadium at Au-HGL/ALP showed a higher response in terms of sensitivity than Au-HGL (Figure 6.14). This confirmed that ALP was responsible of the bio recognition of the catalytic peak of vanadium observed at -0.850 V. The immobilization of ALP enzyme onto the biosensor had an advantage to support and enhanced the catalytic activity of vanadium to the maximum.

6.7. ELECTROCHEMICAL IMPEDANCE ANALYSIS OF Au-HGL/ALP BIOSENSOR RESPONSE TO VANADIUM

The impedance analysis was performed with Voltalab 40 impedance analyzer in the frequency range from 100 mHz – 1 KHz, using a modulation voltage of 10 mV. The impedance spectra were modelled as electrical equivalent circuits based on the method of least squares. The impedance data was modelled as a simple Randle circuit and fit error was kept under 10%. This equivalent circuit included the ohmic resistance of the electrolyte solution R_s , the constant phase element Z_{CPE} and electron transfer resistance R_{ct} . An excellent fitting between the simulated and experimental spectra was obtained for each spectrum. All electrochemical measurements were carried out at room temperature and in a Faraday cage.



WESTERN CAPE
Figure 6.14: Electrical model

Impedance Au-HGL/ALP biosensor was placed in 3 mL of 10 mM Tris buffer and connected as working electrode in a 3 electrodes cell, with Ag/AgCl as reference and 1 mm Pt as counter electrode. EIS spectra were measured across AC frequencies of 100 MHz to 1 KHz, with an amplitude of -0.850 V. Upon successive addition of vanadium concentration an increase in semi cycle in the Nyquist plot was observed (Figure 6.15). A fast rate increase in measured impedance was seen upon first and second additions of vanadium concentration, as the concentration of vanadium was further increased, the measured impedance continued to increase, but at a slower rate (Figure 6.15 and Table 6.5).

Table 6.5: EIS fitting data

[V] mM	CPE	Rct Ω	Rct (% error)
0	1.00E-06	3.01E+05	0.97639
2	9.90E-07	3.15E+05	0.98553
4	9.76E-07	3.63E+05	1.1037
8	9.67E-07	3.87E+05	1.0967
10	9.78E-07	3.88E+05	1.0929
12	9.78E-07	3.92E+05	1.1331

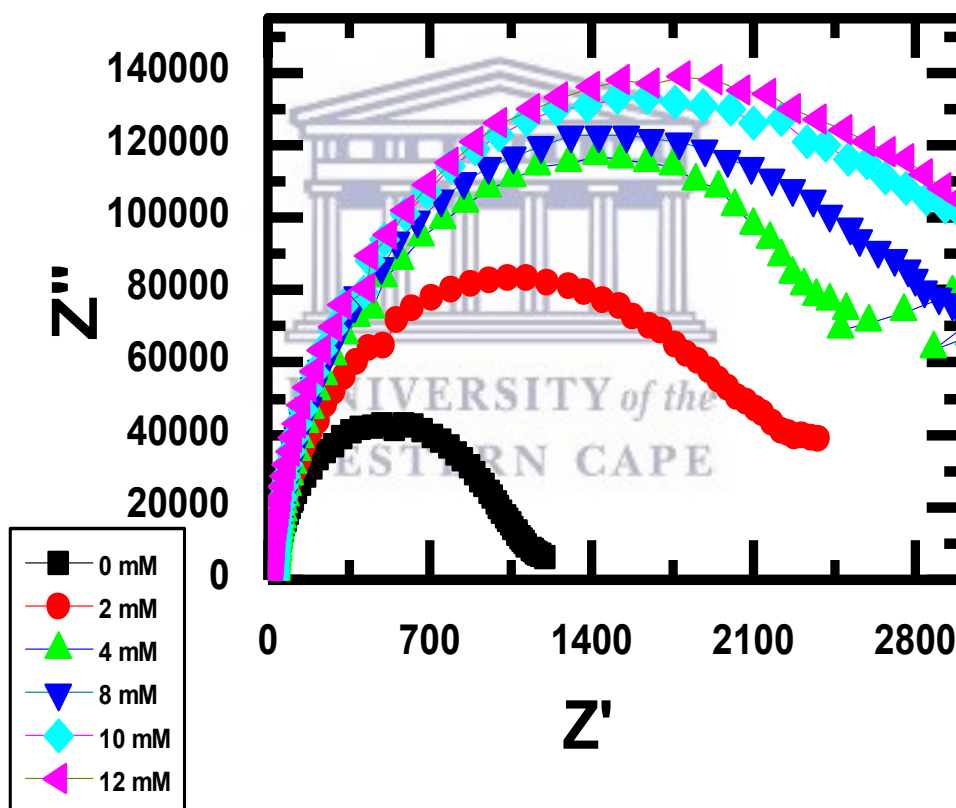


Figure 6.15: EIS (Nyquist plot) of Au-HGL/ALP response to vanadium.

Electrocatalysis of vanadium at Au-HGL/ALP biosensor followed typical diffusion control kinetics as evidenced by semi-circle in the Nyquist plot at low frequency (Figure 6.15). The charge transfer resistance increases as vanadium concentration

increased. The increase was attributed to vanadium inhibition in the enzymatic structure resulting in variation of the dielectric constant. The calibration plot was based on R_{CT} versus vanadium concentration were plotted in (Figure 6.16) and fitting data are in (Table 6.5). R_{CT} represent the change in polarization resistance of the system as a function of vanadium binding to enzyme.

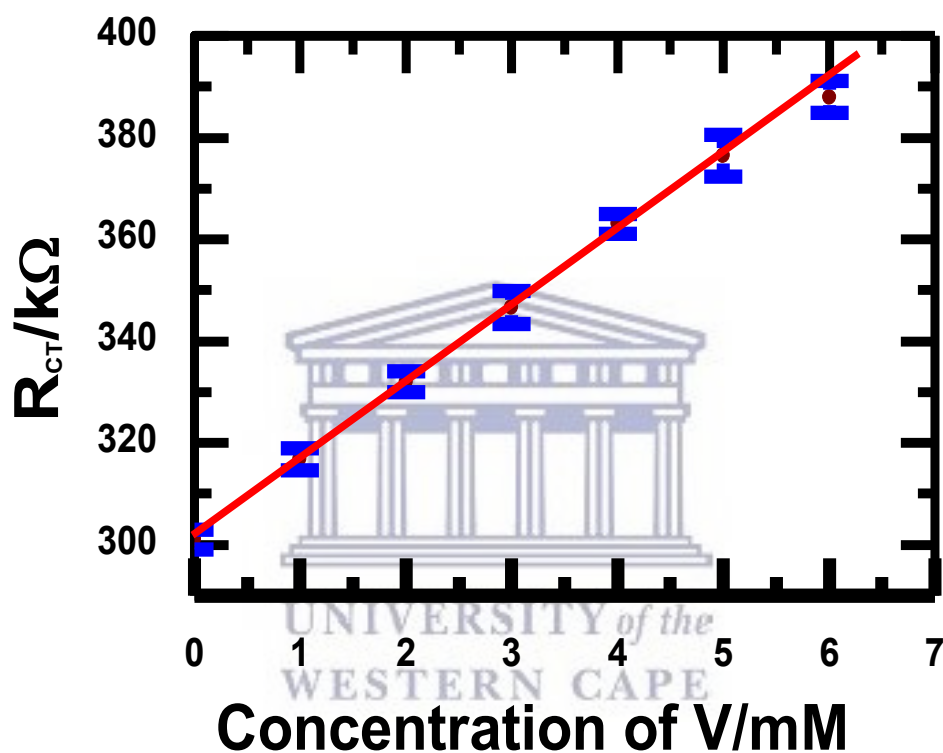


Figure 6.16: Calibration plot for Au-HGL/ALP biosensor response to vanadium (n=4).

The calibration plot showed a linear relationship between the R_{CT} variation and vanadium concentrations, the concentration ranged from 2 to 12 μM with a correlation coefficient of 0.997. A limit of detection (LOD) and limit of quantification (LOQ) of 0.127 μM and 0.366 μM respectively was calculated. The reproducibility of the biosensor was validated by repeating the experiment with four different biosensors prepared in the same way. The results showed that the response of the biosensor had an average standard deviation of 6%.

A Bode plot represents phase angle and total impedance as a function of frequency for the Au-HGL/ALP biosensor response to vanadium (Figure 6.17).

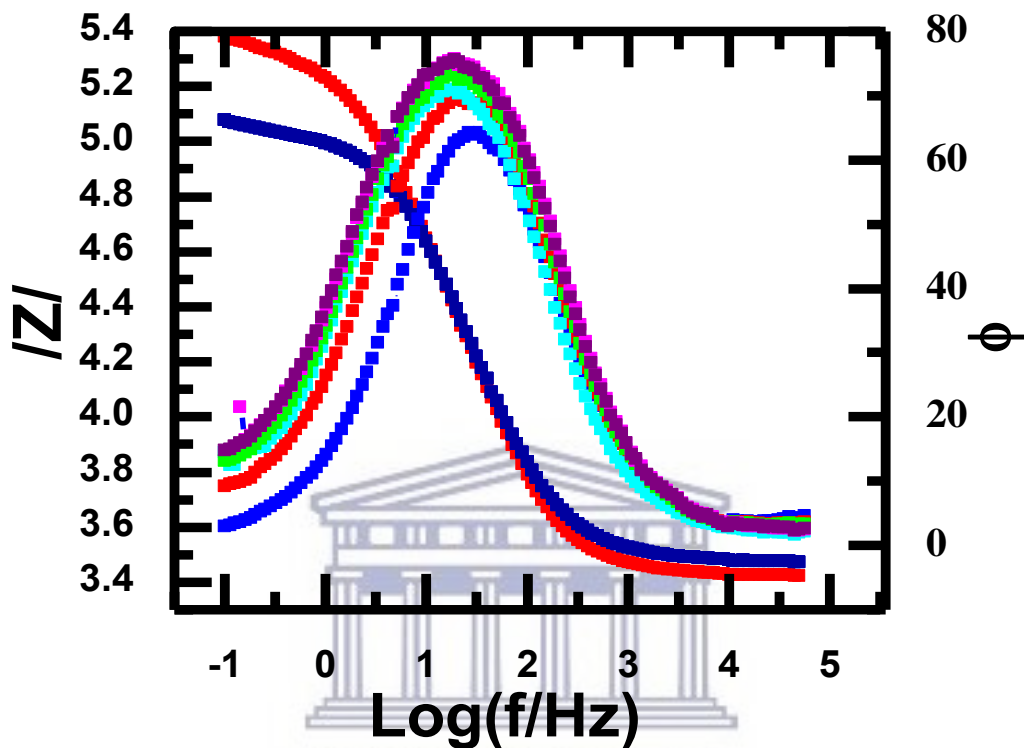


Figure 6.17: EIS (Bode plot) of Au-HGL/ALP response to vanadium.

The binding of vanadium was confirmed to follow a one-step catalytic mechanism as evidenced by the single phase (Figure 6.17). The resistive behavior was observed at high frequencies (electrolyte resistance, R_e), while, at lower frequencies, the increase of impedance with an increased in frequency indicated catalytic behavior (geometric capacitance). The increase of the impedance in the low-frequency range was related to the binding affinity of the enzyme for vanadium as its substrate.

6.8. AMPEROMETRIC RESPONSE OF Au-HGL/ALP BIOSENSOR TO VANADIUM

Amperometric sensor is a type of electrochemical sensor, which continuously measure current as a result of oxidation or reduction of an electroactive species in a biochemical reaction [168,181]. The amperometric experiments were conducted by placing the Au-HGL/ALP amperometry biosensor in 3 mL of 10 mM Tris buffer and connected as working electrode in a 3 electrodes cell, with Ag/AgCl as reference and 1 mm Pt as counter electrode. The potential was fixed at -0.850 V and the current response was measured as function of time (Figure 6.18). For experimental purposes the background was firstly scanned until the current reached a stable value. Than 10 μ L of vanadium solution was added consecutively. After each addition of vanadium a rise in anodic current was recorded before the system reach plateau once more (Figure 6.18).

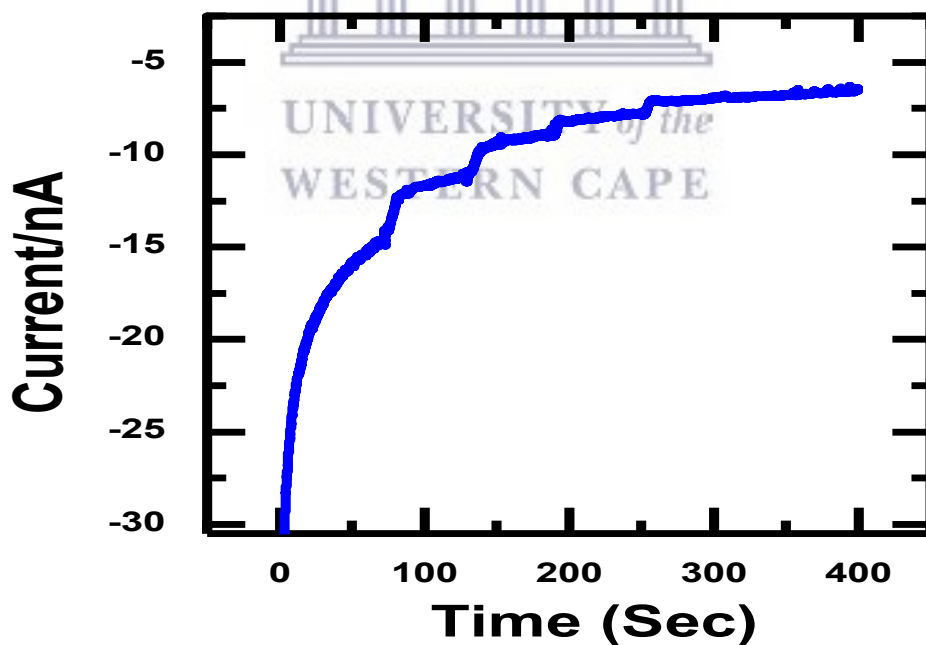


Figure 6.18: Current response of biosensor to concentration addition of vanadium in Tris-buffer vs Ag/AgCl

The amperometric biosensor exhibited a rapid and sensitive response to a change in vanadium concentration. A steady-state current response of the biosensor in the absence of vanadium was observed within 30 seconds. Upon successively addition of vanadium concentration the biosensor showed a response to vanadium within 2 seconds (Figure 6.18). This was attributed to the fast inhibitions processes of vanadium and was in competition with most published amperometric biosensors in terms of response time [182]. The calibration plot of a change in current response vs vanadium concentration are presented (Figure 6.19).

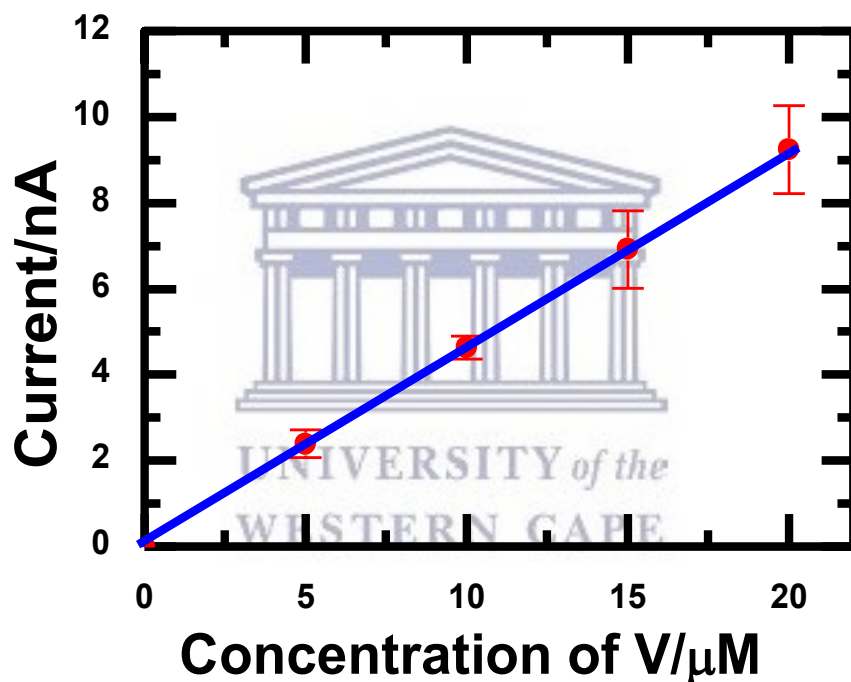


Figure 6.19: Calibration plot of vanadium response to the amperometric biosensor monitored at - 850mV in fresh Tris-buffer vs Ag/AgCl (n=4).

The amperometric Au-HGL/ALP biosensor showed a linear relationship between the current variation and vanadium concentrations. These were found within the range of 2 to 20 μM with a correlation coefficient of 0.999. The calculated LOD and LOQ of the system was found to be 0.312 μM and 0.6955 μM respectively (Table 6.6). The reproducibility of the biosensor was validated by repeating the experiment with four

different biosensors prepared in the same way with average standard deviation of less than 8 %.

Table 6.6: Analytical performance of Au-HGL/ALP response to vanadium

Linear range	R ²	LOD	LOQ	n	RSD
2-25 μM	0.999	0.312 μM	0.696 μM	4	8%

Effect of ALP enzyme in the Au-HGL/ALP biosensor by amperometry

In amperometry we monitor the current response of a peak at -0.850 V as a function of time. Since the potential is fixed it means we only monitor the inhibition process of vanadium at ALP interface, therefore a negative or weak response is expected in the absence of ALP. The experiments were conducted by placing both Au-HGL/ALP amperometry biosensor and Au-HGL amperometry sensor in 3 mL of 10 mM Tris buffer and connected as working electrode in a 3 electrodes cell, with Ag/AgCl as reference and 1 mm Pt as counter electrode respectively. The potential was fixed at -0.850 V and the current response was measured as function of time (Figure 6.20). For experimental purposes the background was firstly scanned until the current reached a stable value. Then 10 μL of vanadium solution was added consecutively. After each addition of vanadium a change in anodic current was observed for both Au-HGL/ALP and Au-HGL (Figure 6.20). The calibration plot of a change in current response vs vanadium concentration for both Au-HGL/ALP biosensor and Au-HGL sensor (Figure 6.20 B) were used to calculate the sensitivity of the system.

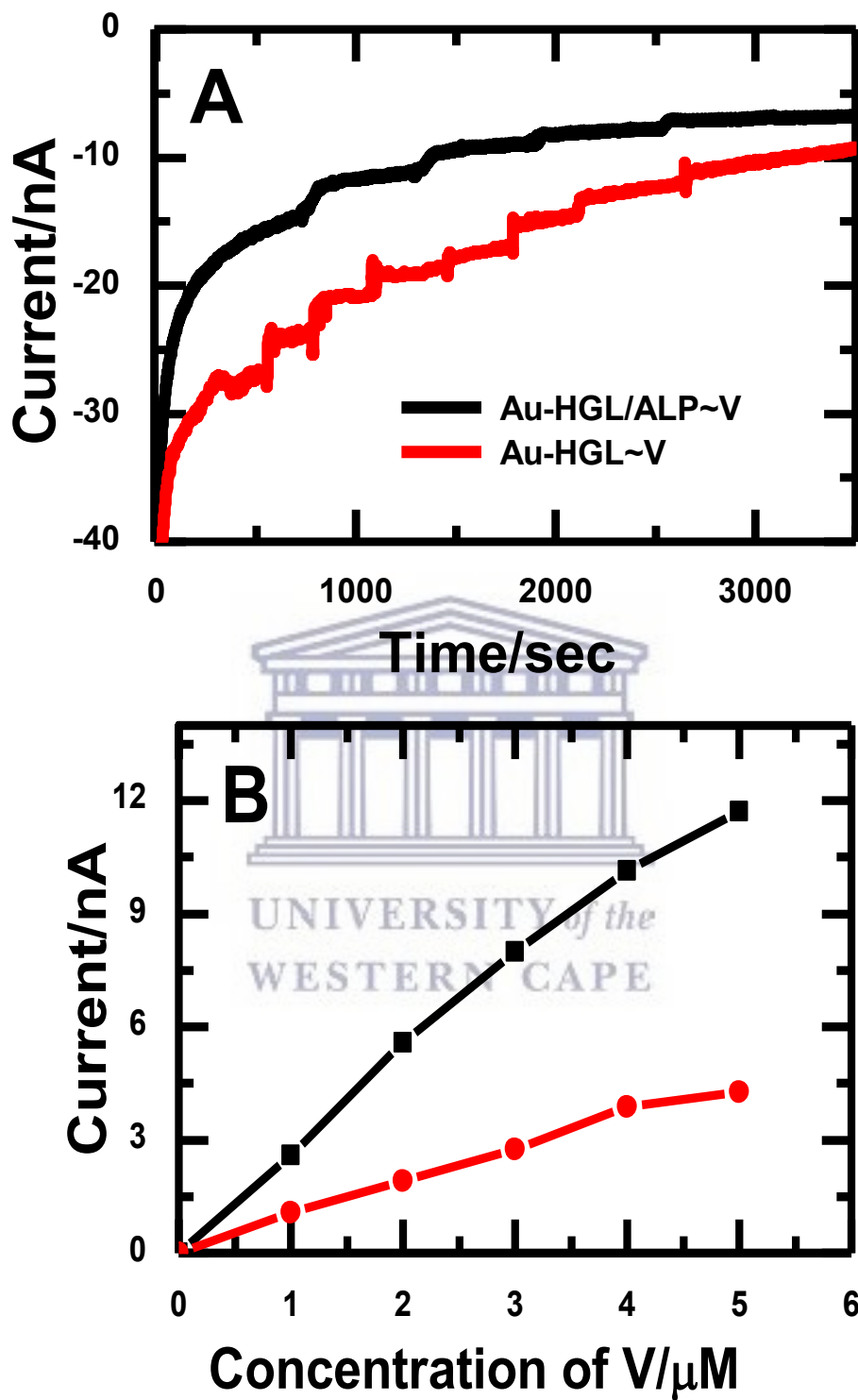


Figure 6.20: Amperometric effects of ALP in Au-HGL/ALP biosensor

The Au-HGL/ALP amperometry biosensor proved to be more sensitive than Au-HGL amperometry sensor with sensitivity of 2.389 nA/ μM and 0.874 nA/ μM respectively and LOD of 0.149 μM irrespectively. High sensitivity of Au-HGL/ALP was associated with inhibition mechanism of vanadium at ALP interface.

6.9. COMPARISON BETWEEN THE VOLTAMMETRY, IMPEDANCE AND AMPEROMETRIC BIOSENSOR FOR DETECTION OF VANADIUM

Various electrochemical techniques (voltammetry, amperometry and impedance spectroscopy) were employed in the evaluation of alkaline phosphatase biosensor. Performance in the detection of vanadium in terms of sensitivity, LOD and LOQ for each method was evaluated. Amperometry and impedance respectively are more sensitivity than voltammetry. These techniques disclosed a relative standard deviation (RSD) of 8% related to their LOD and LOQ (Table 6.6). The performances of the three techniques it's conclusive that amperometry biosensor is more appropriate for the detection of metals of biological significance due to high sensitivity.

Table 6.6: Comparison for various techniques used

	LOD (μM)	LOQ (μM)	Linear range (μM)	Sensitivity Au-HGL/ALP	Sensitivity Au-HGL
Amperometry	0.312	0.696	0-20	0.460 nA/ μM	0.023 nA/ μM
Impedance	0.127	0.366	0-6	14.698 k Ω / μM	-
Voltammetry	0.227	0.758	0-25	0.008 nA/ μM	0.001 nA/ μM

6.10. KINETIC AND METABOLIC STUDIES OF THE AU-HGL/ALP BIOSENSOR

Kinetic models are critically important in understanding and predicting the functional behavior of dynamic system [183]. The actual challenge is resolving uncertainties about parameter values of kinetic reaction. The aim of this investigation by UV-vis was to predict the functional behavior of Au-HGL/ALP biosensor in the presence of inhibitor.

The experiment was conducted by freshly prepared two Au-HGL/ALP biosensors. The first Au-HGL/ALP biosensor was placed in 0.01M vanadium solution and connected as working electrode in a 3 electrodes cell, with Ag/AgCl as reference and 1 mm Pt as counter electrode. Single sweep oxidative SWV was applied to the Au-HGL/ALP biosensor by scanning the potential from -1 V to 1 V at scan rate of 50 mV/s. 10 μ L of 0.01M vanadium solution was collected and its UV-vis absorbance spectra was measured. To the reaming vanadium solution a second Au-HGL/ALP was applied by sweeping the same potential. Another 10 μ L of 0.01M vanadium solution was collected and its UV-vis absorbance spectra was measured (Figure6.21).

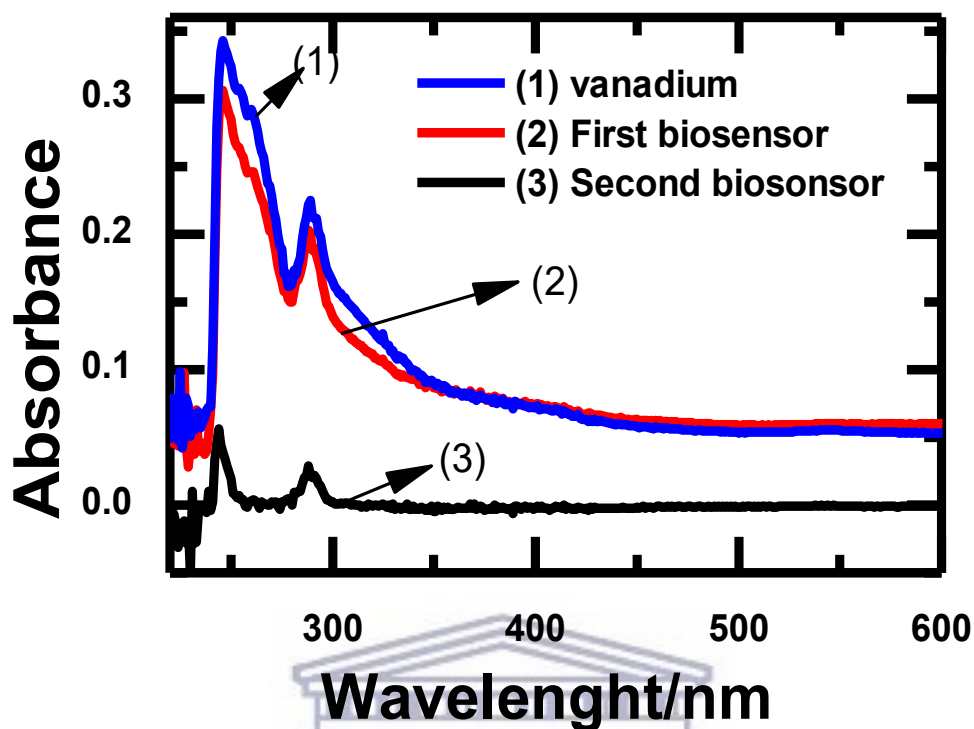


Figure 6.21: UV-vis response of vanadium solution (1) before and (2), (3) after being exposed to the Au-HGL/ALP biosensor

The UV experiment confirmed a 10% reduction in vanadium concentration (Figure 6.21 (2)). After the first sweep and second freshly prepared Au-HGL/ALP was used and the UV showed a reduction in vanadium concentration by 85% (Figure 6.21 (3)). The electrocatalytic kinetic behaviour of ALP monitored by measuring the Faradaic current of vanadium before and after the application of the biosensor was observed. The decrease in Faradaic current was related to adsorptive kinetic as well as the inhibition processes of the ALP toward the analyte as illustrated in (Figure 6.22).

6.11. Au-HGL/ALP BIOSENSOR RESPONSE TO VANADIUM DETECTED IN REAL SAMPLE

The Au-HGL/ALP biosensor was used to detect vanadium in Centrum multivitamin over 50+. Centrum multivitamins over 50+ tablet was selected based on the worldwide classification as one of the most consumed supplements. Each tablet of Centrum multivitamins contained various nutrient such as potassium, boron, nickel, silicon, vanadium, Lutein and Lycopene. The average weight of one tablet was 1.700 g and was proposed to contain 10 μg /tablet of vanadium. The tablets were crushed and 0.987 g was weighed and dissolved in 5 mL of water to yield a concentration of 2.301 μM . The sample was filtered and store for analysis.

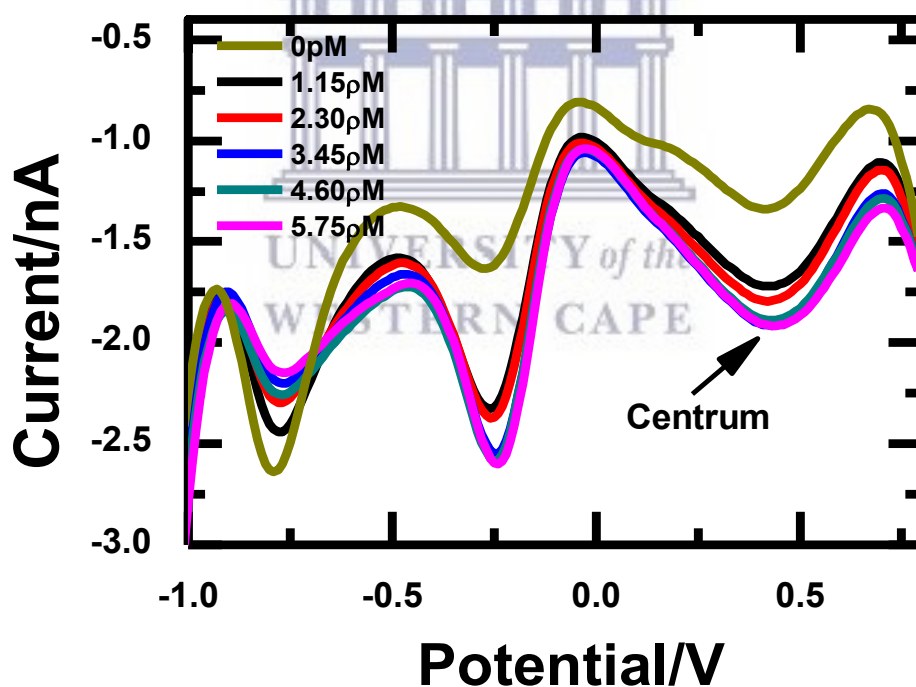


Figure 6.22: Au-HGL/ALP biosensor response to Centrum Tablet in Tris-buffer 1% BSA, scan at 100 mV/s.

The peak current at -0.850 mV showed the characteristic decrease in peak intensity associated with inhibition of ALP by vanadium. Saturation of the biosensor was

observed after 4 additions of sample. However other metal element such as boron, nickel and potassium also exhibited strong affinity to ALP binding side (Figure 6.24). Vanadium oxidation peak at 0.5V was used for Centrum tablet analysis.

Quantification of vanadium concentration in centrum tablet was achieved by applying the AU-HGL/ALP biosensor to various concentration of centrum solution. The oxidative analytical signal of AU-HGL/ALP biosensor to concentration of Centrum was recorded. The concentration of vanadium in Centrum tablet was evaluated by extrapolation method and was estimated to be 2.402 μM (Figure 6.23). This was far below than the label value (10 $\mu\text{g}/1.7\text{g}$), this could be due to the competitive ALP binding to interferents. Therefore, quantification of vanadium in sample matrix by Au-HGL/ALP required a blocking agent which will prevent interferents from binding to ALP.

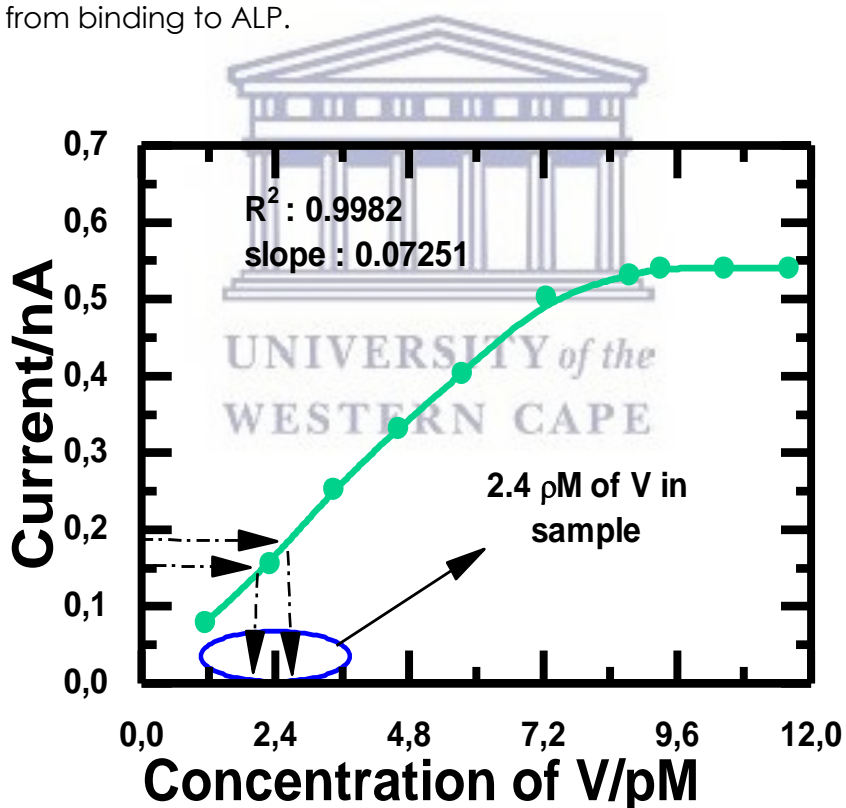


Figure 6.23: Au-HGL/ALP biosensor response to vanadium in centrum

6.12. INTERFERENCE STUDIES

Interferents can be any substance in centrum over 50+ sample matrix which can respond to the Au-HGL/ALP biosensor apart from vanadium. Interferences cause erroneous analytical results. As illustrated above each tablet of Centrum multivitamins also contained potassium, boron, nickel, silicon, vanadium, lutein and lycopene. Therefore Potassium, nickel and Boron were selected as potential interferents for this study. All interferents were purchased from Sigma Aldrich as salts and dissolved in water to yield a concentration of 0.1 M of which 10 μL of each solution was added in 3 mL of 10mM Tris buffer solution pH 7.2. The Au-HGL/ALP biosensor was analyzed by SWV between -1 V to 1 V at a scan rate of 50 mV/s (Figure 6.24).

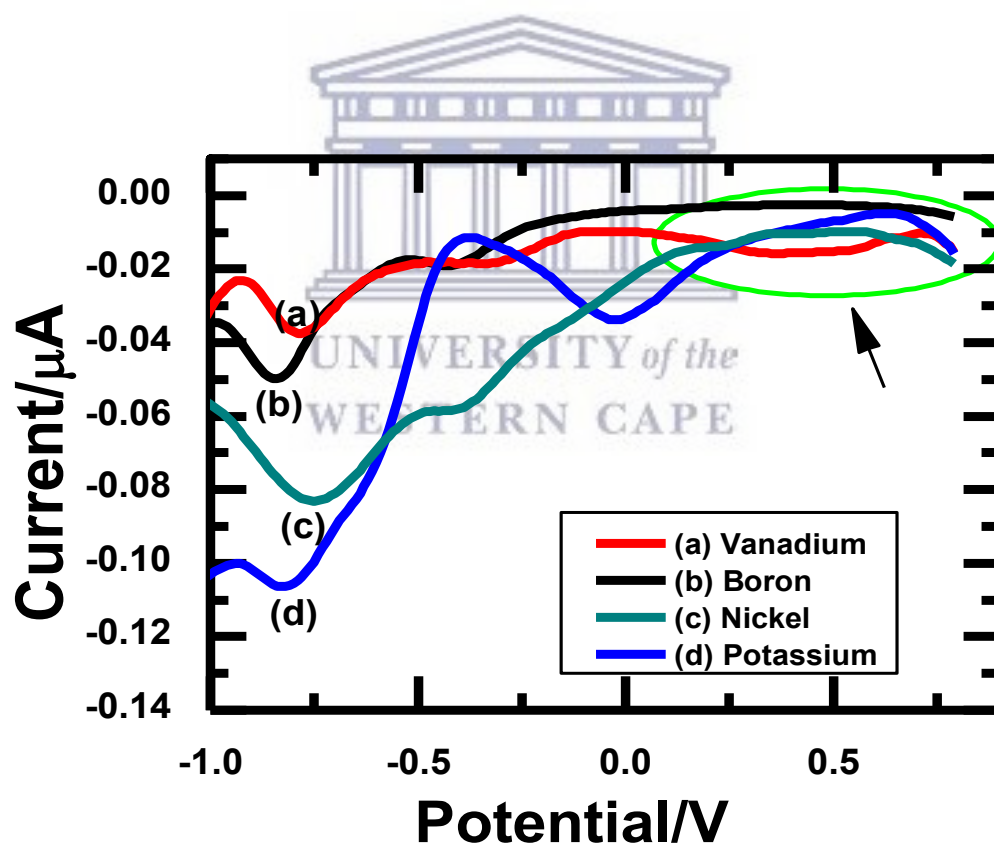


Figure 6.24: Au-HGL/ALP biosensor response to interference (a) Centrum (b) Boron, (c) Nickel and (d) Potassium solution in Tris-buffer 1% BSA, scan at 100 mV/s.

The Au-HGL/ALP biosensor developed showed a positive response to Centrum tablet. Competitive for ALP inhibition by vanadium was demonstrated by other metals (B, Ni and K). The oxidation peak at 0.5V was used to monitor vanadium concentration in Centrum tablet.

6.13. CONCLUSION

Several biosensors based on the immobilization of ALP at different transducers have been described in literature [179,184]. However it is relatively uncommon to approach biosensor construction by direct immobilization of ALP onto an electrode. In this study a covalently modified gold electrode with hydrogel was used for the immobilization of ALP. Hydrogel showed a strong affinity with gold electrode which was characterized by an oxidative peak at -0.150 V. A growth in the hydrogel peak was observed as a function of scan rate with a diffusion coefficient and surface concentration of $1.550 \times 10^{-4} \text{ cm}^2/\text{s}$ and $7.281 \times 10^{-10} \text{ M}$ respectively.

ALP immobilization onto the Au-HGL electrode was achieved by incubation, 30 mins was selected to ensure effective incubation and minimum physical interference effects in the preparation of the biosensor. The analytical performance of the biosensor was evaluated by SWV, amperometry and EIS. Performance in the detection of vanadium in terms of sensitivity, LOD and LOQ for each technique was evaluated. The performances of the three techniques it's conclusive that amperometry biosensor is more appropriate for the detection of vanadium in aqueous medium due to high sensitivity. The sensitivity of Au-HGL/ALP amperometry biosensor towards vanadium was found to be $0.460 \text{ nA}/\mu\text{M}$ which was much high that previously published ALP biosensors [179,184]. The biosensor kinetic parameters modeled as Michaelis-Menten speaks of high sensitive biosensor design, which may be attributed to the simplistic design of the biosensor.

The correlation between electrochemical response for vanadium and Centrum analysis is evidence that Au-HGL/ALP biosensor is selective and sufficient sensitive in its recognition of vanadium. The influence of other interferents in the selective

detection of vanadium by the Au-HGL/ALP biosensor have been investigated and a competitive for ALP inhibition by vanadium was demonstrate by other metals. However another vanadium oxidative peak observed at 0.5V was used for the detection of Centrum. The vanadium concentration in Centrum was calculated by extrapolation method and found to be 2.4 μ M.



UNIVERSITY *of the*
WESTERN CAPE

Chapter 7

Au-HGL/SePP immunosensor for selenium detection

ABSTRACT

The approach in this chapter was the construction of immunosensor using selenoprotein p antibody at Au-HGL for the detection of selenium. Here we present the first results of The Au-HGL/SePP immunosensor response to selenium using voltammetry and amperometric.

7. INTRODUCTION

Selenoprotein p is a protein which contains multiple selenocysteine (Sec) residues [185]. This molecule is a selenium-rich extracellular, plasma protein and has been reported as an index of selenium status in rats [185–187]. Biochemical sensors based on selenoprotein p have been developed previously as analytical device to determine selenium status in rats [188–190]. However here an immunoassay has been developed for human selenoprotein p antibody for the detection of selenium in aqueous as a biomarker for type II diabetes.

7.1. EXPERIMENTAL

The commercial polyclonal Anti-SELS antibody produced in rabbit and stored in solution of phosphate-buffered saline pH 7.2, containing 40% glycerol and 0.02% sodium azide with an immunofluorescence: 1-4 $\mu\text{g}/\text{mL}$ was purchased from sigma Aldrich. The stock solution was prepared by dissolving the antibody into a saline phosphate buffer solution (PBS) pH 7.2 into a molar ration 1:5. From the stock solution further dilution were carried to yield an immunofluorescence concentration of 0.1 $\mu\text{g}/\text{mL}$. The UV-vis spectra were recorded on Nicolet Evolution 100 Spectrometer (Thermo Elctron Corporation, UK). Aliquots 10 μL of selenoprotein p antibody (SePP) solution was placed in 4 cm^3 quartz cuvettes containing 3 mL of PBS solution pH 7.2 and it UV-vis spectra were recorded. The spectra were recorded within the full region. The activity of the antibody was examined by UV-Vis and from the result obtain no signal associated to SePP was observed (Figure 7.1).

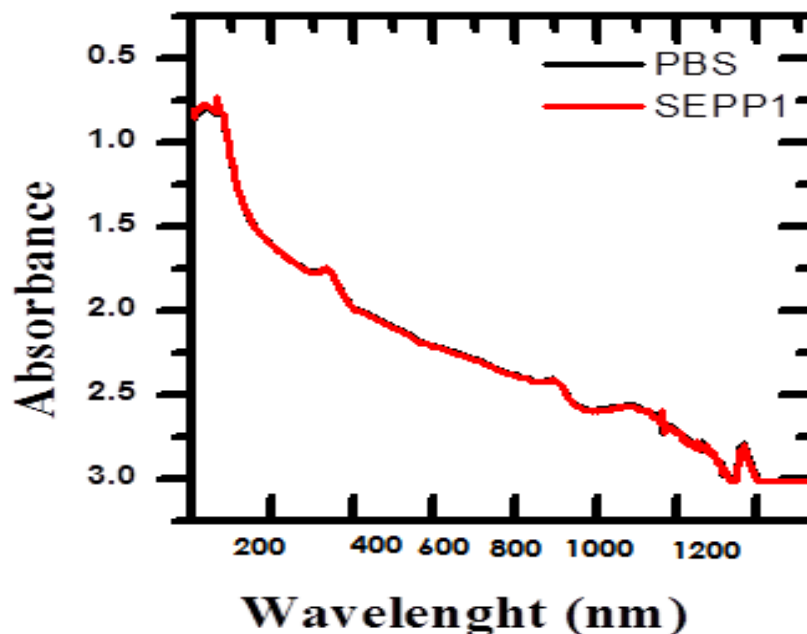


Figure 7.1: UV-vis of SePP in phosphate buffer solution

7.2. ELECTROCHEMICAL RESPONSE OF SELENOPROTEIN P ANTIBODY AT GLASSY CARBON ELECTRODE

Cyclic voltammetry (CV) was used to evaluate the electrochemical behaviour of the Selenoprotein p antibody (SePP) at GCE. The experiment was performed in a 3 cell electrodes and GCE was connected as working electrode, with Ag/AgCl as reference and 1 mm Pt wire as counter electrode. The electrolyte used was 3 mL of PBS solution pH 7.2, to which 10 μ L of SePP was added successively. The characterization was done by cyclic voltammetry and the electrode was scanned from -1.5 V to 1 V at scan rates of 50 mV/s. CV of SePP in solution showed redox couple A/A' at 0.098 V and -0.108 V (Figure 7.2).

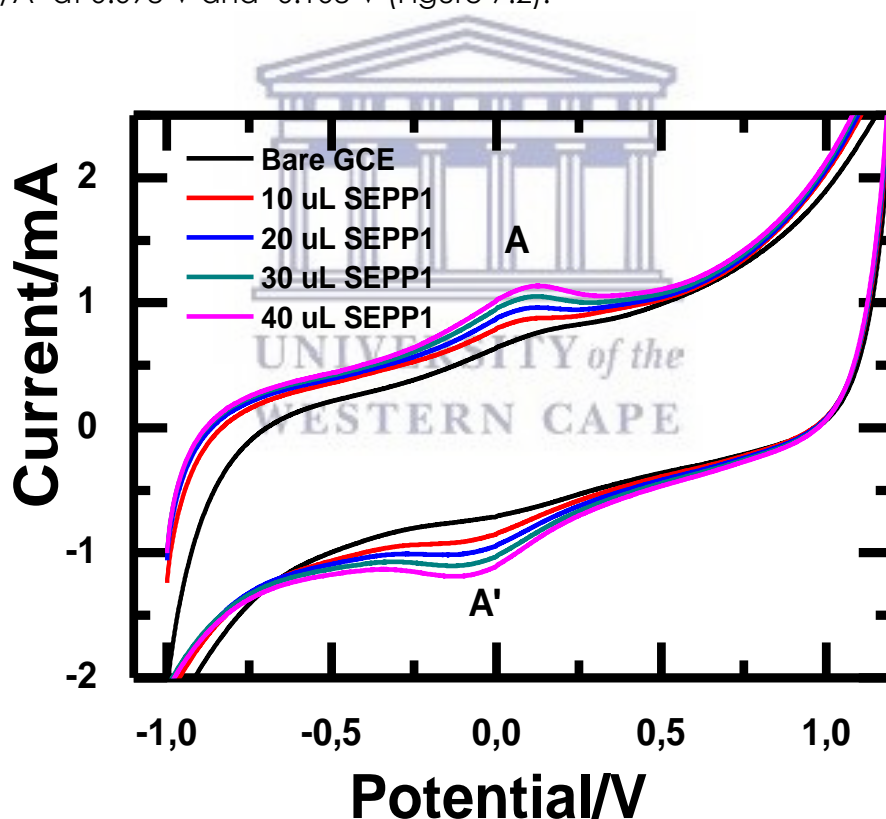


Figure 7.2: Cyclic voltammograms of SePP at GCE in PBS pH 7.1 at 50 mV/s Vs Ag/AgCl.

An increase in current response of a redox couple A/A' as function of an increase in SePP concentration was also observed (Figure 7.2). The kinetic behaviour of SePP in solution was evaluated by cyclic voltammetry and characterized at scan rate ranging from 50 mV/s to 300 mV/s. It was observed that the redox couple A/A' in PBS, shifted positively with increasing scan rate which is an indicative of an electron transfer reaction coupled to a catalytic process. This was an indication of a strong electrochemical affinity of SePP in solution at electrode surface (Figure 7.3).

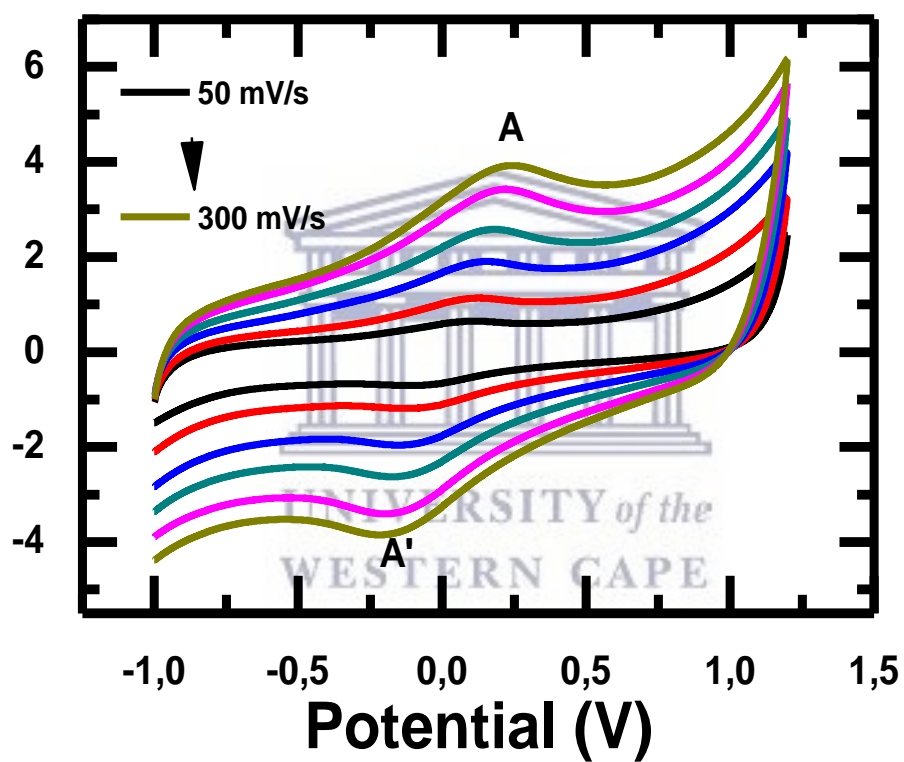


Figure 7.3: Scan rate dependence studies of SePP at Bare GCE in PBS pH 7.1 vs Ag/AgCl

Immobilization of SePP at Au-HGL by incubation

Selenoprotein p antibody (SePP) exhibit a hydrophobic behaviour due to anti-freezing agent used such as glycerol and sodium azide. Glycerol is known as triglycerides and has three hydroxyl groups that are responsible for its hygroscopic nature [191,192]. Sodium azide have been used mainly as a preservative in aqueous laboratory reagents, biologic fluids as a fuel in automobile airbag gas generates [193,194]. The immunosensor prepared by incubation of Au-HGL electrode in SePP solution are discussed in chapter 5. After 24 hours incubation at Au-HGL, Drop shape analyzer (contact angle) was used to evaluate the hydrophobic nature of the antibody (Figure 7.4).

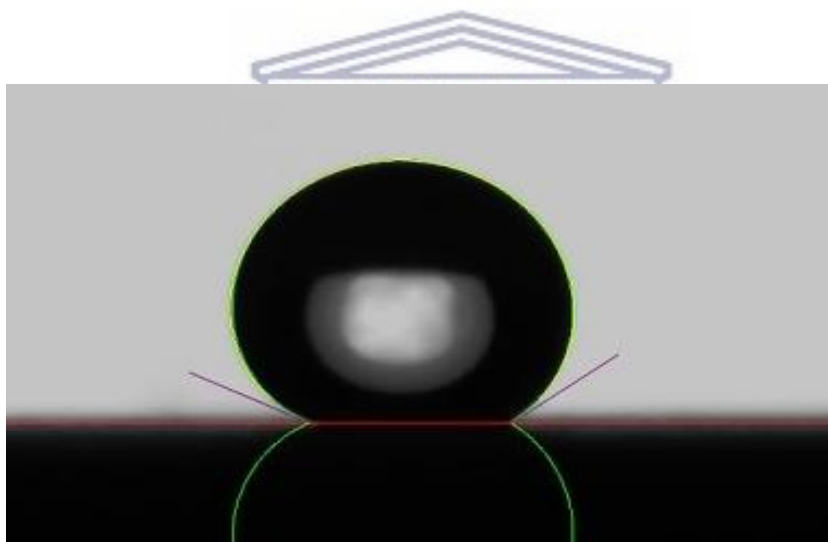
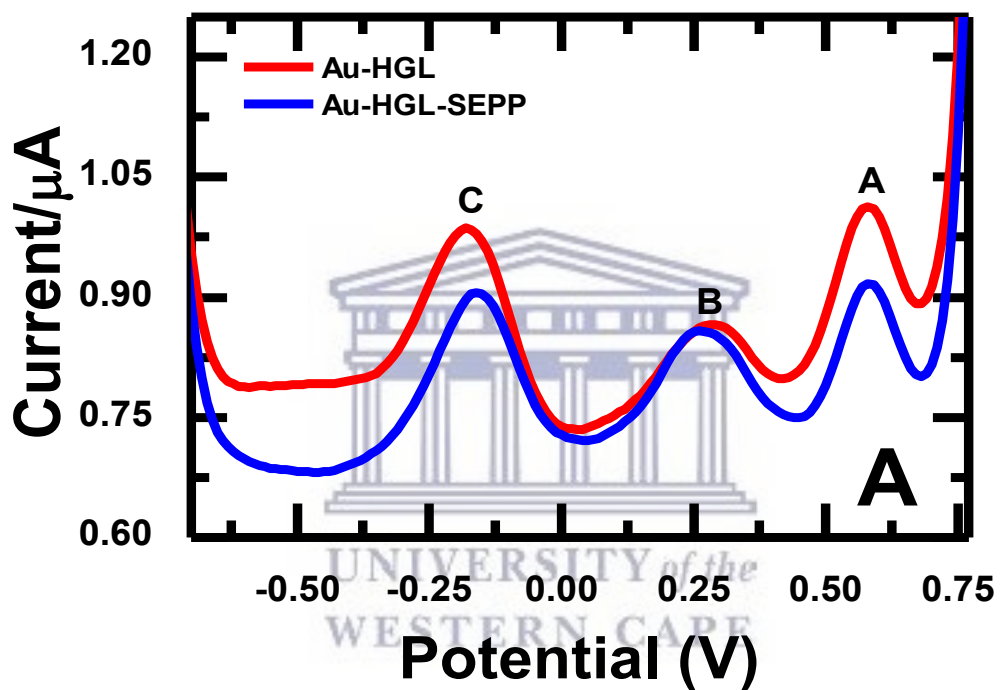


Figure 7.4: Contact angle of SePP

A surface is defined as hydrophobic if it has a contact angle greater than 90° and hydrophilic when it's less than 90° . SePP on its own shows a contact angle of 108° which confirm it hydrophobic nature. SePP comes from supplier as a glycerol based solution which explains the observed hydrophobicity (Figure 7.4). Consequently only a small amount of SePP was incorporated into hydrogel during incubation and the surface excess of SePP was physically removed during drying, to prepare the sample for electrochemical analysis.

The immobilization of SePP at Au-HGL electrode was investigated by SWV in a three electrodes cell. The Au-HGL/SePP electrode was placed in 3 mL of PBS solution and connected as working electrode, with Ag/AgCl as reference and 1mm Pt wire as counter electrode. Single sweep oxidative and reductive SWV was applied to the Au-HGL/SePP immunosensor respectively by scanning the potential from -0.8 V to 0.8 V at scan rate of 50 mV/s and 5 mHz frequency step potential (Figure 7.5).



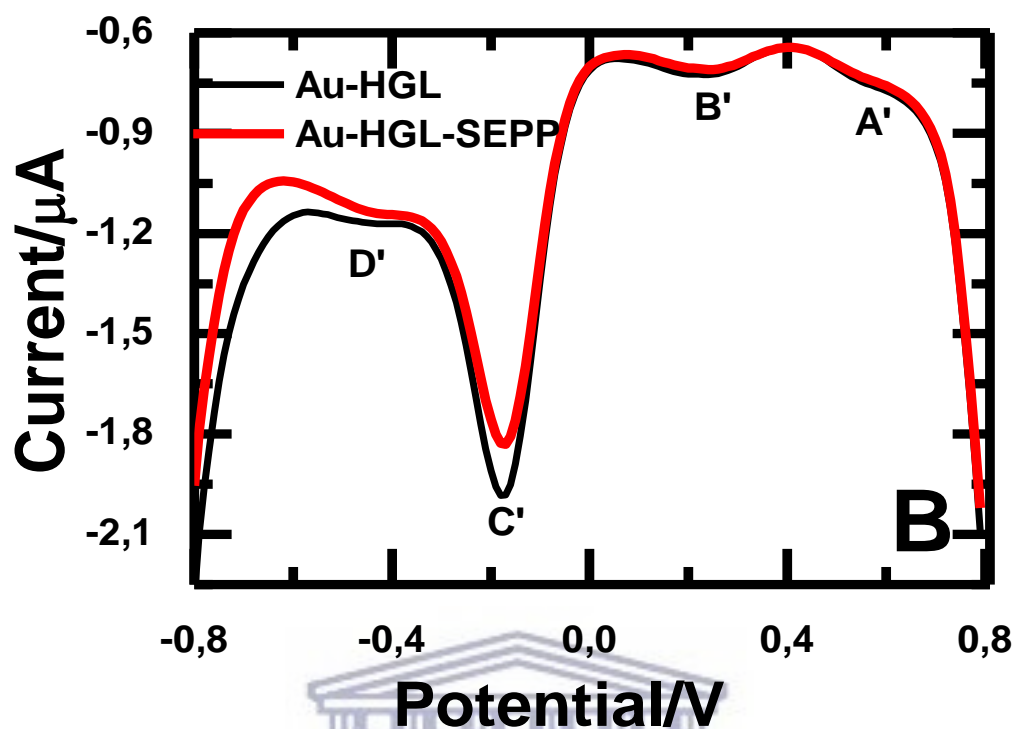


Figure 7.5 OSWV of SePP immobilized at Au-HGL in PBS pH 7.1 Vs Ag/AgCl (A) oxidation and (B) reduction

SWV showed three major redox couples peaks A/A', B/B' and C/C' observed at -0.580 V, 0.278 V and -0.180. The redox couples A/A', B/B' and C/C' are characteristic of hydrogel material (Figure 7.5A). The reduction peak D' observed redox at -0.480 V was associated with SePP binding by hydrogel (Figure 7.5B). This peak D' was monitor to investigate the antibody binding to selenium in solution.

7.3. OSTERYOUNG SQUARE WAVE SPECTROSCOPY OF Au-HGL/SePP IMMUNOSENSOR RESPONSE TO SELENIUM

The response of Au-HGL/SePP immunosensor to selenium concentration was investigated by SWV. The Au-HGL/SePP immunosensor was placed in 3 mL of PBS buffer solution and connected as working electrode in a 3 electrodes cell, with Ag/AgCl as reference and 1 mm Pt as counter electrode. Single sweep reductive SWV was applied to the Au-HGL/SePP immunosensor by scanning the potential from -0.5 V to 0.8 V at scan rate of 100 mV/s and 5 mHz frequency step potential (Figure 7.6). Aliquots 2 μM of selenium solution was added successively after each run (Figure 7.5).

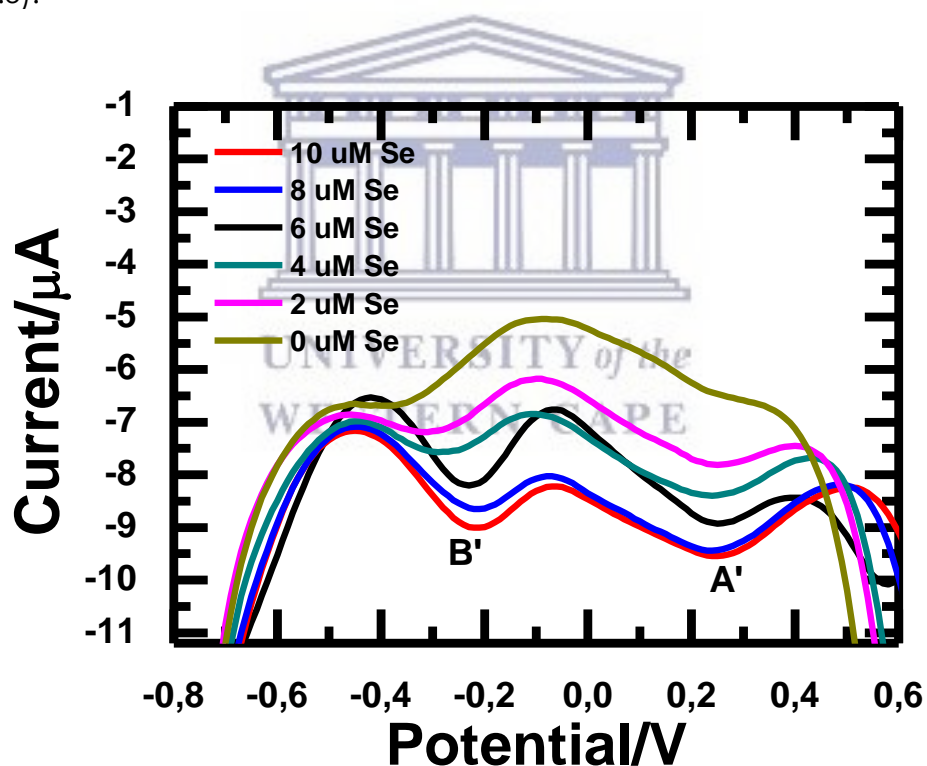


Figure 7.6 OSWV (Reduction) of the increasing in selenium concentration using AuE-HGL/SePP immunosensor in PBS pH 7.1, scan at 100 mV/s

The voltammograms depict a catalytic current resulting from the coupling of the electro-oxidation of the AuE-HGL films to the binding of selenoprotein p antibody.

Au-HGL films are functioning as electron-transfer mediators between the Au electrode and selenium. From the first addition of selenium concentration a positive shift in peak potential B' from -0.450V to -0.202V and a decrease in peak current was observed in (Figure 7.6). Upon successive addition of selenium showed a decrease in reductive peak current which was attributed to selenium binding even though reproducibility still a challenged. The peak B' was modelled as Michaelis-Menten kinetics [177,178] and used to plot a calibration curve of selenium concentration vs peak current (Figure 7.7).

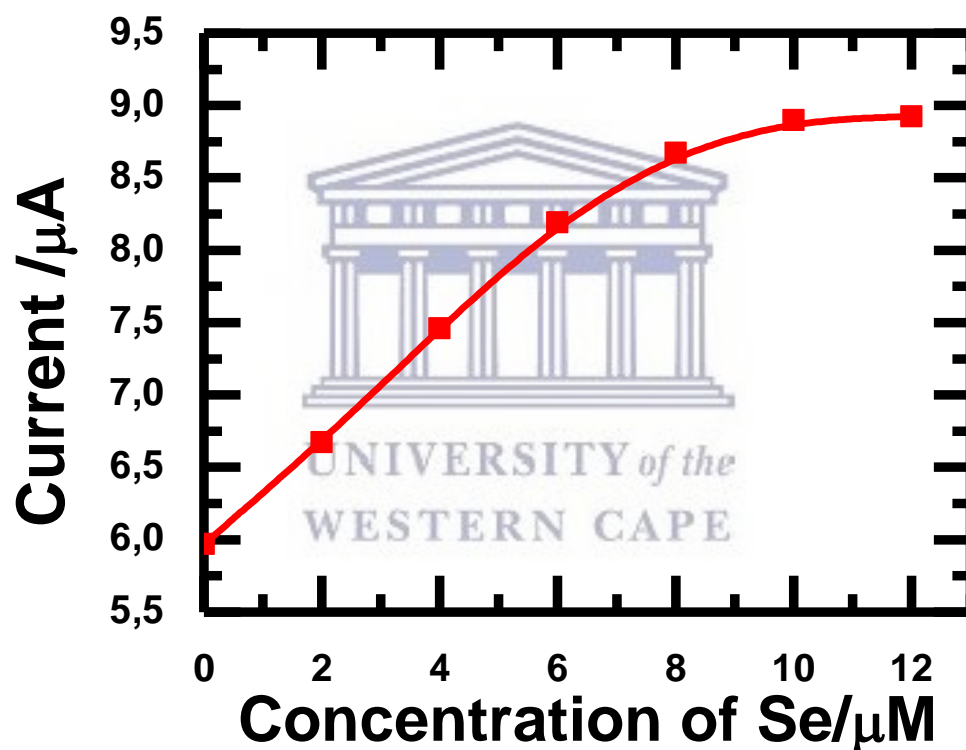


Figure 7.7: Calibration plot for the Au-HGL/SePP immunosensor to the different concentration of selenium in the linear range between 0-8 μM .

From Michaelis-Menten equation, an evaluation of a rate constant, linear range and limit of detection for the Au-HGL/SePP immunosensor was established. K_m and V_{max} was calculated to be 4 μM and 10 μM respectively. The linearity, coefficient

correlation, limit of detection (LOD) and limit of quantification (LOQ) of the immunosensor were calculated and tabulated in (Table 7.1).

Table 7.1: Analytical performance of Au-HGL/SePP response to selenium

Linear range	R ²	LOD	LOQ	n	RSD
0-8 μM	0.992	0.035 μM	0.104 μM	1	-

7.4. AMPEROMETRIC RESPONSE OF Au-HGL/SePP IMMUNOSENSOR TO SELENIUM

The amperometric experiments were conducted by placing the Au-HGL/SePP immunosensor in 3 mL of PBS solution pH 7.2 and connected as working electrode in a 3 electrodes cell, with Ag/AgCl as reference and 1 mm Pt as counter electrode. The potential was fixed at -0.202 V and the current response was measured as function of time (Figure 7.8). For experimental purposes the background was firstly scanned until the current reached a stable value. Than 2 μL of selenium solution was added consecutively. After each addition of selenium a rise in cathodic current was recorded before the system reach plateau once more (Figure 7.8).

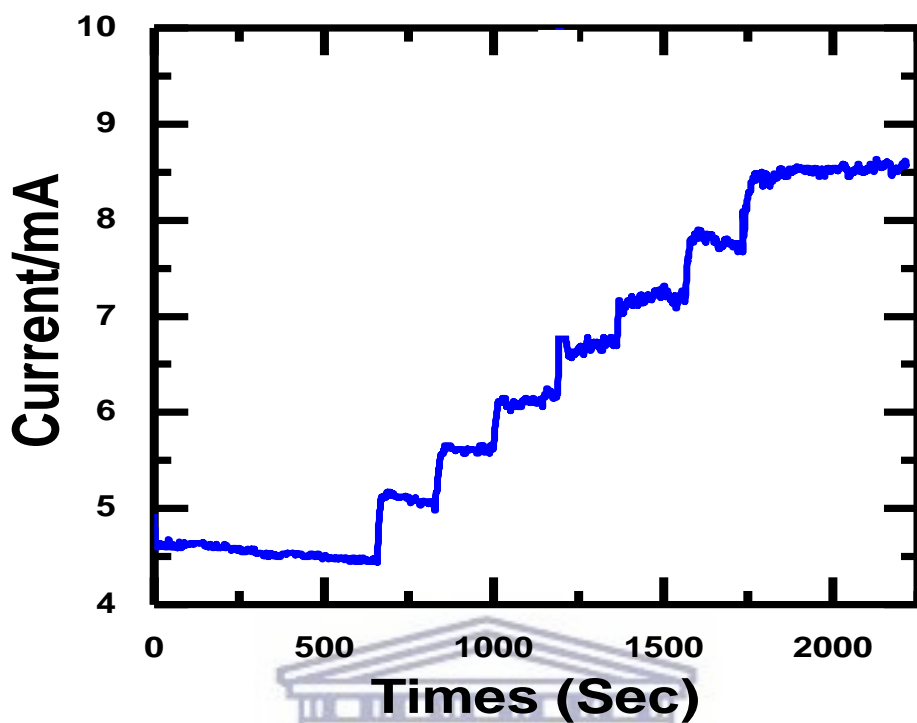


Figure 7.8: Amperometry immunosensor for selenium detection at - 0.200 V in PBS pH 7.1 vs Ag/AgCl

A slow and sensitive response to a change in selenium concentration was observed. A steady-state current response of the immunosensor in the absence of selenium was observed within 150 seconds and the system was allowed to stabilize for longer than that. Upon successive addition of vanadium concentration the immunosensor showed a response to selenium within 60 seconds (Figure 7.8). This was attributed to the slow binding processes of selenium. The calibration plot of a change in current response vs selenium concentration are presented in (Figure 7.9).

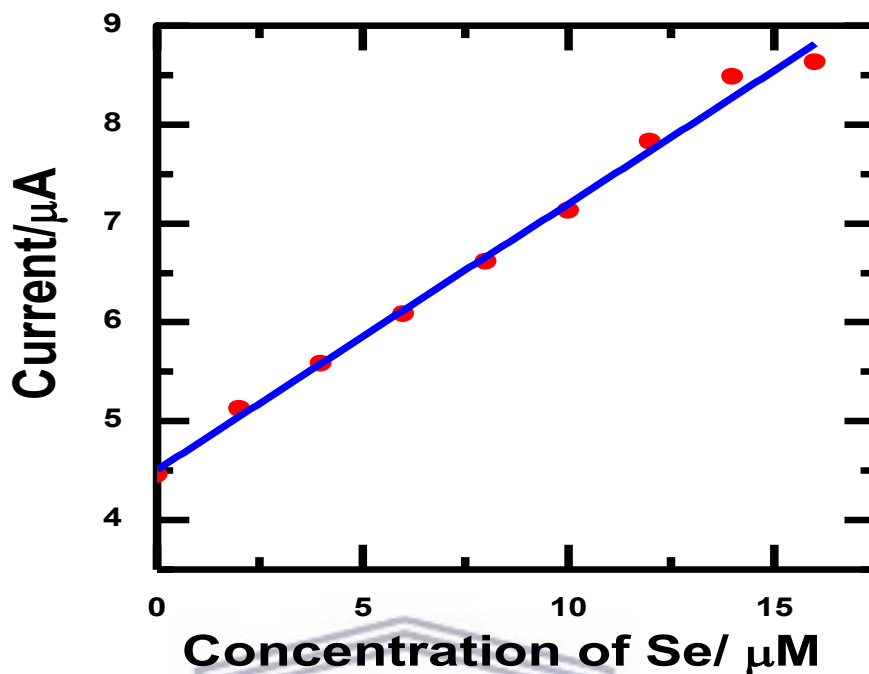


Figure 7.9: Calibration plot of selenium response to the amperometric immunosensor monitored at -0.200 V in PBS pH 7.1 vs Ag/AgCl

The amperometric immunosensor showed a linear relationship between the current variation and selenium concentrations. These were found within the linear range of 0 to 15 μM with a correlation coefficient of 0.993. A limit of detection (LOD) of 0.269 μM and limit of quantification (LOQ) of 0.808 μM was observed (Table 7.2).

Table 7.2: Analytical performance of Au-HGL/SePP response to selenium.

Linear range	R^2	LOD	LOQ	n	RSD
0-15 μM	0.993	0.269 μM	0.808 μM	1	-

7.5. CONCLUSION

To the best of my knowledge not much biological sensors based on selenoprotein p antibody have been reported yet. In the construction of SePP based immunosensor, SePP immobilization onto the Au-HGL electrode was achieved by incubation, 24 hours was selected to ensure effective incubation and maximum physical interaction in the construction of the immunosensor. SePP showed a weak binding affinity due to its hydrophobic nature. The analytical performance of the immunosensor was evaluated by SWV and amperometry. Performance in the detection of selenium in terms of sensitivity, LOD and LOQ was evaluated. The sensitivity of Au-HGL sensor and Au-HGL/SePP immunosensor towards selenium was found to be $1.994 \times 10^{-4} \mu\text{A}/\text{mM}$ and $0.460 \text{ nA}/\mu\text{M}$ respectively. Au-HGL/SePP immunosensor proved to be more sensitive to selenium than Au-HGL sensor. This confirmed that SePP was responsible of the bio recognition of the binding peak of selenium observed at -0.202 V . The immobilization of SePP antibody onto the immunosensor had an advantage to support and enhanced the binding activity of selenium to the maximum. Reproducibility of Au-HGL/SePP immunosensor still a challenge and further studies are in process to improve the performances and reproducibility of the immunosensor.

Chapter 8

Conclusions and recommendations

We have provided evidence in support of PSF-hydrogel material produced by crosslinking two polymers i.e. PSF and PVA using glutaraldehyde as crosslinker. The crosslinking was evaluated using various analytical techniques including FTIR, Raman, Contact angle, AFM, SEM, and CV. The synthesized hydrogel was characterized by 2 well resolved redox peaks with a formal potential of 0.490 V and -0.510 V (vs Ag/AgCl). The diffusion coefficient for the hydrogel thin film electrode in aqueous medium was calculated as $9.060 \text{ e}^{-9} \text{ Cm}^2/\text{s}$. Due to these superior material properties, the hydrogel was applied as a sensor for the detection of vanadium and selenium. The novelty of the hydrogel chemical sensor was based on physisorption onto screen printed carbon electrode that favored Se^{4+} than Se^0 , in terms of sensitivity, diffusion coefficient, and LOD. The hydrogel proved to be a good adsorbent for vanadium and selenium with the adsorption capacities of 0.189 mg/g and 0.559 mg/g respectively, under conditions of low pH.

To overcome the limitation of physisorption of hydrogel onto the SPCE electrodes, a gold electrode was used in subsequent biosensor development, since Au has a good covalent affinity for sulfate group in hydrogel. Thorough characterization of hydrogel showed that the hydrogel material was electrochemically deposited onto Au electrode to provide a platform for ALP (enzyme) and SePP (antibody) immobilizations. ALP and SePP were immobilized by incubation method and produced Au-HGL/ALP biosensor and Au-HGL/SePP immunosensor. The stepwise modification of the biosensors was evaluated by SWV, Raman spectroscopy and AFM. Au modification was confirmed by Raman spectroscopy with two broad peaks in Au-HGL electrode, upon incubation of ALP and SePP respectively a decrease in peak intensity was observed. The reduction in peak intensity was associated with the

incorporation of ALP and SePP in hydrogel matrix. Here we have demonstrated that Raman spectroscopy has emerged as a new tool for sensor and biological sensor characterization.

AFM characterization confirmed the incorporation of ALP onto the Au-HGL matrix by a decrease in peak height distribution and a dramatic change in surface area. The surface area of the Au-HGL electrode significantly decrease by modification with ALP enzyme. The decrease in surface area was an indicative of ALP binding onto the Au-HGL electrode. SWV provided evidence of ALP incorporation by a redox couple present at -0.850 V.

The performance of the novel Au-HGL/ALP biosensor was evaluated by SWV, EIS and amperometry techniques. The apparent Michaelis-Menten constant (K_m and V) calculated for the Au-HGL/ALP biosensor in the presence of vanadium were found to be 20 μM and 0.0592 $\mu\text{A}/\mu\text{M}$ respectively. The low value of V and K_m obtained for the Au-HGL/ALP biosensor confirmed strong binding to ALP by the substrate. The analytical performance of the Au-HGL/ALP biosensor was evaluated by SWV, amperometry and EIS. Amperometry emerged as the preferred for the detection of vanadium in aqueous medium due to high sensitivity. The sensitivity of Au-HGL/ALP biosensor was found to be 0.460 $\text{nA}/\mu\text{M}$ which was much high that previously published ALP biosensors[118]. The developed Au-HGL/ALP biosensor proven to be among the few alkaline phosphatase based biosensor for vanadium in aqueous medium with a LOD of less than 0.127 μM . This biosensor can be used in an application such as environmental health for the monitoring of vanadium in a biological sample.

The Au-HGL/SePP immunosensor is among the first developed immunosensor for selenium based on selenoprotein p antibody binding. The novel immunosensor response to selenium was evaluated by measuring the binding mechanism of selenium using SWV and amperometry. Amperometry appeared as the preferred for selenium monitoring in solution. The novel Au-HGL/SePP immunosensor showed a linear relationship to selenium concentrations ranging from 1-25 μM . The detection limit of 0.269 μM for selenium was observed. A high detection limit found indicating

that hydrogel matrix was not suitable for the immobilization of SePP and subsequent fabrication of electrochemical immunosensor for selenium detection. Au-HGL/SePP immunosensor showed some reproducibility problem associated with the nature of the antibody (SePP). To improve the reproducibility parameters such as antibody purity, anti-freezing agent used, storage solution and electrolyte solution need a thoroughly investigation. SePP has shown to be hydrophobic by nature with a contact angle of 108°. Consequently only a small amount of SePP is incorporated into hydrogel matrix during incubation.

Future work and recommendation

My thesis opens up an entirely new approach in the application of Raman spectroscopy as useful tool in the construction of the biosensor. The biosensor and immunosensor were constructed by electrochemical deposition of polysulfone hydrogel onto Au electrode. For future work it's important to further establish how other hydrogels would behave for the immobilization of ALP and SePP in the detection of V and Se is worthwhile.

- Further optimization of the biosensors to improve selectivity and its application in the detection of vanadium and selenium in environmental waste water is important.
- Investigation on the use of the developed biosensors in the detection of more than two competitive metals in waste water.
- Application of the developed biosensors for the detection of vanadium and selenium in a clinical samples (Blood and urine).
- More work need to be done to improve sensitivity and reproducibility of the immunosensor response to selenium. This can be achieved by changing the hydrophobic nature of the antibody which will result in strong binding of the SePP at hydrogel interface.

REFERENCES

- [1] K. Tsekova, D. Todorova, S. Ganeva, Removal of heavy metals from industrial wastewater by free and immobilized cells of *Aspergillus niger*, *Int. Biodeterior. Biodegradation*. 64 (2010) 447–451. doi:<http://dx.doi.org/10.1016/j.ibiod.2010.05.003>.
- [2] D.C. Crans, A.M. Trujillo, P.S. Pharazyn, M.D. Cohen, How environment affects drug activity: Localization, compartmentalization and reactions of a vanadium insulin-enhancing compound, dipicolinatooxovanadium(V), *Coord. Chem. Rev.* 255 (2011) 2178–2192. doi:<http://dx.doi.org/10.1016/j.ccr.2011.01.032>.
- [3] J. Wu, R. Li, R. Ding, T. Li, H. Sun, City expansion model based on population diffusion and road growth, *Appl. Math. Model.* 43 (2017) 1–14. doi:[10.1016/j.apm.2016.08.002](https://doi.org/10.1016/j.apm.2016.08.002).
- [4] M. Tibayrenc, Chapter 6 – Human Population Variability and Its Adaptive Significance, in: *Hum. Nat.*, 2017: pp. 85–109. doi:[10.1016/B978-0-12-420190-3.00006-5](https://doi.org/10.1016/B978-0-12-420190-3.00006-5).
- [5] H. Sasaki, Population growth and trade patterns in semi-endogenous growth economies, *Struct. Chang. Econ. Dyn.* 41 (2017) 1–12. doi:[10.1016/j.strueco.2017.01.001](https://doi.org/10.1016/j.strueco.2017.01.001).
- [6] K. Jurczynska, B. Kuang, Population Growth, in: *Int. Encycl. Public Heal.*, 2017: pp. 533–540. doi:[10.1016/B978-0-12-803678-5.00339-8](https://doi.org/10.1016/B978-0-12-803678-5.00339-8).
- [7] Q. Liu, H. Cai, Y. Xu, L. Xiao, M. Yang, P. Wang, Detection of heavy metal toxicity using cardiac cell-based biosensor, *Biosens. Bioelectron.* 22 (2007) 3224–3229. doi:<http://dx.doi.org/10.1016/j.bios.2007.03.005>.
- [8] B. Boulassel, N. Sadeg, O. Roussel, M. Perrin, H. Belhadj-Tahar, Fatal poisoning by vanadium, *Forensic Sci. Int.* 206 (2011) e79–e81. doi:<http://dx.doi.org/10.1016/j.forsciint.2010.10.027>.
- [9] H.-J. Sun, B. Rathinasabapathi, B. Wu, J. Luo, L.-P. Pu, L.Q. Ma, Arsenic and selenium toxicity and their interactive effects in humans, *Environ. Int.* 69 (2014) 148–158.

doi:<http://dx.doi.org/10.1016/j.envint.2014.04.019>.

- [10] G.A. Souza, J.J. Hart, J.G. Carvalho, M.A. Rutzke, J.C. Albrecht, L.R.G. Guilherme, L. V Kochian, L. Li, Genotypic variation of zinc and selenium concentration in grains of Brazilian wheat lines, *Plant Sci.* 224 (2014) 27–35. doi:<http://dx.doi.org/10.1016/j.plantsci.2014.03.022>.
- [11] S. Li, F. Bian, L. Yue, H. Jin, Z. Hong, G. Shu, Selenium-dependent antitumor immunomodulating activity of polysaccharides from roots of *A. membranaceus*, *Int. J. Biol. Macromol.* 69 (2014) 64–72. doi:<http://dx.doi.org/10.1016/j.ijbiomac.2014.05.020>.
- [12] G.-B. Ding, R.-H. Nie, L.-H. Lv, G.-Q. Wei, L.-Q. Zhao, Preparation and biological evaluation of a novel selenium-containing exopolysaccharide from *Rhizobium* sp. N613, *Carbohydr. Polym.* 109 (2014) 28–34. doi:<http://dx.doi.org/10.1016/j.carbpol.2014.03.038>.
- [13] F. Natella, M. Fidale, F. Tubaro, F. Ursini, C. Scaccini, Selenium supplementation prevents the increase in atherogenic electronegative LDL (LDL minus) in the postprandial phase, *Nutr. Metab. Cardiovasc. Dis.* 17 (2007) 649–656. doi:<http://dx.doi.org/10.1016/j.numecd.2006.05.002>.
- [14] M. Hasanuzzaman, K. Nahar, M. Fujita, Chapter 16 – Silicon and Selenium: Two Vital Trace Elements that Confer Abiotic Stress Tolerance to Plants, in: P. Ahmad, S. Rasool (Eds.), *Emerg. Technol. Manag. Crop Stress Toler.*, Academic Press, San Diego, 2014: pp. 377–422. doi:<http://dx.doi.org/10.1016/B978-0-12-800876-8.00016-3>.
- [15] K. Rees, L. Hartley, C. Day, N. Flowers, A. Clarke, S. Stranges, Selenium supplementation for the primary prevention of cardiovascular disease., *Cochrane Database Syst. Rev.* 1 (2013) CD009671. doi:10.1002/14651858.CD009671.pub2.
- [16] M.M. Bordbar, H. Khajehsharifi, A. Solhjoo, PC-ANN assisted to the determination of Vanadium (IV) ion using an optical sensor based on immobilization of Eriochrome Cyanine R on a triacetylcellulose film., *Spectrochim. Acta. A. Mol. Biomol. Spectrosc.* 151 (2015) 225–231. doi:10.1016/j.saa.2015.06.025.

- [17] A. Ayala Quezada, K. Ohara, N. Ratanawimarnwong, D. Nacapricha, H. Murakami, N. Teshima, T. Sakai, Stopped-in-loop flow analysis system for successive determination of trace vanadium and iron in drinking water using their catalytic reactions☆, *Talanta*. 144 (2015) 844–850. doi:10.1016/j.talanta.2015.07.006.
- [18] C. Rameshan, M.L. Ng, A. Shavorskiy, J.T. Newberg, H. Bluhm, Water adsorption on polycrystalline vanadium from ultra-high vacuum to ambient relative humidity, *Surf. Sci.* 641 (2015) 141–147. doi:10.1016/j.susc.2015.06.004.
- [19] M.A. Larsson, M. D'Amato, F. Cubadda, A. Raggi, I. Öborn, D.B. Kleja, J.P. Gustafsson, Long-term fate and transformations of vanadium in a pine forest soil with added converter lime, *Geoderma*. 259–260 (2015) 271–278. doi:10.1016/j.geoderma.2015.06.012.
- [20] Y. Wang, M. Zuo, Y. Li, Theoretical investigation of the mechanism of ethylene polymerization with salicylaldiminato vanadium(III) complexes, *Chinese J. Catal.* 36 (2015) 657–666. doi:10.1016/S1872-2067(14)60271-0.
- [21] X. Liu, L. Zhang, Insight into the adsorption mechanisms of vanadium(V) on a high-efficiency biosorbent (Ti-doped chitosan bead), *Int. J. Biol. Macromol.* 79 (2015) 110–117. doi:10.1016/j.ijbiomac.2015.04.065.
- [22] E. Kioseoglou, S. Petanidis, C. Gabriel, A. Salifoglou, The chemistry and biology of vanadium compounds in cancer therapeutics, *Coord. Chem. Rev.* (2015). doi:10.1016/j.ccr.2015.03.010.
- [23] M. Xie, D. Chen, F. Zhang, G.R. Willsky, D.C. Crans, W. Ding, Effects of vanadium (III, IV, V)-chlorodipicolinate on glycolysis and antioxidant status in the liver of STZ-induced diabetic rats, *J. Inorg. Biochem.* 136 (2014) 47–56. doi:http://dx.doi.org/10.1016/j.jinorgbio.2014.03.011.
- [24] Z. Wang, J. Bai, L. Kong, X. Wen, X. Li, Z. Bai, W. Li, Y. Shi, Viscosity of coal ash slag containing vanadium and nickel, *Fuel Process. Technol.* 136 (2015) 25–33. doi:10.1016/j.fuproc.2014.07.025.
- [25] J. Huotari, R. Bjorklund, J. Lappalainen, A. Lloyd Spetz, Pulsed Laser Deposited

Nanostructured Vanadium Oxide Thin Films Characterized as Ammonia Sensors, *Sensors Actuators B Chem.* 217 (2015) 22–29. doi:10.1016/j.snb.2015.02.089.

- [26] J. Mazloom, F.E. Ghodsi, H. Golmojdeh, Synthesis and characterization of vanadium doped SnO₂ diluted magnetic semiconductor nanoparticles with enhanced photocatalytic activities, *J. Alloys Compd.* 639 (2015) 393–399. doi:10.1016/j.jallcom.2015.03.184.
- [27] Z. Li, G. Liu, M. Guo, L.-X. Ding, S. Wang, H. Wang, Electrospun porous vanadium pentoxide nanotubes as a high-performance cathode material for lithium-ion batteries, *Electrochim. Acta.* 173 (2015) 131–138. doi:10.1016/j.electacta.2015.05.057.
- [28] B. Mukherjee, B. Patra, S. Mahapatra, P. Banerjee, A. Tiwari, M. Chatterjee, Vanadium—an element of atypical biological significance, *Toxicol. Lett.* 150 (2004) 135–143. doi:http://dx.doi.org/10.1016/j.toxlet.2004.01.009.
- [29] C. Scriver, S. Kaufman, Hyperphenylalaninemia: phenylalanine hydroxylase deficiency, *Metab. Mol. Bases Inherit. Dis.* (2001) 1667–1724. doi:10.1036/ommbid.97.
- [30] B.N. Ames, DNA damage from micronutrient deficiencies is likely to be a major cause of cancer, *Mutat. Res. Mol. Mech. Mutagen.* 475 (2001) 7–20. doi:10.1016/S0027-5107(01)00070-7.
- [31] M.A. Fik, A. Gorczyński, M. Kubicki, Z. Hnatejko, A. Wadas, P.J. Kulesza, A. Lewińska, M. Giel-Pietraszuk, E. Wyszko, V. Patroniak, New vanadium complexes with 6,6''-dimethyl-2,2':6',2''-terpyridine in terms of structure and biological properties, *Polyhedron.* 97 (2015) 83–93. doi:10.1016/j.poly.2015.05.021.
- [32] L. Phelane, F.N. Muya, H.L. Richards, P.G.L. Baker, E.I. Iwuoha, Polysulfone Nanocomposite Membranes with improved hydrophilicity, *Electrochim. Acta.* 128 (2014) 326–335. doi:10.1016/j.electacta.2013.11.156.
- [33] F.N. Muya, L. Phelane, P.G.L. Baker, E.I. Iwuoha, Synthesis and Characterization of Polysulfone Hydrogels, *J. Surf. Eng. Mater. Adv. Technol.* 4 (2014) 227–236. doi:10.4236/jsemat.2014.44025.
- [34] X. Wang, G. Ye, X. Wang, Hydrogel diffraction gratings functionalized with crown ether

for heavy metal ion detection, *Sensors Actuators B Chem.* 193 (2014) 413–419. doi:<http://dx.doi.org/10.1016/j.snb.2013.11.098>.

- [35] Z.Q. Tou, T.W. Koh, C.C. Chan, Poly(vinyl alcohol) hydrogel based fiber interferometer sensor for heavy metal cations, *Sensors Actuators B Chem.* 202 (2014) 185–193. doi:<http://dx.doi.org/10.1016/j.snb.2014.05.006>.
- [36] S.R. Smith, A critical review of the bioavailability and impacts of heavy metals in municipal solid waste composts compared to sewage sludge, *Environ. Int.* 35 (2009) 142–156. doi:<http://dx.doi.org/10.1016/j.envint.2008.06.009>.
- [37] G.R. Willsky, A.B. Goldfine, P.J. Kostyniak, J.H. McNeill, L.Q. Yang, H.R. Khan, D.C. Crans, Effect of vanadium(IV) compounds in the treatment of diabetes: in vivo and in vitro studies with vanadyl sulfate and bis(maltolato)oxovanadium(IV), *J. Inorg. Biochem.* 85 (2001) 33–42. doi:[http://dx.doi.org/10.1016/S0162-0134\(00\)00226-9](http://dx.doi.org/10.1016/S0162-0134(00)00226-9).
- [38] A.N. Wilson, A. Guiseppi-Elie, Targeting homeostasis in drug delivery using bioresponsive hydrogel microforms, *Int. J. Pharm.* 461 (2014) 214–222. doi:<http://dx.doi.org/10.1016/j.ijpharm.2013.11.061>.
- [39] S.W. Won, P. Kotte, W. Wei, A. Lim, Y.-S. Yun, Biosorbents for recovery of precious metals, *Bioresour. Technol.* 160 (2014) 203–212. doi:<http://dx.doi.org/10.1016/j.biortech.2014.01.121>.
- [40] M. Morsy, H. Abdel-Razek, O. Osman, Effect of vanadium on renal Na⁺,K⁺-ATPase activity in diabetic rats: a possible role of leptin, *J. Physiol. Biochem.* 67 (2011) 61–69. doi:10.1007/s13105-010-0049-z.
- [41] M.H. Oster, J.M. Llobet, J.L. Domingo, J. Bruce German, C.L. Keen, Vanadium treatment of diabetic Sprague-Dawley rats results in tissue vanadium accumulation and pro-oxidant effects, *Toxicology.* 83 (1993) 115–130. doi:[http://dx.doi.org/10.1016/0300-483X\(93\)90096-B](http://dx.doi.org/10.1016/0300-483X(93)90096-B).
- [42] H. Holback, Y. Yeo, K. Park, 1 - Hydrogel swelling behavior and its biomedical applications, in: S. Rimmer (Ed.), *Biomed. Hydrogels*, Woodhead Publishing, 2011: pp. 3–24. doi:<http://dx.doi.org/10.1533/9780857091383.1.3>.

- [43] J. Costa Pessoa, Thirty years through vanadium chemistry., *J. Inorg. Biochem.* 147 (2015) 4–24. doi:10.1016/j.jinorgbio.2015.03.004.
- [44] R. Odunayo, NANOSTRUCTURED POLYPYRROLE IMPEDIMETRIC SENSORS FOR ANTHROPOGENIC ORGANIC, (2007).
- [45] K. Kustin, Aqueous vanadium ion dynamics relevant to bioinorganic chemistry: A review., *J. Inorg. Biochem.* 147 (2015) 32–8. doi:10.1016/j.jinorgbio.2014.12.009.
- [46] D. Rehder, Biological and medicinal aspects of vanadium, *Inorg. Chem. Commun.* 6 (2003) 604–617. doi:http://dx.doi.org/10.1016/S1387-7003(03)00050-9.
- [47] D.M. Facchini, V.G. Yuen, M.L. Battell, J.H. McNeill, M.D. Grynypas, The effects of vanadium treatment on bone in diabetic and non-diabetic rats, *Bone*. 38 (2006) 368–377. doi:http://dx.doi.org/10.1016/j.bone.2005.08.015.
- [48] S.C. Gad, T. Pham, Vanadium, in: P. Wexler (Ed.), *Encycl. Toxicol.* (Third Ed., Academic Press, Oxford, 2014: pp. 909–911. doi:http://dx.doi.org/10.1016/B978-0-12-386454-3.00960-X.
- [49] A.M. Evangelou, Vanadium in cancer treatment, *Crit. Rev. Oncol. Hematol.* 42 (2002) 249–265. doi:http://dx.doi.org/10.1016/S1040-8428(01)00221-9.
- [50] D.C. Crans, Chemistry and insulin-like properties of vanadium(IV) and vanadium(V) compounds, *J. Inorg. Biochem.* 80 (2000) 123–131. doi:http://dx.doi.org/10.1016/S0162-0134(00)00048-9.
- [51] I. Goldwasser, D. Gefel, E. Gershonov, M. Fridkin, Y. Shechter, Insulin-like effects of vanadium: basic and clinical implications, *J. Inorg. Biochem.* 80 (2000) 21–25. doi:http://dx.doi.org/10.1016/S0162-0134(00)00035-0.
- [52] Y. Shechter, I. Goldwasser, M. Mironchik, M. Fridkin, D. Gefel, Historic perspective and recent developments on the insulin-like actions of vanadium; toward developing vanadium-based drugs for diabetes, *Coord. Chem. Rev.* 237 (2003) 3–11. doi:http://dx.doi.org/10.1016/S0010-8545(02)00302-8.
- [53] L. He, X. Wang, C. Zhao, D. Zhu, W. Du, Inhibition of human amylin fibril formation by

insulin-mimetic vanadium complexes, *Metallomics*. 6 (2014) 1087–1096. doi:10.1039/c4mt00021h.

- [54] J.B. Vincent, Y. Neggers, Chapter 46 - Roles of Chromium(III), Vanadium, and Zinc in Sports Nutrition, in: D. Bagchi, S. Nair, C.K. Sen (Eds.), *Nutr. Enhanc. Sport. Perform.*, Academic Press, San Diego, 2013: pp. 447–454. doi:http://dx.doi.org/10.1016/B978-0-12-396454-0.00046-1.
- [55] A. Bishayee, A. Waghray, M.A. Patel, M. Chatterjee, Vanadium in the detection, prevention and treatment of cancer: The in vivo evidence, *Cancer Lett.* 294 (2010) 1–12. doi:http://dx.doi.org/10.1016/j.canlet.2010.01.030.
- [56] G. Cabrera, R. Pérez, J.M. Gómez, A. Ábalos, D. Cantero, Toxic effects of dissolved heavy metals on *Desulfovibrio vulgaris* and *Desulfovibrio* sp. strains, *J. Hazard. Mater.* 135 (2006) 40–46. doi:http://dx.doi.org/10.1016/j.jhazmat.2005.11.058.
- [57] M. Kammerer, O. Mastain, S. Le Dréan-Quenech'du, H. Pouliquen, M. Larhantec, Liver and kidney concentrations of vanadium in oiled seabirds after the Erika wreck, *Sci. Total Environ.* 333 (2004) 295–301. doi:http://dx.doi.org/10.1016/j.scitotenv.2004.05.014.
- [58] X. Zhu, Y. Lu, Chapter 16 - Selenium Supplementation and Cataract, in: V.R. Preedy (Ed.), *Handb. Nutr. Diet Eye*, Academic Press, San Diego, 2014: pp. 157–165. doi:http://dx.doi.org/10.1016/B978-0-12-401717-7.00016-2.
- [59] B. Santhosh Kumar, K.I. Priyadarsini, Selenium nutrition: How important is it?, *Biomed. Prev. Nutr.* 4 (2014) 333–341. doi:http://dx.doi.org/10.1016/j.bionut.2014.01.006.
- [60] S.C. Gad, T. Pham, Selenium, in: P. Wexler (Ed.), *Encycl. Toxicol.* (Third Ed., Academic Press, Oxford, 2014: pp. 232–235. doi:http://dx.doi.org/10.1016/B978-0-12-386454-3.00926-X.
- [61] O. Ozay, S. Ekici, Y. Baran, N. Aktas, N. Sahiner, Removal of toxic metal ions with magnetic hydrogels, *Water Res.* 43 (2009) 4403–4411. doi:http://dx.doi.org/10.1016/j.watres.2009.06.058.
- [62] S. Chatterjee, T. Chatterjee, S.H. Woo, A new type of chitosan hydrogel sorbent

generated by anionic surfactant gelation, *Bioresour. Technol.* 101 (2010) 3853–3858. doi:<http://dx.doi.org/10.1016/j.biortech.2009.12.089>.

- [63] W.S. Wan Ngah, M.A.K.M. Hanafiah, Removal of heavy metal ions from wastewater by chemically modified plant wastes as adsorbents: A review, *Bioresour. Technol.* 99 (2008) 3935–3948. doi:<http://dx.doi.org/10.1016/j.biortech.2007.06.011>.
- [64] D. Sud, G. Mahajan, M.P. Kaur, Agricultural waste material as potential adsorbent for sequestering heavy metal ions from aqueous solutions – A review, *Bioresour. Technol.* 99 (2008) 6017–6027. doi:<http://dx.doi.org/10.1016/j.biortech.2007.11.064>.
- [65] S.S. Kalaivani, T. Vidhyadevi, A. Murugesan, K.V. Thiruvengadaravi, D. Anuradha, S. Sivanesan, L. Ravikumar, The use of new modified poly(acrylamide) chelating resin with pendent benzothiazole groups containing donor atoms in the removal of heavy metal ions from aqueous solutions, *Water Resour. Ind.* 5 (2014) 21–35. doi:<http://dx.doi.org/10.1016/j.wri.2014.04.001>.
- [66] G. Narender Reddy, M.N. V Prasad, Heavy metal-binding proteins/peptides: Occurrence, structure, synthesis and functions. A review, *Environ. Exp. Bot.* 30 (1990) 251–264. doi:[http://dx.doi.org/10.1016/0098-8472\(90\)90037-5](http://dx.doi.org/10.1016/0098-8472(90)90037-5).
- [67] K.H. Thompson, C. Orvig, Vanadium in diabetes: 100 years from Phase 0 to Phase I, *J. Inorg. Biochem.* 100 (2006) 1925–1935. doi:<http://dx.doi.org/10.1016/j.jinorgbio.2006.08.016>.
- [68] K.H. Thompson, J. Lichter, C. LeBel, M.C. Scaife, J.H. McNeill, C. Orvig, Vanadium treatment of type 2 diabetes: A view to the future, *J. Inorg. Biochem.* 103 (2009) 554–558. doi:<http://dx.doi.org/10.1016/j.jinorgbio.2008.12.003>.
- [69] Y. Zhang, X.-D. Yang, K. Wang, D.C. Crans, The permeability and cytotoxicity of insulin-mimetic vanadium (III,IV,V)-dipicolinate complexes, *J. Inorg. Biochem.* 100 (2006) 80–87. doi:<http://dx.doi.org/10.1016/j.jinorgbio.2005.10.006>.
- [70] J. Chen, M. Liu, H. Liu, L. Ma, Synthesis, swelling and drug release behavior of poly(N,N-diethylacrylamide-co-N-hydroxymethyl acrylamide) hydrogel, *Mater. Sci. Eng. C.* 29 (2009) 2116–2123. doi:<http://dx.doi.org/10.1016/j.msec.2009.04.008>.

- [71] J. Wang, C. Chen, Chitosan-based biosorbents: Modification and application for biosorption of heavy metals and radionuclides, *Bioresour. Technol.* 160 (2014) 129–141. doi:<http://dx.doi.org/10.1016/j.biortech.2013.12.110>.
- [72] A. Demirbas, Heavy metal adsorption onto agro-based waste materials: A review, *J. Hazard. Mater.* 157 (2008) 220–229. doi:<http://dx.doi.org/10.1016/j.jhazmat.2008.01.024>.
- [73] D. Buenger, F. Topuz, J. Groll, Hydrogels in sensing applications, *Prog. Polym. Sci.* 37 (2012) 1678–1719. doi:<http://dx.doi.org/10.1016/j.progpolymsci.2012.09.001>.
- [74] M.M. Abeer, M.C.I.M. Amin, A.M. Lazim, M. Pandey, C. Martin, Synthesis of a novel acrylated abietic acid-g-bacterial cellulose hydrogel by gamma irradiation, *Carbohydr. Polym.* 110 (2014) 505–512. doi:<http://dx.doi.org/10.1016/j.carbpol.2014.04.052>.
- [75] Y. Zheng, A. Wang, Evaluation of ammonium removal using a chitosan-g-poly (acrylic acid)/rectorite hydrogel composite, *J. Hazard. Mater.* 171 (2009) 671–677. doi:<http://dx.doi.org/10.1016/j.jhazmat.2009.06.053>.
- [76] T. Jamnongkan, A. Wattanakornsiri, P. Wachirawongsakorn, S. Kaewpirom, Effects of crosslinking degree of poly(vinyl alcohol) hydrogel in aqueous solution: kinetics and mechanism of copper(II) adsorption, *Polym. Bull.* 71 (2014) 1081–1100. doi:10.1007/s00289-014-1112-7.
- [77] C. Liu, Y. Tan, K. Xu, Y. Li, C. Lu, P. Wang, Synthesis of poly(2-(2-methoxyethoxy)ethyl methacrylate) hydrogel using starch-based nanosphere cross-linkers, *Carbohydr. Polym.* 105 (2014) 270–275. doi:<http://dx.doi.org/10.1016/j.carbpol.2014.01.078>.
- [78] Y.H.F. Al-qudah, G.A. Mahmoud, M.A. Abdel Khalek, Radiation crosslinked poly (vinyl alcohol)/acrylic acid copolymer for removal of heavy metal ions from aqueous solutions, *J. Radiat. Res. Appl. Sci.* 7 (2014) 135–145. doi:<http://dx.doi.org/10.1016/j.jrras.2013.12.008>.
- [79] A.H. Kaksonen, M.L. Riekkola-Vanhanen, J.A. Puhakka, Optimization of metal sulphide precipitation in fluidized-bed treatment of acidic wastewater, *Water Res.* 37 (2003)

255–266. doi:[http://dx.doi.org/10.1016/S0043-1354\(02\)00267-1](http://dx.doi.org/10.1016/S0043-1354(02)00267-1).

- [80] Z. Cao, J. Guo, X. Fan, J. Xu, Z. Fan, B. Du, Detection of heavy metal ions in aqueous solution by P(MBTVBC-co-VIM)-coated QCM sensor, *Sensors Actuators B Chem.* 157 (2011) 34–41. doi:<http://dx.doi.org/10.1016/j.snb.2011.03.023>.
- [81] R. Villalonga, S. Tachibana, R. Cao, H.L. Ramirez, Y. Asano, Supramolecular-mediated thermostabilization of phenylalanine dehydrogenase modified with β -cyclodextrin derivatives, *Biochem. Eng. J.* 30 (2006) 26–32. doi:10.1016/j.bej.2006.01.013.
- [82] Y. Liu, X. Cao, R. Hua, Y. Wang, Y. Liu, C. Pang, Y. Wang, Selective adsorption of uranyl ion on ion-imprinted chitosan/PVA cross-linked hydrogel, *Hydrometallurgy.* 104 (2010) 150–155. doi:<http://dx.doi.org/10.1016/j.hydromet.2010.05.009>.
- [83] B.-Y. Chen, V.P. Utgikar, S.M. Harmon, H.H. Tabak, D.F. Bishop, R. Govind, Studies on biosorption of zinc(II) and copper(II) on *Desulfovibrio desulfuricans*, *Int. Biodeterior. Biodegradation.* 46 (2000) 11–18. doi:[http://dx.doi.org/10.1016/S0964-8305\(00\)00054-8](http://dx.doi.org/10.1016/S0964-8305(00)00054-8).
- [84] J.J. Chen, A.L. Ahmad, B.S. Ooi, Poly(N-isopropylacrylamide-co-acrylic acid) hydrogels for copper ion adsorption: Equilibrium isotherms, kinetic and thermodynamic studies, *J. Environ. Chem. Eng.* 1 (2013) 339–348. doi:<http://dx.doi.org/10.1016/j.jece.2013.05.012>.
- [85] S. Bekin, S. Sarmad, K. Gürkan, G. Keçeli, G. Gürdağ, Synthesis, characterization and bending behavior of electroresponsive sodium alginate/poly(acrylic acid) interpenetrating network films under an electric field stimulus, *Sensors Actuators B Chem.* 202 (2014) 878–892. doi:<http://dx.doi.org/10.1016/j.snb.2014.06.051>.
- [86] E.S. Dragan, Design and applications of interpenetrating polymer network hydrogels. A review, *Chem. Eng. J.* 243 (2014) 572–590. doi:<http://dx.doi.org/10.1016/j.cej.2014.01.065>.
- [87] B. Singh, G.S. Chauhan, S.S. Bhatt, K. Kumar, Metal ion sorption and swelling studies of psyllium and acrylic acid based hydrogels, *Carbohydr. Polym.* 64 (2006) 50–56. doi:<http://dx.doi.org/10.1016/j.carbpol.2005.10.022>.

- [88] S.R. Shirsath, A.P. Patil, R. Patil, J.B. Naik, P.R. Gogate, S.H. Sonawane, Removal of Brilliant Green from wastewater using conventional and ultrasonically prepared poly(acrylic acid) hydrogel loaded with kaolin clay: A comparative study, *Ultrason. Sonochem.* 20 (2013) 914–923. doi:<http://dx.doi.org/10.1016/j.ultsonch.2012.11.010>.
- [89] H. Yan, L. Yang, Z. Yang, H. Yang, A. Li, R. Cheng, Preparation of chitosan/poly(acrylic acid) magnetic composite microspheres and applications in the removal of copper(II) ions from aqueous solutions, *J. Hazard. Mater.* 229–230 (2012) 371–380. doi:<http://dx.doi.org/10.1016/j.jhazmat.2012.06.014>.
- [90] R. Akkaya, U. Ulusoy, Adsorptive features of chitosan entrapped in polyacrylamide hydrogel for Pb²⁺, UO₂²⁺, and Th⁴⁺, *J. Hazard. Mater.* 151 (2008) 380–388. doi:<http://dx.doi.org/10.1016/j.jhazmat.2007.05.084>.
- [91] K.R. Vogel, E. Arning, B.L. Wasek, S. McPherson, T. Bottiglieri, K.M. Gibson, Brain-blood amino acid correlates following protein restriction in murine maple syrup urine disease., *Orphanet J. Rare Dis.* 9 (2014) 73. doi:[10.1186/1750-1172-9-73](https://doi.org/10.1186/1750-1172-9-73).
- [92] N.K. Lazaridis, E.N. Peleka, T.D. Karapantsios, K.A. Matis, Copper removal from effluents by various separation techniques, *Hydrometallurgy.* 74 (2004) 149–156. doi:<http://dx.doi.org/10.1016/j.hydromet.2004.03.003>.
- [93] S.A. El-Sayed, M.E. Mostafa, Pyrolysis characteristics and kinetic parameters determination of biomass fuel powders by differential thermal gravimetric analysis (TGA/DTG), *Energy Convers. Manag.* 85 (2014) 165–172. doi:<http://dx.doi.org/10.1016/j.enconman.2014.05.068>.
- [94] L.A. Féris, A.T. De León, M. Santander, J. Rubio, Advances in the adsorptive particulate flotation process, *Int. J. Miner. Process.* 74 (2004) 101–106. doi:<http://dx.doi.org/10.1016/j.minpro.2003.09.005>.
- [95] Y. Cheng, X. Sun, X. Liao, B. Shi, Adsorptive Recovery of Uranium from Nuclear Fuel Industrial Wastewater by Titanium Loaded Collagen Fiber, *Chinese J. Chem. Eng.* 19 (2011) 592–597. doi:[http://dx.doi.org/10.1016/S1004-9541\(11\)60027-X](http://dx.doi.org/10.1016/S1004-9541(11)60027-X).
- [96] E. Doelsch, A. Masion, G. Moussard, C. Chevassus-Rosset, O. Wojciechowicz, Impact

of pig slurry and green waste compost application on heavy metal exchangeable fractions in tropical soils, *Geoderma*. 155 (2010) 390–400. doi:<http://dx.doi.org/10.1016/j.geoderma.2009.12.024>.

- [97] R. Hua, Z. Li, Sulfhydryl functionalized hydrogel with magnetism: Synthesis, characterization, and adsorption behavior study for heavy metal removal, *Chem. Eng. J.* 249 (2014) 189–200. doi:<http://dx.doi.org/10.1016/j.cej.2014.03.097>.
- [98] D. Liu, Z. Li, Y. Zhu, Z. Li, R. Kumar, Recycled chitosan nanofibril as an effective Cu(II), Pb(II) and Cd(II) ionic chelating agent: Adsorption and desorption performance, *Carbohydr. Polym.* 111 (2014) 469–476. doi:<http://dx.doi.org/10.1016/j.carbpol.2014.04.018>.
- [99] R. Oun, J.A. Plumb, N.J. Wheate, A cisplatin slow-release hydrogel drug delivery system based on a formulation of the macrocycle cucurbit[7]uril, gelatin and polyvinyl alcohol, *J. Inorg. Biochem.* 134 (2014) 100–105. doi:<http://dx.doi.org/10.1016/j.jinorgbio.2014.02.004>.
- [100] J. Liu, Q. Li, Y. Su, Q. Yue, B. Gao, Characterization and swelling–deswelling properties of wheat straw cellulose based semi-IPNs hydrogel, *Carbohydr. Polym.* 107 (2014) 232–240. doi:<http://dx.doi.org/10.1016/j.carbpol.2014.02.073>.
- [101] B. Mandal, S.K. Ray, Synthesis of interpenetrating network hydrogel from poly(acrylic acid-co-hydroxyethyl methacrylate) and sodium alginate: Modeling and kinetics study for removal of synthetic dyes from water, *Carbohydr. Polym.* 98 (2013) 257–269. doi:<http://dx.doi.org/10.1016/j.carbpol.2013.05.093>.
- [102] I.S. Ng, X. Wu, X. Yang, Y. Xie, Y. Lu, C. Chen, Synergistic effect of *Trichoderma reesei* cellulases on agricultural tea waste for adsorption of heavy metal Cr(VI), *Bioresour. Technol.* 145 (2013) 297–301. doi:<http://dx.doi.org/10.1016/j.biortech.2013.01.105>.
- [103] P.K. Seyed Morteza Naghib, Mohammad Rabiee, Eskandar Omidinia, Investigation of a Biosensor Based on Phenylalanine Dehydrogenase Immobilized on a Polymer-Blend Film for Phenylketonuria Diagnosis, *Electroanalysis*. 24 (2012) 407–417.
- [104] Z. Wang, P.M. Lee, Graphene thin film electrodes synthesized by thermally treating co-

- sputtered nickel-carbon mixed layers for detection of trace lead, cadmium and copper ions in acetate buffer solutions, *Thin Solid Films*. 544 (2013) 341–347. doi:10.1016/j.tsf.2013.02.102.
- [105] G. Qin, Z. Zhu, S. Li, A.M. McDermott, C. Cai, Development of ciprofloxacin-loaded contact lenses using fluoros chemistry, *Biomaterials*. 124 (2017) 55–64. doi:10.1016/j.biomaterials.2017.01.046.
- [106] Y.-K. Lee, Y.-C. Lin, S.-H. Tsai, W.-L. Chen, Y.-M. Chen, Therapeutic outcomes of combined topical autologous serum eye drops with silicone-hydrogel soft contact lenses in the treatment of corneal persistent epithelial defects: A preliminary study, *Contact Lens Anterior Eye*. 39 (2016) 425–430. doi:10.1016/j.clae.2016.06.003.
- [107] K. Filipecka, R. Miedziński, M. Sitarz, J. Filipecki, M. Makowska-Janusik, Optical and vibrational properties of phosphorylcholine-based contact lenses—Experimental and theoretical investigations, *Spectrochim. Acta Part A Mol. Biomol. Spectrosc.* 176 (2017) 83–90. doi:10.1016/j.saa.2017.01.013.
- [108] D.C. Crans, M. Mahroof-Tahir, M.D. Johnson, P.C. Wilkins, L. Yang, K. Robbins, A. Johnson, J.A. Alfano, M.E. Godzala Iii, L.T. Austin, G.R. Willsky, Vanadium(IV) and vanadium(V) complexes of dipicolinic acid and derivatives. Synthesis, X-ray structure, solution state properties: and effects in rats with STZ-induced diabetes, *Inorganica Chim. Acta*. 356 (2003) 365–378. doi:http://dx.doi.org/10.1016/S0020-1693(03)00430-4.
- [109] J.B. Vincent, Chapter 30 - Beneficial Effects of Chromium(III) and Vanadium Supplements in Diabetes, in: D. Bagchi, N. Sreejayan (Eds.), *Nutr. Ther. Interv. Diabetes Metab. Syndr.*, Academic Press, San Diego, 2012: pp. 381–391. doi:http://dx.doi.org/10.1016/B978-0-12-385083-6.00030-9.
- [110] R.K. Sharma, P. Kumar, G.B. Reddy, Synthesis of vanadium pentoxide (V₂O₅) nanobelts with high coverage using plasma assisted PVD approach, *J. Alloys Compd.* 638 (2015) 289–297. doi:10.1016/j.jallcom.2015.02.178.
- [111] Y. Zhao, L. Ye, H. Liu, Q. Xia, Y. Zhang, X. Yang, K. Wang, Vanadium compounds induced mitochondria permeability transition pore (PTP) opening related to oxidative stress, *J. Inorg. Biochem.* 104 (2010) 371–378.

doi:<http://dx.doi.org/10.1016/j.jinorgbio.2009.11.007>.

- [112] K.A. Doucette, K.N. Hassell, D.C. Crans, Selective speciation improves efficacy and lowers toxicity of platinum anticancer and vanadium antidiabetic drugs, *J. Inorg. Biochem.* 165 (2016) 56–70. doi:10.1016/j.jinorgbio.2016.09.013.
- [113] J.H. Duffus, Carcinogenicity classification of vanadium pentoxide and inorganic vanadium compounds, the NTP study of carcinogenicity of inhaled vanadium pentoxide, and vanadium chemistry, *Regul. Toxicol. Pharmacol.* 47 (2007) 110–114. doi:10.1016/j.yrtph.2006.08.006.
- [114] Office of Dietary Supplements - Dietary Supplement Fact Sheet: Selenium, (n.d.). <https://ods.od.nih.gov/factsheets/Selenium-healthProfessional/> (accessed July 22, 2015).
- [115] S. Reinberg, Selenium Supplements May Slow Progression of HIV, *Arch. Intern. Med.* 1 (2007) 922. <http://consumer.healthday.com/general-health-information-16/misc-drugs-news-218/selenium-supplements-may-slow-progression-of-hiv-601153.html> (accessed August 26, 2015).
- [116] J. Gebicki, T. Dymerski, Chapter 11 – Application of Chemical Sensors and Sensor Matrixes to Air Quality Evaluation, *Compr. Anal. Chem.* 73 (2016) 267–294. doi:10.1016/bs.coac.2016.02.007.
- [117] E.A. Bagshaw, A. Beaton, J.L. Wadham, M. Mowlem, J.R. Hawkings, M. Tranter, Chemical sensors for in situ data collection in the cryosphere, *TrAC Trends Anal. Chem.* 82 (2016) 348–357. doi:10.1016/j.trac.2016.06.016.
- [118] A.L. Alvarado-Gómez, M.A. Alonso-Lomillo, O. Domínguez-Renedo, M.J. Arcos-Martínez, A disposable alkaline phosphatase-based biosensor for vanadium chronoamperometric determination., *Sensors (Basel)*. 14 (2014) 3756–67. doi:10.3390/s140203756.
- [119] K.M. Holtz, B. Stec, E.R. Kantrowitz, A Model of the Transition State in the Alkaline Phosphatase Reaction, *J. Biol. Chem.* 274 (1999) 8351–8354. doi:10.1074/jbc.274.13.8351.

- [120] E. Sergienko, Y. Su, X. Chan, B. Brown, A. Hurder, S. Narisawa, J.L. Millán, Identification and characterization of novel tissue-nonspecific alkaline phosphatase inhibitors with diverse modes of action., *J. Biomol. Screen.* 14 (2009) 824–37. doi:10.1177/1087057109338517.
- [121] P.L. Walter, H. Steinbrenner, A. Barthel, L.-O. Klotz, Stimulation of selenoprotein P promoter activity in hepatoma cells by FoxO1a transcription factor, *Biochem. Biophys. Res. Commun.* 365 (2008) 316–321. doi:10.1016/j.bbrc.2007.10.171.
- [122] H. Steinbrenner, L. Aili, E. Bilgic, H. Sies, P. Brenneisen, Involvement of selenoprotein P in protection of human astrocytes from oxidative damage, *Free Radic. Biol. Med.* 40 (2006) 1513–1523. doi:10.1016/j.freeradbiomed.2005.12.022.
- [123] P. Brenneisen, H. Steinbrenner, H. Sies, Selenium, oxidative stress, and health aspects, *Mol. Aspects Med.* 26 (2005) 256–267. doi:10.1016/j.mam.2005.07.004.
- [124] • R. N. Adams, *Electrochemistry at Solid Electrodes*, 10th ed., Marcel Dekker, New York, 1968.
- [125] R.G. Compton and C.E. Banks, *Understanding Voltammetry*, in: World Sci., Singapore, 2007.
- [126] S.W. Feldberg, A general method for simulation, *Electroanal. Chem. Ser.* 3 (1969).
- [127] Louis Ramaley and Matthew.S. Krause, Theory of square wave voltammetry, *Anal. Chem.* 41 (1969) 1362–1365.
- [128] Mark.E. Orazem and Bernard Tribollet, *Electrochemical Impedance spectroscopy*, John Wiley and sons, Pennington, 2011.
- [129] P.H. Rodrigues Júnior, K. de Sá Oliveira, C.E.R. de Almeida, L.F.C. De Oliveira, R. Stephani, M. da S. Pinto, A.F. de Carvalho, Í.T. Perrone, FT-Raman and chemometric tools for rapid determination of quality parameters in milk powder: Classification of samples for the presence of lactose and fraud detection by addition of maltodextrin, *Food Chem.* 196 (2016) 584–588. doi:10.1016/j.foodchem.2015.09.055.
- [130] J. Jehlička, H.G.M. Edwards, I. Němec, A. Oren, Raman spectroscopic study of the

Chromobacterium violaceum pigment violacein using multiwavelength excitation and DFT calculations., *Spectrochim. Acta. A. Mol. Biomol. Spectrosc.* 151 (2015) 459–67. doi:10.1016/j.saa.2015.06.051.

- [131] A. Daniel, A. Prakasarao, K. Dornadula, S. Ganesan, Polarized Raman spectroscopy unravels the biomolecular structural changes in cervical cancer., *Spectrochim. Acta. A. Mol. Biomol. Spectrosc.* 152 (2015) 58–63. doi:10.1016/j.saa.2015.06.053.
- [132] C. Kyomugasho, S. Christiaens, A. Shpigelman, A.M. Van Loey, M.E. Hendrickx, FT-IR spectroscopy, a reliable method for routine analysis of the degree of methylesterification of pectin in different fruit- and vegetable-based matrices, *Food Chem.* 176 (2015) 82–90. doi:10.1016/j.foodchem.2014.12.033.
- [133] S. Sudhakara, A. Chadha, A fourier transform infrared spectroscopy (FTIR) based assay for *Candida parapsilosis* ATCC 7330 mediated oxidation of aryl alcohols., *J. Biotechnol.* 209 (2015) 102–7. doi:10.1016/j.jbiotec.2015.06.398.
- [134] S.A. Shlykov, D.Y. Osadchiy, N.N. Chipanina, L.P. Oznobikhina, B.A. Shainyan, Molecular structure and conformational analysis of 3-methyl-3-silathiane by gas phase electron diffraction, FTIR spectroscopy and quantum chemical calculations, *J. Mol. Struct.* 1100 (2015) 555–561. doi:10.1016/j.molstruc.2015.08.005.
- [135] R. Rygula, N. Abumaria, E. Domenici, C. Hiemke, E. Fuchs, Effects of fluoxetine on behavioral deficits evoked by chronic social stress in rats., *Behav. Brain Res.* 174 (2006) 188–92. doi:10.1016/j.bbr.2006.07.017.
- [136] J. Siegel, O. Kvítek, P. Slepíčka, J. Náhlík, J. Heitz, V. Švorčík, Structural, electrical and optical studies of gold nanostructures formed by Ar plasma-assisted sputtering, *Nucl. Instruments Methods Phys. Res. Sect. B Beam Interact. with Mater. Atoms.* 272 (2012) 193–197. doi:10.1016/j.nimb.2011.01.063.
- [137] B.J. Inkson, 2 – Scanning electron microscopy (SEM) and transmission electron microscopy (TEM) for materials characterization, in: *Mater. Charact. Using Nondestruct. Eval. Methods*, 2016: pp. 17–43. doi:10.1016/B978-0-08-100040-3.00002-X.
- [138] E. Ginting, E.W. Peterson, J. Zhou, Scanning tunneling microscopy studies of Mn-doped

CeOx(111) interfaces, *Appl. Catal. B Environ.* 197 (2016) 337–342. doi:10.1016/j.apcatb.2016.04.020.

- [139] P. Kusch, D. Schroeder-Obst, V. Obst, G. Knupp, W. Fink, J. Steinhaus, Chapter 17 – Application of pyrolysis-gas chromatography/mass spectrometry (Py-GC/MS) and scanning electron microscopy (SEM) in failure analysis for the identification of organic compounds in chemical, rubber, and automotive industry, in: *Handb. Mater. Fail. Anal. with Case Stud. from Chem. Concr. Power Ind.*, 2016: pp. 441–469. doi:10.1016/B978-0-08-100116-5.00017-X.
- [140] A.D. Ozkan, A.E. Topal, A. Dana, M.O. Guler, A.B. Tekinay, Atomic force microscopy for the investigation of molecular and cellular behavior, *Micron*. 89 (2016) 60–76. doi:10.1016/j.micron.2016.07.011.
- [141] H. Liu, H. Qiao, D. Krajcikova, Z. Zhang, H. Wang, I. Barak, J. Tang, Physical interaction and assembly of *Bacillus subtilis* spore coat proteins CotE and CotZ studied by atomic force microscopy, *J. Struct. Biol.* 195 (2016) 245–251. doi:10.1016/j.jsb.2016.06.010.
- [142] F.J. Flores-Ruiz, F.J. Espinoza-Beltrán, C.J. Dilliegros-Godines, J.M. Siqueiros, A. Herrera-Gómez, Atomic force acoustic microscopy: Influence of the lateral contact stiffness on the elastic measurements, *Ultrasonics*. 71 (2016) 271–277. doi:10.1016/j.ultras.2016.07.003.
- [143] M.R. Maurya, B. Uprety, N. Chaudhary, F. Avecilla, Synthesis and characterization of di- μ -oxidovanadium(V), oxidoperoxido-vanadium(V) and polymer supported dioxidovanadium(V) complexes and catalytic oxidation of isoeugenol, *Inorganica Chim. Acta*. 434 (2015) 230–238. doi:10.1016/j.ica.2015.05.027.
- [144] M. Nasehnejad, M. Gholipour Shahraki, G. Nabiyouni, Atomic force microscopy study, kinetic roughening and multifractal analysis of electrodeposited silver films, *Appl. Surf. Sci.* 389 (2016) 735–741. doi:10.1016/j.apsusc.2016.07.134.
- [145] R. Akhtar, H.K. Graham, B. Derby, M.. Sherratt, A.W. Trafford, R.S. Chadwick, N. Gavara, Frequency-modulated atomic force microscopy localises viscoelastic remodelling in the ageing sheep aorta, *J. Mech. Behav. Biomed. Mater.* 64 (2016) 10–17. doi:10.1016/j.jmbbm.2016.07.018.

- [146] J. Moffat, V.J. Morris, S. Al-Assaf, A.P. Gunning, Visualisation of xanthan conformation by atomic force microscopy, *Carbohydr. Polym.* 148 (2016) 380–389. doi:10.1016/j.carbpol.2016.04.078.
- [147] M. Prokopowicz, Atomic force microscopy technique for the surface characterization of sol-gel derived multi-component silica nanocomposites, *Colloids Surfaces A Physicochem. Eng. Asp.* 504 (2016) 350–357. doi:10.1016/j.colsurfa.2016.05.092.
- [148] D. Lazarev, F.R. Zypman, Determination of charge and size of rings by atomic force microscopy, *J. Electrostat.* 83 (2016) 69–72. doi:10.1016/j.elstat.2016.07.008.
- [149] A.K. Bajpai, R. Bhatt, R. Katare, Atomic force microscopy enabled roughness analysis of nanostructured poly (diaminonaphthalene) doped poly (vinyl alcohol) conducting polymer thin films, 2016. doi:10.1016/j.micron.2016.07.012.
- [150] X. Gui, Y. Xing, G. Rong, Y. Cao, J. Liu, Interaction forces between coal and kaolinite particles measured by atomic force microscopy, *Powder Technol.* 301 (2016) 349–355. doi:10.1016/j.powtec.2016.06.026.
- [151] M.-C. Chen, H.-W. Tsai, C.-T. Liu, S.-F. Peng, W.-Y. Lai, S.-J. Chen, Y. Chang, H.-W. Sung, A nanoscale drug-entrapment strategy for hydrogel-based systems for the delivery of poorly soluble drugs, *Biomaterials* 30 (2009) 2102–2111. doi:http://dx.doi.org/10.1016/j.biomaterials.2008.12.047.
- [152] F.N. Muya, P.G.L. Baker, E. Ewuoha, Development of Hydrogel Sensors for Detection of Trace Metals of Biological Significance, (2014) 2014.
- [153] L.P. Muya, F. N. P. Baker* and E. Iwouha, Synthesis and characterization of polysulfone Hydrogels, *J. Surf. Eng. Mater. Adv. Technol.* (4) (2014) 227–236.
- [154] S.S. Vaghani, M.M. Patel, C.S. Satish, Synthesis and characterization of pH-sensitive hydrogel composed of carboxymethyl chitosan for colon targeted delivery of ornidazole, *Carbohydr. Res.* 347 (2012) 76–82. doi:http://dx.doi.org/10.1016/j.carres.2011.04.048.
- [155] E.I.I. F. N. Muya, X. T. Ngema, P. G. L. Baker, Sensory Properties of Polysulfone Hydrogel for Electro-Analytical Profiling of Vanadium and Selenium in Aqueous Solutions, *J.*

Nano Res. 44 (2016) 142–157. doi:10.4028/www.scientific.net/JNanoR.44.142.

- [156] A. Isha, N.A. Yusof, M. Ahmad, D. Suhendra, W.M.Z.W. Yunus, Z. Zainal, Optical fibre chemical sensor for trace vanadium(V) determination based on newly synthesized palm based fatty hydroxamic acid immobilized in polyvinyl chloride membrane, *Spectrochim. Acta Part A Mol. Biomol. Spectrosc.* 67 (2007) 1398–1402. doi:10.1016/j.saa.2006.10.031.
- [157] F.-J. Huo, J. Su, Y.-Q. Sun, C.-X. Yin, H.-B. Tong, Z.-X. Nie, A rhodamine-based dual chemosensor for the visual detection of copper and the ratiometric fluorescent detection of vanadium, *Dye. Pigment.* 86 (2010) 50–55. doi:10.1016/j.dyepig.2009.11.007.
- [158] M. Paczkowska, M. Mizera, J. Dzitko, K. Lewandowska, P. Zalewski, J. Cielecka-Piontek, Vibrational (FT-IR, Raman) and DFT analysis on the structure of labile drugs. The case of crystalline tebipenem and its ester, *J. Mol. Struct.* 1134 (2017) 135–142. doi:10.1016/j.molstruc.2016.12.074.
- [159] T. Virtanen, S.-P. Reinikainen, M. Kögler, M. Mänttari, T. Viitala, M. Kallioinen, Real-time fouling monitoring with Raman spectroscopy, *J. Memb. Sci.* 525 (2017) 312–319. doi:10.1016/j.memsci.2016.12.005.
- [160] Q. Dai, X. Zhu, J. Yu, E. Karangwa, S. Xia, X. Zhang, C. Jia, Critical desiccation state Raman spectroscopy for simple, rapid and sensitive detection of native and glycosylated protein, 2017. doi:10.1016/j.foodhyd.2016.12.026.
- [161] A. V. Markin, N.E. Markina, I.Y. Goryacheva, Raman spectroscopy based analysis inside photonic-crystal fibers, *TrAC Trends Anal. Chem.* 88 (2017) 185–197. doi:10.1016/j.trac.2017.01.003.
- [162] A. Daniel, A. P., S. Ganesan, L. Joseph, Biochemical assessment of human uterine cervix by micro-Raman mapping, *Photodiagnosis Photodyn. Ther.* 17 (2017) 65–74. doi:10.1016/j.pdpdt.2016.08.011.
- [163] Y. Yue, J.J. Wang, P.A.M. Basheer, J.J. Boland, Y. Bai, Characterisation of carbonated Portland cement paste with optical fibre excitation Raman spectroscopy, *Constr.*

Build. Mater. 135 (2017) 369–376. doi:10.1016/j.conbuildmat.2017.01.008.

- [164] D.-W. Li, W.-L. Zhai, Y.-T. Li, Y.-T. Long, Recent progress in surface enhanced Raman spectroscopy for the detection of environmental pollutants, *Microchim. Acta.* 181 (2014) 23–43. doi:10.1007/s00604-013-1115-3.
- [165] M.L. Fernández-Cruz, M.L. Mansilla, J.L. Tadeo, Mycotoxins in fruits and their processed products: Analysis, occurrence and health implications, *J. Adv. Res.* 1 (2010) 113–122. doi:10.1016/j.jare.2010.03.002.
- [166] A. Amine, F. Arduini, D. Moscone, G. Palleschi, Recent advances in biosensors based on enzyme inhibition., *Biosens. Bioelectron.* 76 (2016) 180–94. doi:10.1016/j.bios.2015.07.010.
- [167] A. Homaei, Immobilization of *Penaeus merguensis* alkaline phosphatase on gold nanorods for heavy metal detection, *Ecotoxicol. Environ. Saf.* 136 (2017) 1–7. doi:10.1016/j.ecoenv.2016.10.023.
- [168] E. Akyilmaz, M. Turemis, An inhibition type alkaline phosphatase biosensor for amperometric determination of caffeine, *Electrochim. Acta.* 55 (2010) 5195–5199. doi:10.1016/j.electacta.2010.04.038.
- [169] M. Čadková, V. Dvořáková, R. Metelka, Z. Bílková, L. Korecká, Alkaline phosphatase labeled antibody-based electrochemical biosensor for sensitive HE4 tumor marker detection, 2015. doi:10.1016/j.elecom.2015.06.014.
- [170] S.K. Mwilu, V.A. Okello, F.J. Osonga, S. Miller, O.A. Sadik, A new substrate for alkaline phosphatase based on quercetin pentaphosphate, *Analyst.* 139 (2014) 5472–5481. doi:10.1039/C4AN00931B.
- [171] K.C. Luk, D.J. Covell, V.M. Kehm, B. Zhang, I.Y. Song, M.D. Byrne, R.M. Pitkin, S.C. Decker, J.Q. Trojanowski, V.M.-Y. Lee, Molecular and Biological Compatibility with Host Alpha-Synuclein Influences Fibril Pathogenicity, *Cell Rep.* 16 (2016) 3373–3387. doi:10.1016/j.celrep.2016.08.053.
- [172] H. Santana, Y. González, P.T. Campana, J. Noda, O. Amarantes, R. Itri, A. Beldarraín, R. Páez, Screening for stability and compatibility conditions of recombinant human

epidermal growth factor for parenteral formulation: Effect of pH, buffers, and excipients, *Int. J. Pharm.* 452 (2013) 52–62. doi:10.1016/j.ijpharm.2013.04.054.

- [173] T. Shimomura, T. Itoh, T. Sumiya, F. Mizukami, M. Ono, Electrochemical biosensor for the detection of formaldehyde based on enzyme immobilization in mesoporous silica materials, *Sensors Actuators B Chem.* 135 (2008) 268–275. doi:10.1016/j.snb.2008.08.025.
- [174] N.M. Selivanova, N.V. Sautina, D.V. Vezenov, O.V. Stoyanov, Y.G. Galyametdinov, Evaluation of interactions between liquid crystal films and silane monolayers by atomic force microscopy, *J. Mol. Liq.* 230 (2017) 574–578. doi:10.1016/j.molliq.2017.01.068.
- [175] B. Legrand, J.-P. Salvetat, B. Walter, M. Faucher, D. Théron, J.-P. Aimé, Multi-MHz micro-electro-mechanical sensors for atomic force microscopy, *Ultramicroscopy.* 175 (2017) 46–57. doi:10.1016/j.ultramic.2017.01.005.
- [176] L.C. Powell, N. Hilal, C.J. Wright, Atomic force microscopy study of the biofouling and mechanical properties of virgin and industrially fouled reverse osmosis membranes, *Desalination.* 404 (2017) 313–321. doi:10.1016/j.desal.2016.11.010.
- [177] B. Limoges, J.-M. Savéant, Cyclic voltammetry of immobilized redox enzymes. Interference of steady-state and non-steady-state Michaelis–Menten kinetics of the enzyme–redox cosubstrate system, *J. Electroanal. Chem.* 549 (2003) 61–70. doi:10.1016/S0022-0728(03)00285-7.
- [178] Š. Komorsky-Lovrić, M. Lovrić, Influence of product adsorption on catalytic reaction determined by Michaelis–Menten kinetics, *J. Electroanal. Chem.* 748 (2015) 47–51. doi:10.1016/j.jelechem.2015.04.028.
- [179] I. Daryaei, M. Mohammadebrahim Ghaffari, K.M. Jones, M.D. Pagel, Detection of Alkaline Phosphatase Enzyme Activity with a CatalyCEST MRI Biosensor, *ACS Sensors.* 1 (2016) 857–861. doi:10.1021/acssensors.6b00203.
- [180] R.L. Dean, Kinetic studies with alkaline phosphatase in the presence and absence of inhibitors and divalent cations, *Biochem. Mol. Biol. Educ.* 30 (2002) 401–407.

doi:10.1002/bmb.2002.494030060138.

- [181] W.O. Ho, D. Athey, C.J. McNeil, Amperometric detection of alkaline phosphatase activity at a horseradish peroxidase enzyme electrode based on activated carbon: potential application to electrochemical immunoassay, *Biosens. Bioelectron.* 10 (1995) 683–691. doi:10.1016/0956-5663(95)96959-3.
- [182] P.A. Fiorito, S.I.C. de Torresi, Glucose Amperometric Biosensor Based on the Co-immobilization of Glucose Oxidase (GOx) and Ferrocene in Poly(pyrrole) Generated from Ethanol / Water Mixtures, *J. Braz. Chem. Soc.* 12 (2001) 729–733. doi:10.1590/S0103-50532001000600007.
- [183] P. Manimozhi, L. Rajendran, Derivation of nonsteady-state analytical solution for surface enzyme kinetics, 2010. doi:10.1016/j.jelechem.2010.05.019.
- [184] J.H. Wang, K. Wang, B. Bartling, C.-C. Liu, The Detection of Alkaline Phosphatase Using an Electrochemical Biosensor in a Single-Step Approach, *Sensors (Basel)*. 9 (2009) 8709–8721. doi:10.3390/s91108709.
- [185] Y. Xia, X. Zhao, L. Zhu, P.D. Whanger, Metabolism of selenate and selenomethionine by a selenium-deficient population of men in China, 1992. doi:10.1016/0955-2863(92)90041-G.
- [186] M.-S. Zeng, X. Li, Y. Liu, H. Zhao, J.-C. Zhou, K. Li, J.-Q. Huang, L.-H. Sun, J.-Y. Tang, X.-J. Xia, K.-N. Wang, X.G. Lei, A high-selenium diet induces insulin resistance in gestating rats and their offspring, *Free Radic. Biol. Med.* 52 (2012) 1335–1342. doi:10.1016/j.freeradbiomed.2012.01.017.
- [187] B.A. Zachara, U. Trafikowska, A. Adamowicz, E. Nartowicz, J. Manitus, Selenium, glutathione peroxidases, and some other antioxidant parameters in blood of patients with chronic renal failure, *J. Trace Elem. Med. Biol.* 15 (2001) 161–166. doi:10.1016/S0946-672X(01)80061-4.
- [188] S. Hybsier, T. Schulz, Z. Wu, I. Demuth, W.B. Minich, K. Renko, E. Rijntjes, J. Köhrle, C.J. Strasburger, E. Steinhagen-Thiessen, L. Schomburg, Sex-specific and inter-individual differences in biomarkers of selenium status identified by a calibrated ELISA for

selenoprotein P, *Redox Biol.* 11 (2017) 403–414. doi:10.1016/j.redox.2016.12.025.

- [189] K.A. Guertin, R.K. Grant, K.B. Arnold, L. Burwell, J. Hartline, P.J. Goodman, L.M. Minasian, S.M. Lippman, E. Klein, P.A. Cassano, Effect of long-term vitamin E and selenium supplementation on urine F2-isoprostanes, a biomarker of oxidative stress, *Free Radic. Biol. Med.* 95 (2016) 349–356. doi:10.1016/j.freeradbiomed.2016.03.010.
- [190] R.A. Hauser-Davis, J.A.N. Silva, R.C.C. Rocha, T. Saint'Pierre, R.L. Ziolli, M.A.Z. Arruda, Acute selenium selenite exposure effects on oxidative stress biomarkers and essential metals and trace-elements in the model organism zebrafish (*Danio rerio*), *J. Trace Elem. Med. Biol.* 33 (2016) 68–72. doi:10.1016/j.jtemb.2015.09.001.
- [191] J. Prywer, E. Mielniczek-Brzóska, Chemical equilibria of complexes in urine. A contribution to the physicochemistry of infectious urinary stone formation, *Fluid Phase Equilib.* 425 (2016) 282–288. doi:http://dx.doi.org/10.1016/j.fluid.2016.06.009.
- [192] P. Huang, S.T. Mukherji, S. Wu, J. Muller, R. Goel, Fate of 17 β -Estradiol as a model estrogen in source separated urine during integrated chemical P recovery and treatment using partial nitrification-anammox process, *Water Res.* 103 (2016) 500–509. doi:http://dx.doi.org/10.1016/j.watres.2016.07.044.
- [193] K.E. Williams, O. Miroshnychenko, E.B. Johansen, R.K. Niles, R. Sundaram, K. Kannan, M. Albertolle, Y. Zhou, N. Prasad, P.M. Drake, L.C. Giudice, S.C. Hall, H.E. Witkowska, G.M. Buck Louis, S.J. Fisher, Urine, peritoneal fluid and omental fat proteomes of reproductive age women: Endometriosis-related changes and associations with endocrine disrupting chemicals, *J. Proteomics.* 113 (2015) 194–205. doi:http://dx.doi.org/10.1016/j.jprot.2014.09.015.
- [194] I. Yaroshenko, D. Kirsanov, L. Kartsova, A. Sidorova, I. Borisova, A. Legin, Determination of urine ionic composition with potentiometric multisensor system, *Talanta.* 131 (2015) 556–561. doi:http://dx.doi.org/10.1016/j.talanta.2014.08.030.